National Library of Canada
Bibliothèque nationale du Canada

Canadian Theses Service
Service des thèses canadiennes

Ottawa, Canada
K1A 0N4

NOTICE

The quality of this microform is heavily dependent upon the quality of the original thesis submitted for microfilming. Every effort has been made to ensure the highest quality of reproduction possible.

If pages are missing, contact the university which granted the degree.

Some pages may have indistinct print especially if the original pages were typed with a poor typewriter ribbon or if the university sent us an inferior photocopy.

Reproduction in full or in part of this microform is governed by the Canadian Copyright Act, R.S.C. 1970, c. C-30, and subsequent amendments.

AVIS

La qualité de cette microforme dépend grandement de la qualité de la thèse soumise au microfilmage. Nous avons tout fait pour assurer une qualité supérieure de reproduction.

S'il manque des pages, veuillez communiquer avec l'université qui a conféré le grade.

La qualité d'impression de certaines pages peut laisser à désirer, surtout si les pages originales ont été dactylographiées à l'aide d'un ruban usé ou si l'université nous a fait parvenir une photocopie de qualité inférieure.

La reproduction, même partielle, de cette microforme est soumise à la Loi canadienne sur le droit d'auteur, SRC 1970, c. C-30, et ses amendements subséquents.

NL-339 (r. 88/04) c

Canada

THE UNIVERSITY OF ALBERTA

DETERMINATION OF TRACE ELEMENTS IN NATURAL WATERS BY INDUCTIVELY COUPLED PLASMA-MASS SPECTROMETRY

by

MOHAMED D. SANKOH

A THESIS

SUBMITTED TO THE FACULTY OF GRADUATE STUDIES AND RESEARCH IN PARTIAL FULFILLMENT OF THE REQUIREMENTS FOR THE DEGREE OF MASTER OF SCIENCE

DEPARTMENT OF CHEMISTRY

EDMONTON, ALBERTA

SPRING, 1989

Permission has been granted to the National Library of Canada to microfilm this thesis and to lend or sell copies of the film.

The author (copyright owner) has reserved other publication rights, and neither the thesis nor extensive extracts from it may be printed or otherwise reproduced without his/her written permission.

L'autorisation a été accordée à la Bibliothèque nationale du Canada de microfilmer cette thèse et de prêter ou de vendre des exemplaires du film.

L'auteur (titulaire du droit d'auteur) se réserve les autres droits de publication; ni la thèse ni de longs extraits de celle-ci ne doivent être imprimés ou autrement reproduits sans son autorisation écrite.

ISBN 0-315-52839-7

THE UNIVERSITY OF ALBERTA

RELEASE FORM

NAME OF AUTHOR: MOHAMED D. SANKOH

TITLE OF THESIS: DETERMINATION OF TRACE ELEMENTS IN NATURAL WATERS BY INDUCTIVELY COUPLED PLASMA-MASS SPECTROMETRY

DEGREE FOR WHICH THESIS WAS PRESENTED M.Sc

YEAR THIS DEGREE GRANTED 1989

Permission is hereby granted to the UNIVERSITY OF ALBERTA LIBRARY to produce single copies of this thesis and to lend or sell such copies for private, scholarly or scientific research purposes only.

The author reserves other publication rights, and neither the thesis nor extensive extracts from it may be printed or otherwise reproduced without the author's written permission.

(Signed) M. D. Sankoh

PERMANENT ADDRESS
21 Henry Street
Freetown
Sierra Leone

DATED Dec. 19th 1988.

THE UNIVERSITY OF ALBERTA

FACULTY OF GRADUATE STUDIES AND RESEARCH

The undersigned certify that they have read, and recommend to the Faculty of Graduate Studies and Research, for acceptance, a thesis entitled DETERMINATION OF TRACE ELEMENTS IN NATURAL WATERS BY INDUCTIVELY COUPLED PLASMA-MASS SPECTROMETRY by MOHAMED D. SANKOH in partial fulfillment of the requirement for the degree of Master of Science.

.....Gary Horlick.....
(Supervisor)

.....

.....Frederick J. Cantwell.....

.....

.....

Date ..1 Dec. 19th..... 19 88....

ABSTRACT

Inductively coupled plasma-mass spectrometry is a fairly new technique that is gaining popularity in trace element analysis.

The studies undertaken in this thesis delve into both the effect of plasma operating parameters on analyte signals in ICP-MS and the application of ICP-MS to trace element analysis in natural waters.

Utilizing the Sciex Elan Model 250 ICP-MS a study was done on the effects of plasma operating parameters (nebulizer flowrate, plasma rf power and sampling dep+h), on analyte signals. Data obtained were graphed in different formats and compared and optimum parameter values for trace element analysis were selected.

The effect of Na on matrix induced signal suppression and the use of an internal standard to reduce such signal suppression were investigated.

Finally, the ICP-MS was utilized for trace element analysis of natural water and the occurrence of isobaric interferences is illustrated. Accuracy of analytical results was verified by the utilization of more than one isotope when possible and by analysis with another techique: inductively coupled plasma atomic emission spectrometry (ICP-AES). Precision and detection limits of both techniques are reports.

ACKNOWLEDGEMENT

The Author wishes to extend his unreserved thanks and appreciation to his research group and especially to Dr. Youbin Shao, Margaret-Ann Vaughan and Joseph Lam who were of great assistant in operating the ICP-MS and for many valuable discussions.

The author would also like to extend his gratitude and love to his wife Fiona, for her encouragement and companionship.

Finally, the author is deeply indebted to Dr. Gary Horlick for his continuous support and leadership.

TABLE OF CONTENTS

CHAPTER			Page
I.	A.	Introduction	1
	B.	Summary of Analytical Techniques	5
		1. Colorimetry and Spectrometry	6
		2. Flame-Emission Spectrometry	7
		3. Atomic-absorption Spectrometry	7
		4. Atomic-fluorescence Spectrometry	10
		5. X-Ray Fluorescence Spectrometry	10
		6. Activation Analysis	12
		7. Other Measurement Techniques	13
	C.	The ICP as a Spectrochemical Source	16
	D.	Inductively Coupled Plasma-Mass Spectrometry (ICP-MS)	20
II.	INSTRUMENTATION AND SAMPLES		24
	A.	ICP-MS	24
	B.	ICP-AES	26
	C.	Sample Description	26

III. COMPARISON OF DATA DISPLAY FORMAT FOR ICP-MS..... 31

A. Introduction..... 31

B. Signal vs. Nebulizer Flow Rate..... 31

1. Power family at different sampling depths..... 32

2. Sampling depth family at different powers..... 42

C. Signal v.s Sampling Depth..... 51

1. Power family at different Flow rates..... 51

2. Flowrate family at different powers..... 61

D. Conclusion..... 70

IV. DETERMINATION OF MAJOR ELEMENTS..... 72

A. Introduction..... 72

B. Semiquantitative Analysis by ICP-MS..... 72

C. Results and Discussion..... 73

D. Quantitative Determination of Major Elements by ICP-AES..... 79

E. Results & Discussion..... 81

V. DETERMINATION OF TRACE ELEMENTS..... 86

A. Introduction..... 86

B. Na Matrix Effect and Internal Standardization.. 87

1. Experimental..... 87

2. Results & Discussion..... 87

C. ICP-MS and ICP-AES Quantitative Analysis..... 98

1. Standard Preparation..... 98

2. Experimental..... 99

3. Results and Discussion..... 103

D. Spectral Interference Assessment in ICP-MS..... 122

VI. CONCLUSIONS..... 137

BIBLIOGRAPHY..... 140

LIST OF TABLES

Table	Description	Page
I	Degree of ionization of elements in an argon ICP	19
II	Specifications for the ARL34000 ICP spectrometer	27
III	Elements and their wavelengths and detection limits on the ARL 34000 ICP spectrometer	28
IV	ICP-MS semiquantitative analysis data acquisition and experimental parameters	74
V	Major elements semiquantative analysis results for WW39-WW66	75
VI	Isobaric interfering species associated with S	77
VII	Isobaric interfering species associated with Ca, Mg, Fe, Na and Al	78
VIII	Calibration scheme for ICP-AES: major element analysis	80
IX	Major element analysis report; WW27-WW52	83
X	Major element analysis report; WW53-WW76	84
XI	Data acquisition and instrumental parameters for ICP-MS optimization studies	88
XII	Calibration scheme for ICP-MS trace element analysis	100
XIII	Data acquisition and instrumental parameters for ICP-MS trace element analysis	101
XIV	Data acquisition and instrumental parameters for ICP-AES trace element analysis	102
XV	Slopes of ICP-MS and ICP-AES log-log calibration curves	107
XVI	ICP-MS and ICP-AES trace element analysis report for Sr and Ba in WW27-WW52	109
XVII	ICP-MS and ICP-AES trace element analysis report for Sr and Ba in WW53-WW77	110

XVIII	ICP-MS and ICP-AES trace element analysis report for Ni, Cu, V and Co in WW27-WW52	111
XIX	ICP-MS and ICP-AES trace element analysis report for Ni, Cu, V and Co in WW27-WW52	112
XX	ICP-MS and ICP-AES trace element analysis report for Li, Zn, and U in WW27-WW52	113
XXI	ICP-MS and ICP-AES trace element analysis report for Li, Zn, and U in WW53-WW77	114
XXII	Precision comparison of ICP-MS and ICP-AES results for Li in WW27-WW52	123
XXIII	Precision comparison of ICP-MS and ICP-AES results for Li in WW53-WW77	124
XXIV	Precision comparison of ICP-MS and ICP-AES results for Zn in WW27-WW52	125
XXV	Precision comparison of ICP-MS and ICP-AES results for Zn in WW53-WW77	126
XXVI	ICP-MS and ICP-AES detection limits	127
XXVII	Isobaric interfering species associated with Cl	136
XXVIII	ICP-MS semiquantitative and quantitative trace analysis results comparison	138

LIST OF FIGURES

Figure	Description	Page
1.	Main features of the ICP discharge.	16
2.	Schematic diagram of the Sciex Elan Model 250 ICP-MS system.	21
3.	Schematic diagram of mass filter and lenses.	25
4.	Periodic chart showing only the elements available on the ARL 34000 ICP spectrometer.	29
5.	Nebulizer flowrate-power parameter plots for Ba at sampoing depths of 10,15,20 and 25 mm from the load coil.	33
6.	Nebulizer flowrate-power parameter plots for Cd at sampling depths of 10,15,20 and 25mm from the load coil	34
7.	Nebulizer flowrate-power parameter plots for La at sampling depths of 10,15,20 and 25 mm from the load coil.	35
8.	Nebulizer flowrate-power parameter plots for Sr at sampling depths of 10,15,20 and 25 mm form the load coil.	36
9.	Nebulizer flowrate-power parameter plots for Y at sampling depths of 10,15,20 and 25 mm from the load coil.	37
10.	Nebulizer flowrate-power parameter plots for Zn at sampling depths of 10,15,20 and 25mm from the load coil.	38
11.	Nebulizer flowrate-power parameter plots for Ba^{2+} at sampling depths of 10,15,20 and 25mm from the load coil.	39
12.	Nebulizer flowrate-power parameter plots for La^{2+} at sampling depths of 10,15,20 and 25mm from the load coil.	40
13.	Nebulizer flowrate-depth parameter plots for Ba at plasma rf poer of 0.09, 1.1, 1.3 and 1.5kW.	43

14. Nebulizer flowrate–depth parameter plots for Cd at plasma rf powers of 0.9, 1.1, 1.3 and 1.5kW. 44

15. Nebulizer flowrate–depth parameter plots for La at plasma rf powers of 0.9, 1.1, 1.3 and 1.5kW. 45

16. Nebulizer flowrate–depth parameter plots for Sr at plasma rf powers of 0.9, 1.1, 1.3 and 1.5kW. 46

17. Nebulizer flowrate–depth parameter plots for Y at plasma rf powers of 0.9, 1.1, 1.3 and 1.5kW. 47

18. Nebulizer flowrate–depth parameter plots for Zn at plasma rf powers of 0.9, 1.1, 1.3 and 1.5kW. 48

19. Nebulizer flowrate–depth parameter plots for Ba^{2+} at plasma rf powers of 0.9, 1.1, 1.3 and 1.5kW. 49

20. Nebulizer flowrate–depth parameter plots for La^{2+} at plasma rf powers of 0.9, 1.1, 1.3 and 1.5kW. 50

21. Sampling depth-power parameter plots for Ba at nebulizer flowrates of 0.7, 0.8, 0.9 and 1.0 and 1.1 ℓ/min. 52

22. Sampling depth-power parameter plots for Cd at nebulizer flowrates of 0.7, 0.8, 0., 1.0 and 1.1 ℓ/min. 53

23. Sampling depth-power parameter plots for La at nebulizer flowrates of 0.7, 0.8, .09, 1.0 and 1.1 ℓ/min. 54

24. Sampling depth-power parameter plots for Sr at nebulizer flowrates of 0.7, 0.8, 0.9, 1.0 and 1.1 ℓ/min. 55

25. Sampling depth-power parameter plots for Y at nebulizer flowrates of 0.7, 0.8, 0.9, 1.0 and 1.1 ℓ/min. 56

26. Sampling depth-power parameter plots for Zn at nebulizer flowrates of 0.7, 0.8, 0.9, 1.0 and 1.1 ℓ/min. 57

27. Sampling depth-power parameter plots for Ba^{2+} at nebulizer flowrates of 0.7, 0.8, 0.9, 1.0 and 1.1 ℓ/min 58

28. Sampling depth-power parameter plots for La^{2+} at nebulizer flowrates of 0.7, 0.8, 0.9, 1.0 and 1.1 ℓ/min 59

29. Sampling depth-nebulizer Flowrate parameter plots for Ba at plasma rf powers of 0.9, 1.1, 1.3 and 1.5kW; nebulizer flowrate in ℓ/min shown on each line 62

30. Sampling depth-nebulizer flowrate parameter plots for Cd at plasma rf powers of 0.9, 1.1, 1.3 and 1.5kW; nebulizer flowrate in ℓ/min shown on each line 63

31. Sampling depth-nebulizer flowrate parameter plots for La at plasma rf powers of 0.9, 1.1, 1.3 and 1.5kW; nebulizer flowrate in ℓ/min shown on each line 64

32. Sampling depth-nebulizer flowrate parameter plots for Sr at plasma rf powers of 0.9, 1.1, 1.3 and 1.5kW; nebulizer flowrate in ℓ/min shown on each line 65

33. Sampling depth-nebulizer flowrate parameter plots for Y at plasma rf powers of 0.9, 1.1, 1.3 and 1.5kW; nebulizer flowrate in ℓ/min shown on each line 66

34. Sampling depth-nebulizer flowrate parameter plots for Zn at plasma rf powers of 0.9, 1.1, 1.3 and 1.5kW; nebulizer flowrate in ℓ/min shown on each line 67

35. Sampling depth-nebulizer flowrate parameter plots for Ba^{2+} at plasma rf powers of 0.9, 1.1, 1.3 and 1.5kW; nebulizer flowrate in ℓ/min shown on each line 68

36. Sampling depth-nebulizer flowrate parameter plots for La^{2+} at plasma rf powers of 0.9, 1.1, 1.3 and 1.5kW; nebulizer flowrate in ℓ/min shown on each line 69

37. ICP-AES calibration curves for S, Ca, Na, Mg, B and Fe 82

38. Effects of varying nebulizer flowrate and Na concentration on the Co signal. 89

39. Effects of varying nebulizer flowrate and Na concentration on the Cu signal. 90

40. Effects of varying nebulizer flowrate and Na concentration on the Li signal. 91

41. Effects of varying nebulizer flowrate and Na concentration on the Ni signal. 92

42. Effects of varying nebulizer flowrate and Na concentration on the Sr signal. 93

43. Effects of varying nebulizer flowrate and Na concentration on the U signal. 94

44. Effects of varying nebulizer flowrate and Na concentration on the V signal. 95

45. Effects of varying nebulizer flowrate and Na concentration on the Zn signal. 96

46. ICP-MS calibration curves for ^{136}Ba, ^{137}Ba, ^{138}Ba, ^{88}Sr, ^{86}Sr, ^{52}V, Co, ^{235}U 104

47. ICP-MS calibration curves for ^{6}Li, ^{7}Li, ^{66}Zn ^{67}Zn 105

48. ICP-AES calibration curves for Ba, Cu, Li, Ni, V and Zn 106

49. Column plots of ICP-MS concentration results of ^{137}Ba and ^{138}Ba 115

50. Column plots of ICP-MS concentration results of ^{86}Sr and ^{88}Sr 116

51. Column plots of ICP-MS concentration results of ^{66}Zn and ^{67}Zn 117

52. Column plots of ICP-MS and ICP-AES concentration results of Ba 119

53. Column plots of ICP-MS and ICP-AES concentration results of Li 120

54. Column plots of ICP-MS and ICP-AES concentration results of Zn 121

55. Column plots of ^{60}Ni and Ca 129

56. Column plots of ^{62}Ni and Na 130

57. Column plots of ^{62}Ni and Ca 131

58. Column plots of ^{63}Cu and Na 132

59. Line plots of ^{65}Cu and S 134

60. Column plots of ^{65}Cu-^{63}Cu and S 135

CHAPTER I

Determination of Trace Elements in Natural Waters

A. Introduction

An abundant supply of water is one of the most important factors in the development of modern societies. The convenience of water available in the home improves the quality of life. Inexpensive water allows individuals and communities to beautify their surroundings and to use water as a carrier for household wastes. A modern society depends upon an available supply of clean water. Ground water provides about half the drinking water in the U.S. and is extensively used in industry and agriculture. The natural quality and quantity of ground-water varies and instances of ground water contamination have been found in most countries. The contamination of ground-water may result from all aspects of human activities; agriculture, industry, transportation, domestic wastes and resource exploitation.

The contaminants found in ground-water vary from simple inorganic ions to complex synthetic organic chemicals. Inorganic species enter natural water from a variety of sources. The weathering of rocks and soils directly exposed to surface water is usually the largest natural source. Atmospheric fallout of particulate matter from natural sources as well as from anthropogenic inputs, which include the combination of fossil fuels and material processing, can introduce relatively large quantities of inorganic species into natural water systems. Other inputs such as the discharging of various treated and

untreated liquid wastes to the receiving waters or the contaminations of the aquatic system through construction, mining, lumbering, or similar activities, can introduce large quantities of inorganic constituents into natural water. The origin and nature of major inorganic species are described in great detail in most water-chemistry textbooks [1-3].

At a first glance, the analysis of water would seem to be the simplest of all analytical tasks. While this may be correct for distilled water solutions containing an easily detectable amount of a single inorganic salt, it is far from the truth for natural waters. The latter contain living as well as nonliving, organic together with inorganic, and dissolved as well as insoluble substances. Problems can occur during or after sampling which may change the sample composition drastically from its true form. This may be caused by a variety of problems including contamination and loss of a substance due to precipitation, complexation, absorption or ion-exchange on a container wall.

Another problem is that natural waters vary greatly in matrix constituents. Samples range from precipitation, rivers and lakes which are low in impurities, to highly polluted effluents. A single analytical method will not necessarily be applicable to such a wide range of compositions.

Sampling is another major problem which is generally given little attention, hence it is common for it to be the largest source of error in the final result. Natural water can be very heterogeneous

vertically, horizontally, and with time. This is due not only to man-made pollution, but also can be caused by natural phenomena such as erosion, currents, thermodines, and precipitation washout of dust. No agreement can be found in the literature on sampling methods. However, in designing a sampling strategy, the objective of the work must be borne in mind together with the problems associated with any sampling method under consideration.

Contamination of samples is an ever-present danger in water analysis. Thiers [4] classifies the problem as follows:

i. Positive contamination results from the addition of contaminants to the sample.

ii. Negative contamination occurs when losses of the substance in question (analyte) occur.

iii. Pseudo-Contamination is an error introduced by the presence of a substance other than the analyte (i.e. a matrix effect).

Positive and negative contamination pose the most serious problems. Causes of positive contamination are many and generally obvious. Negative contamination can be caused by precipitation, adsorption, or ion exchange on the surface of containers. Particulate matter, if present, may also adsorb analyte species.

Storage containers to be used will depend on the parameters being measured. In some cases the constraints can be very severe e.g. determination of heavy metals. In others e.g. determination of major ions, almost any clean leak-proof container will suffice. Plastic

bottles have almost entirely superceded glass for the storage of waters for inorganic analysis. Compared to borosilicate glass most plastic bottles are inexpensive, less fragile and have minimal problems due to ion exchange. On the negative side most plastics have a porosity which allows samples to evaporate slightly over long storage periods.

Positive and pseudo contamination can result from contaminated plastic bottles hence cleaning is essential. Metallic impurities, present as a result of the fabrication process or past usages can cause serious positive contamination in trace metal analysis. Additives used as stabilizers may leach out, causing negative or pseudo-contamination problems. At the very least, most inorganic analysis applications require that the container be washed with detergent, rinsed thoroughly with tap and finally distilled and the sampled water. In trace analysis and when heavy metals are to be analyzed, an acid soaking following the detergent-wash is essential.

To prevent adverse changes to the samples during storage, it may be necessary to add a preservative to all samples. Such a procedure is generally recommended for trace metal analysis where the sample should be acidified [11].

It is very important in trace metal analysis to use reagents of high purity. Analytical reagents will suffice in most cases but when working at very low concentrations it may be necessary to use specially purified material. A blank must be run with any trace analysis. The magnitude of the blank will control the detection limit

which can be obtained.

Great care is essential in the preparation of standards, and water used for dilutions and standard preparation should be of high quality.

Since good precision does not necessarily signify that an accurate result has been obtained, the possibility of the latter should be maximized by testing natural and or synthetic reference samples on a routine basis during analysis.

B. Summary of Analytical Techniques

Methods for analyzing water are reviewed biennially in odd-numbered years in 'Analytical Chemistry' [5]. These reviews are very comprehensive, and no attempt has therefore, been made to give an exhaustive coverage of the literature. Some reviews on the subject include books by Mancy [6] and Ciaccio [7-10]. The latter is particularily comprehensive, gives many references, and deals with the following measuring techniques: flame spectrometry (atomic emission, absorption, and fluorescence), emission spectroscopy, X-ray spectroscopy, activation analysis, determination of radionuclides, gas chromatography, mass spectometry, infra-red spectroscopy, luminescence analysis, electroanalysis. Other techniques are touched on, and in addition pre-concentration and separation techniques are discussed in great detail. Minear and Keith [11] also edited an excellent book which deals with the use of plasma excitation sources in water analysis as well as many of the other techniques listed above. A

brief review of some of these techniques follows.

1. Colorimetry and Spectrophotometry

Several different colormetric and spectrophotometric procedures are available [12] but only two are widely used for analyzing water. When the analyte is coloured in solution, analysis is done by visual comparison of the sample solution with standard solutions. In spectrophotometry, photoelectric measurement of the degree of absorption for a selected wavelength band is done. If the determinant is weakly absorbing, chemical pretreatment may be required so as to obtain a strongly-absorbing substance.

Yan et al [13] reported a detection limit of 4.5 ppb for the determination of phenol in natural waters. Phenols were extracted with butyl acetate and determined spectrophotometrically. They used three different wavelengths to eliminate natural water background interference.

Rathmore et al [14] reported a method for determining citric acid in river water using spectrophotometry. The method is based on the red colour developed upon treating the acid with acetic anhydride at 65^{o}C in the presence of sodium acetate and phenyl acetate.

Due to the simplicity of colorimetry, and because equipment is inexpensive and less liable to failure, it is used widely under field conditions. It requires less analytical skill and experience and is very rapid when permanent comparison standards can be used. However, the lengthy chemical treatment of samples that may be required is a big disadvantage. It also tends to give poor accuracy and precision

compared with spectrophotometry.

2. Flame-Emission Spectrometry

Flame emission spectometry has also been used in water analysis. A variety of factors affect the analytical performance of flame-emission spectrometers including instrumental and experimental parameters. A good description of these are given by Mavrodineau [15] and by Dean and Rains [16, 17]. Compared with the newer plasma spectrochemical excitation sources, flames are very complex and several different types of interferences [17] occur in flame spectrometry. Their relatively lower temperature also results in poor detection limits and sensitivity for most elements. The technique is now mainly used only for the determination of the alkali metals (Na, K, Li, Rb, Cs).

3. Atomic Absorption Spectrometry

This is the method of choice for water analysis and standard procedure for analysis are described in the ASTM manual on Water Analysis [18].

Flame atomic absorption is closely related to flame emission, and its principle advantages stem from its simplicity and ability to determine many elements. As with flame emission, good precision is usually easily and rapidly achieved except when concentrations close to the detection limit are present. Relative standard deviations of 1% and less are often reported.

Interferences do occur in flame AAS but they are often not a big problem in water analysis. Simple means of overcoming most effects

are available, eg. the addition of 'releasing' reagents to the sample.

Application of flame atomic absorption spectrometry to water analysis has developed very rapidly. Lead and calcium were determined in organic — and silica-rich sediments by Hsu and Locke [19]. They used both an open beaker and bomb procedure to digest the samples with nitric, perchloric and hydrochloric acids. Flame atomic absorption spectrometry was used to measure the concentrations in the digestates. Sukhareva, Zolotareva, and Ryzhak [20] determined calcium, magnesium and iron in natural water and waste water with an air-acetylene flame atomic absorption procedure. Methanol was added to the samples to enhance sensitivity. Detection limits were determined to be 1, 0.05 and 0.2 µg/L for calcium, magnesium and iron, respectively. Lead and Zinc in seawater were effectively extracted into carbon tetrachloride with added octanoic acid. A detection limit of 0.1 µg/L was achieved by this method.

Other AAS techniques like graphite-furnace atomic absorption spectrometry and electrothermal vaporization atomic absorption spectrometry (ETV-AAS) have superior sensitivity to flame-AAS and have been used in water analysis. In ETV-AAS, a small amount of a sample is resistively heated in a container by the passage of an electric current. Most systems allow for a number of heating steps and the rate of heating, time and temperature can be programmed so as to select an optimum sequence for drying, heating and vaporization of the sample components on the vaporizer surface. Sample volumes are typically from 5 to 100µℓ and almost all the sample is converted to

an atomic vapour.

This efficient sample utilization accounts for the extreme sensitivity of the technique. Detection limits are typically 10 to 100 times better than those obtained using solution nebulization flame -AAS and rivals the detection limits in anodic stripping and pulse polarographic techniques. The technique, however, has inferior precision when compared with solution nebulization flame-AAS techniques and matrix effects are complex and background correction can be a serious problem.

Io et al [21] described a method utilizing a solvent extraction of dithio carbamate complexes into chloroform followed by back extraction with a dilute Mercury [II] solution. Several elements were simultaneously preconcentrated from seawater by this technique including calcium, cobalt, copper, iron, maganese, nickel, lead and zinc. Graphite-furnace AAS was used to make the final analysis. Sperling and Bahr [22] reported the determination of heavy metals in sea water and marine organisms by atomic absorption spectrometry. They used electrothermal atomizatien and reported poor precision and accuracy due to variations in graphite quality. This imprecision was minimized by the addition of an acid matrix modifier to the final analysis digest.

4. Atomic Fluorescence Spectrometry

Atomic-fluorescence spectrometry is closely related to atomic-emission and absorption spectrometry. However, at present few applications to water analysis have been described. This may be due to the fact that the technique has not yet been commercialized and is mainly confined within academic institutions. However, it is more sensitive than flame-AAS.

Olivo et al [23] used atomic fluorescence for the determination of arsenic and other elements in water. $NaBH_4$ was used as a reductant and a H_2-air mini-flame was used for atomization. A detection limit of 0.04 µg/L was reported for arsenic. Tao et al [24] used atomic fluorescence in the determination of arsenic in water. Hydride generation was employed. Han and Wang [25] also determined arsenic by atomic fluorescence after reduction to the hydride by KBH_4.

5. X-Ray Fluorescence Spectrometry

In X-Ray fluorescence spectrometry, the sample is irradiated with a beam of X-rays which are absorbed by the constituent atoms of the sample. The atoms so excited then emit fluorescence X-rays at wavelengths (energies) characteristic of the elements present. These fluorescent rays are separated into their constituent wavelengths by the dispersive system and the intensity at each wavelength - which is dependent on the concentration of the corresponding element — is measured in the detector system. Scanning the spectrum of fluorescent radiation indicates which elements are present and calibration of the system with known amounts of elements allows quantitative analysis.

Elements of atomic number greater than 9 can be determined often with relative standard deviations of 1-5% provided concentrations are not too close to the limits of detection. Elements of low atomic number (less than 9) can be determined but special techniques are required. The time required to determine one element when the sample has been placed in the instrument is often of the order of 1 minute, though times of 10 minutes have been used to improve precision and sensitivity in water analysis. One of the main problems of the technique is that the results obtained can be markedly affected (positively and negatively) by other elements present in the sample.

In water analysis there is usually the need to achieve high sensitivity for trace elements, and problems may also arise when solutions are analyzed directly. Accordingly recent methods have all adopted some pre-treatment of the sample so that the trace elements are concentrated and then presented to the instrument in a solid form. With these concentration procedures limits of detection between 0.1 and 1μg/ℓ have been reported [26]. Clechet and Eschalier [27] reported determining traces of Mercury and Barium in water by selective retention on ion-exchange paper and X-ray fluorescence spectrometry. Ellis et al [28, 29] studied seven methods for the preconcentration of chromium, maganese, iron, cobalt, nickel, copper, zinc, arsenic, selenium, silver, cadmium, antimony, mercury, thallium, and lead from water prior to energy or wavelength-dispersive X-ray fluorescence spectrometry. The final step of each pre-concentration required the formation of a solid residue which could be introduced

directly into the spectrometer.

6. Activation Analysis

The general principle of this technique is to irradiate the sample with energetic particles (eg. neutrons, protons) or radiation (eg. gamma-rays) which by interaction with the atoms in the sample, lead to formation of radionuclides. The nature and amount of the radionuclides formed is indicative of the elements and their concentrations present in the original sample.

In application to water analysis neutron activation of water samples leads to the formation of many different radionuclides so that either chemical separation is needed before or after irradiation or instrumental methods (eg. gamma-ray spectrometry) of resolving the emitted radiation is necessary. The latter approach is being increasingly used because of its speed but is applicable only to gamma-emitters.

Imai et al [30] reported the use of dithiocarboxy-piperazinyl cellulose ammonium salt to preconcentrate trace elements prior to neutron activation analysis. Ten litres of water was passed through a column packed with the cellulose salt at a given pH. The packing was then ashed in a low-temperature plasma asher, and the resulting ash was encapsulated in polyethylene and subjected to neutron activation. Gamma-spectrometry was then performed to determine 19 elements. Procedures were described by Greenberg and Kingston [31] to preconcentrate trace elements with a chelating resin and subsequent analysis by neutron activation analysis. This technique essentially

removes all alkali, alkaline-earth metals, and halogens from the sample.

Detection limits obtained in NAA are inversely proportional to the neutron flux, and for fluxes of approximately 10^{12} neutrons $cm^{-2}s^{-1}$ many elements can be determined with limits of detection in the range 0.1-100 ng. Such neutron fluxes are achieved only in nuclear reactors and this represents a disadvantage of the technique since few water laboratories have direct access to a suitable reactor.

7. Other Measurement Techniques

Several other techniques have been used in analyzing water. Brihaye and Duyckaerts [32] used a rotating glassy-carbon ring-disk electrode to determine calcium, lead, copper, antimony, and bismuth in seawater by both linear sweep and differential-pulse anodic stripping voltammetry. Concentrations were determined in the ng/L range. Andruzzi, Trazza, and Marrosu [33] compared the performance of the sessile drop mercury electrode to the conventional hanging mercury drop electrode in the direct determination of trace metals by differential-pulse anodic stripping voltammetry. Their studies showed that in seawater, the sessile-drop electrode offered better stability, reproducibility and detection limits (50ng/L) than other electrodes.

Hu, Dessy, and Graneli [34] described a potentiometric stripping analysis procedure for the determination of heavy metals in groundwater. Flow injection techniques provided a convenient automated method for the determination of copper, calcium, and lead. Drabaek, Madsen and Soerensen [35] described the analysis of Seawater

by potentiometric stripping analysis. They determined lead, cadmium, and zinc with a precision of 5-16% relative standard deviation, depending upon the concentration level. The accuracy of the method was evaluated by comparison with other techniques.

Excellent sensitivities and detection limits can be obtained with mass spectrometric and plasma spectrometric techniques. Foss, Svec and Conzemius [36] determined trace elements in an aqueous medium without preconcentration using a cryogenic hollow cathode ion source on a mass spectrometer. A glow discharge in a hollow cathode containing 20-50 µl of aqueous sample held at liquid nitrogen temperatures was used as a source of ions in a double-focusing mass spectrometer. Fluorine, phosphorus, sulfur, selenium, manganese, nickel, and tantalum could not be determined because of interferences. All other elements were determined at detection limits ranging from sub-ng/mL to µg/mL levels. Shelpakova et al [37] reported a method for the analysis of high purity water. It consisted of the preconcentration of impurities by evaporation on a thin layer silicon substrate, followed by ionization by a high-frequency spark. The ions were then measured with a mass spectrometer. The detection limits for 60 elements were reported to range from 10^{-9} to 10^{-12}% with a relative standard deviation of 0.17 to 0.36.

Among the several different plasma spectrochemical techniques that have been used for water analysis are: radio frequency inductively coupled plasma atomic emission spectrometry (ICP-AES) and plasma jet direct direct current arc (DC Plasma) spectrometry.

Blackmore, Casey and Collins [38] described an electrothermal carbon atomizer for the simultaneous determination of 10 elements in wastewater by inductively coupled plasma atomic emission spectrometry. Buchanan and Hannaker [39] determined minor elements in concentrated brines using inductively coupled plasma spectrometry. Magnesium present in the brine solution was used as a carrier by adjusting the pH of the sample to 8.0-9.0 with sodium hydroxide. The resulting precipitate was redissolved and analyzed for 14 cation and 3 anion species. Urasa [40] determined arsenic, boron, carbon, phosphorus, selenium, and silicon in natural waters by a direct-current plasma atomic emission technique. He evaluated the method in terms of the detection limits, sensitivity, linear dynamic range, precision, interference effects, matrix effects and element selectivity. He found that in most cases the detection limits and sensitivities were equal to or better than those achieved with other techniques.

C. The Inductively Coupled Plasma (ICP) as a Spectrochemical Source

The operating principles and characteristics of the ICP have been studied in detail by Fassel et al [41, 42]. The main features of the ICP discharge are shown in Figure 1. The torch consists of three concentric quartz tubes and their argon gas flows as shown. Surrounding the top of the torch is a 3-4 turn induction coil to which radio frequency (rf) power is applied (27MHz, 1-3kW). To ignite the plasma, the argon gas is made electrically conductive by partial ionization with a tesla coil and then coupled with the time varying magnetic field produced by the induction coil. The electrons and ions

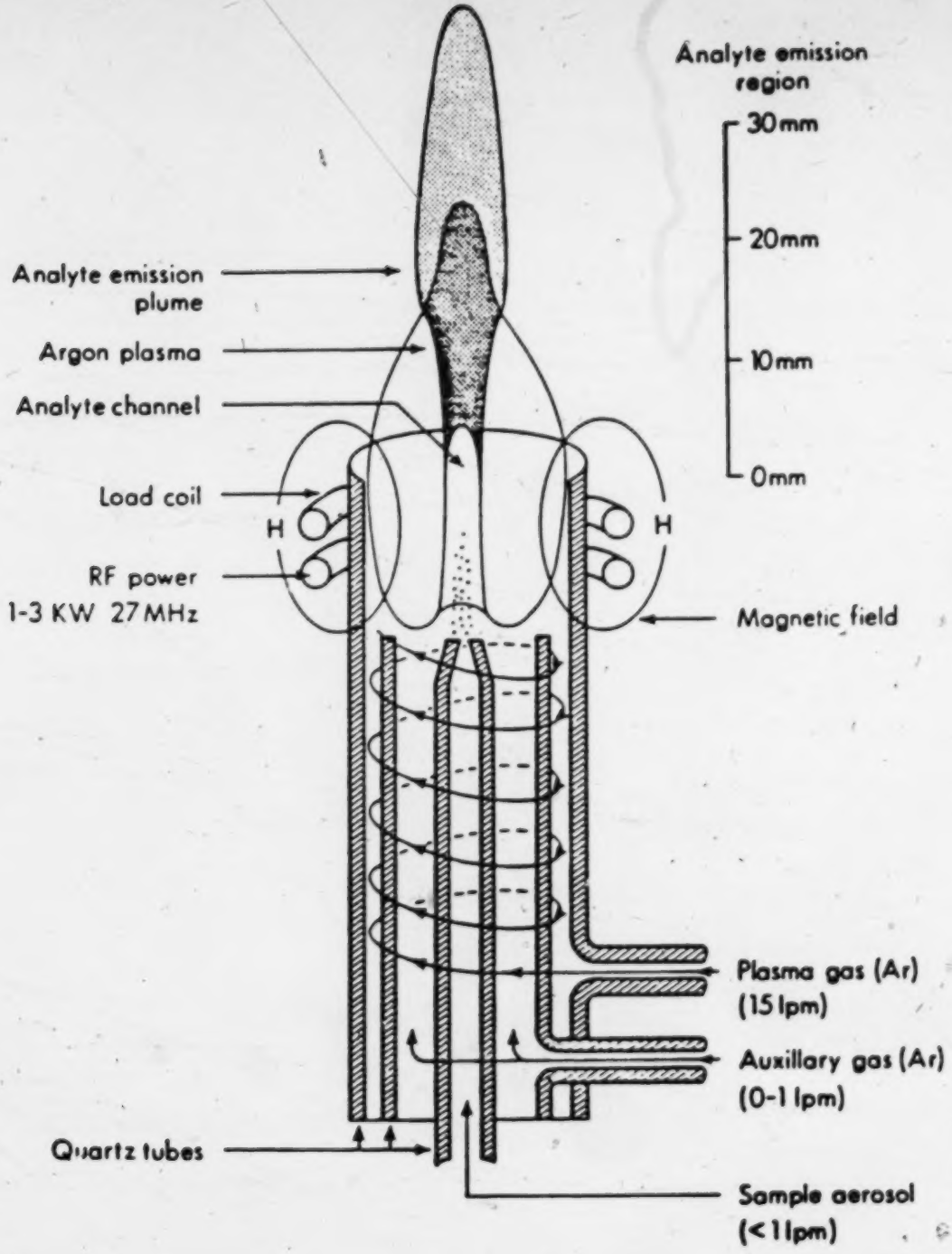

Figure 1. Main features of the ICP discharge.

produced are accelerated in this field to high enough energies to ionize neutral argon atoms, creating an "avalanche" of electrons. The accelerated charged particles also experience resistance to their motion due to collisional processes. This results in an ohmic heating effect, which in turn causes additional ionization.

The characteristics of the plasma are: high temperature, chemical inertness and optical thinness. These features account for its favorable analytical performance as a spectrochemical emission source when compared with other sources like flames, arcs or sparks. The matrix interference effects are comparatively low, solute vaporization interference is negligible, detection limits are low, sensitivity high and the linear dynamic range is wide; about five to six orders of magnitude.

The high temperature and chemical inertness of the ICP makes it an excellent ion source. In the sample solution uptake process the solution is first nebulized and converted to fine aerosol droplets by the spray chamber and then transported to the plasma. The sample takes about (2-3 ms) to travel through the plasma. During this period, the aerosol droplets are desolvated, vaporized, atomized, ionized and excited.

The degree of ionization , is defined as follows.

$$\alpha = \frac{n_i}{n_i + n_a} = \frac{n_i n_e / n_a}{(n_i n_e / n_a) + n_e} = \frac{K_m}{K_m + n_e} \qquad (1)$$

where n_a = number density of atoms

n_i = number density of ions

n_e = electron number density

k_m = Saha Equilibrium Constant

The Saha equilibrium constant is dependent on the ionization temperature T_{ion} and is expressed as [37]:

$$K_m = \frac{n_i n_e}{n_a} = 4.83 \times 10^{15} T_{ion}^{3/2} \frac{Z_i}{Z_a} \exp\left(-\frac{V_i}{kT_{ion}}\right),$$

where Z_a = Partition function of the atom

Z_i = Partition function of the ion

V_i = Ionization potential

K = Boltzman Constant

The degree of ionization α can be calculated if T_{ion} and N_e are known. The data presented in Table I were calculated using n_e = $1.475 \times 10^{14} Cm^{-3}$, T_{ion} (Ar) = 6680 K and assuming local thermodynamic equilibrium [43, 44].

It can be seen that the degree of ionization for an element with an ionization potential of less than 8eV is close to 100%, confirming that the ICP is a good source of elemental ions.

Several excellent reviews and books [45-47] dealing with the analytical applications of ICP have been published. In principal, any element other than the constituents of the plasma gas, can be determined by ICP-emission spectrometry, and in practice, all but a few can be determined by commercially available equipment.

D. Inductively Coupled Plasma-Mass Spectrometry (ICP-MS)

ICP-MS has developed into a significant, new technique for trace element analysis. It combines the advantages of the ICP mentioned in

Table I. Degree of ionization of elements in an argon ICP

Element	IP (eV)	Degree of Ionization	Element	IP (eV)	Degree of Ionization
Cs	3.894	99.98	Au	9.225	48.87
Rb	4.177	99.98	Be	9.322	75.36
K	4.341	99.97	Zn	9.394	74.50
Na	5.139	99.91	Se	9.754	30.53
Ba	5.212	99.96	As	9.81	48.87
Ra	5.279	99.95	S	10.360	11.47
Li	5.392	99.85	Hg	10.437	32.31
La	5.577	99.91	I	10.451	24.65
Sr	5.695	99.92	P	10.486	28.79
In	5.786	99.42	Rn	10.748	35.74
Al	5.986	98.92	Br	11.814	3.183
Ga	5.99	99.00	C	11.260	3.451
Tl	6.108	99.38	Xe	12.130	5.039
Ca	6.113	99.86	Cl	12.967	0.4558
Y	6.38	98.99	O	13.618	0.04245
Sc	6.54	99.71	Kr	13.999	0.2263
V	6.74	99.23	N	14.534	0.04186
Cr	6.766	98.89	Ar	15.759	0.01341
Ti	6.82	99.49	F	17.422	0.0001919
Zr	6.84	99.31	Ne	21.564	0.000005468
Nb	6.88	98.94	He	24.587	1.007E-11
Hf	7.0	98.89			
Mo	7.099	98.54			
Tc	7.28	97.50			
Bi	7.289	94.14			
Sn	7.344	96.72			
Ru	7.37	96.99			
Pb	7.416	97.93			
Mn	7.435	97.10			
Rh	7.46	95.87			
Ag	7.576	94.45			
Ni	7.635	92.55			
Mg	7.646	98.25			
Cu	7.726	91.59			
Co	7.86	94.83			
Fe	7.870	96.77			
Re	7.88	94.54			
Ta	7.89	96.04			
Ge	7.899	91.64			
W	7.98	94.86			
Si	8.151	87.90			
B	8.298	62.03			
Pb	8.34	94.21			
Sb	8.461	81.07			
Os	8.7	79.96			
Cd	8.993	85.43			
Pt	9.0	61.83			
Te	9.009	66.74			
Au	9.225	48.87			
Be	9.322	75.36			
Zn	9.394	74.50			
Se	9.754	30.53			
As	9.81	48.87			
S	10.360	11.47			
Hg	10.437	32.31			

the previous section with the high sensitivity inherent in mass spectrometry. Ions are sampled from the plasma by a cone called the sampling cone (See Figure 2). This cone has an orifice with a diameter of almost 1mm. A second cone, the skimmer, samples part of the ions from the sampler. The diameter of the skimmer orifice is the same as the sampler, but the former is more sharply tapered and is about 6mm behind the sampler. The region between the two cones is differentially pumped to a pressure of about 4 torr. The sampled ions are mass analyzed using a quadruple mass spectrometer.

Pioneering work in ICP-MS was conducted primarily in three laboratories: the Ames Laboratory at Iowa State University headed by Fassel [48-50], the Laboratory at Sciex [51] and the University of Surray (Gray), the British Geological Survey (Date) and VG instrument [52-55]. Houk [54] and Gray [55] published recent reviews on the technique.

Detection limits are in the range of 10 to 100 pg/ml for most elements, and for certain elements, detection limits approach 1 pg/ml (0.001 ppb). Compared with ICP-AES, these limits are 100 to 1000 times superior. Other advantages of the techniques are: simplicity of mass spectra obtained compared with the complexity of optical emission spectra, facile measurement of elemental isotope ratio which allows routine utilization of isotope ratio information and the isotope dilution technique to solve and study analytical problems, and the qualitative identification of elements from their natural abundance spectral pattern.

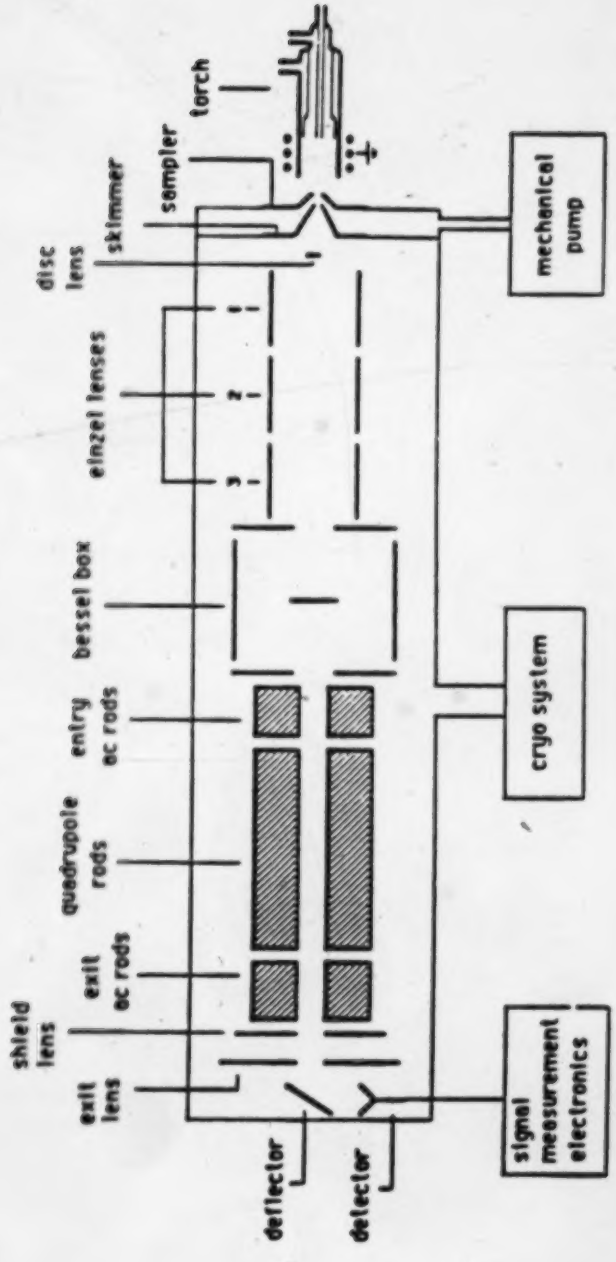

Figure 2. Schematic diagram of the Sciex Elan Model 250 ICP-MS system.

Complications do occur in ICP-MS due to molecular ions formed either in the ICP or in the ion extraction device. Studies have already been done to identify problems that may result from isobaric and oxide interference [58, 59], but very little has been done to illustrate these and other interferences in real sample analysis. It is one of the aims of these studies to illustrate interferences that can occur in water analysis using ICP-MS.

Experience gained from previous studies of the ICP-MS have shown that the areas to address during method development include: compromise instrument setting [59-62], spectral interferences [58, 60, 62], and matrix effects [60, 63-65]. In this study all these aspects of the technique will be covered with respect to the analysis of ground water. In the next chapter a detailed study of the effect of plasma operating parameters on the analyte signal is presented. Parameters studied include: nebulizer flow rate, rf power and sampling depth. The response of the signal is mapped out over a wide range of these variables. The results of this study allow the establishment of effective compromise instrument settings. Then ICP-MS is applied to the determination of trace elements in ground water. Matrix effects are assessed and semi-quantitative analysis is carried out. Since matrix effects originate mostly from the major elements in the matrix, an analysis for major elements will be carried out so as to properly assess matrix interferences. An internal standard will also be selected so as to reduce matrix effects and improve precision. Finally to check the accuracy of the analytical results two

complimentary techniques can be used for the analysis. In this work, ICP-AES was used with ICP-MS.

CHAPTER II

Instrumentation and Samples

A. ICP-MS

All experiments were carried out on the Sciex Elan model 250 inductively coupled plasma mass spectrometer. A schematic diagram of the instrument is shown in Figure 2.

The solution to be analyzed is aspirated by a nebulizer through a spray chamber into the plasma. Argon is used as the nebulizing gas. A Meinhard nebulizer and a Scott type spray chamber were used in all experiments. The plasma torch was a standard torch. The torch is mounted on the impedance matching network box and the whole unit was built so that the torch could be moved both laterally and vertically for alignment with the sampling orifice.

Ions formed in the plasma are sampled into the housing of the quadruple mass spectrometer through a differentially pumped region. Once in the mass spectrometer, the ions are focused and collimated by the ion lenses and deflected according to their m/z ratio by the quadruple rods (mass filter). A detailed diagram of the mass filter and lenses is shown in Figure 3.

Ion detection is achieved with a Channel Electron Multiplier (CEM) which produces a pulse of current in response to each ion impact. The signal generated by the CEM is processed by the signal handling unit and then transmitted to a computer. The computer is an Intel 16-bit microprocessor with one flexible disk drive and a 10Mbyte hard disk

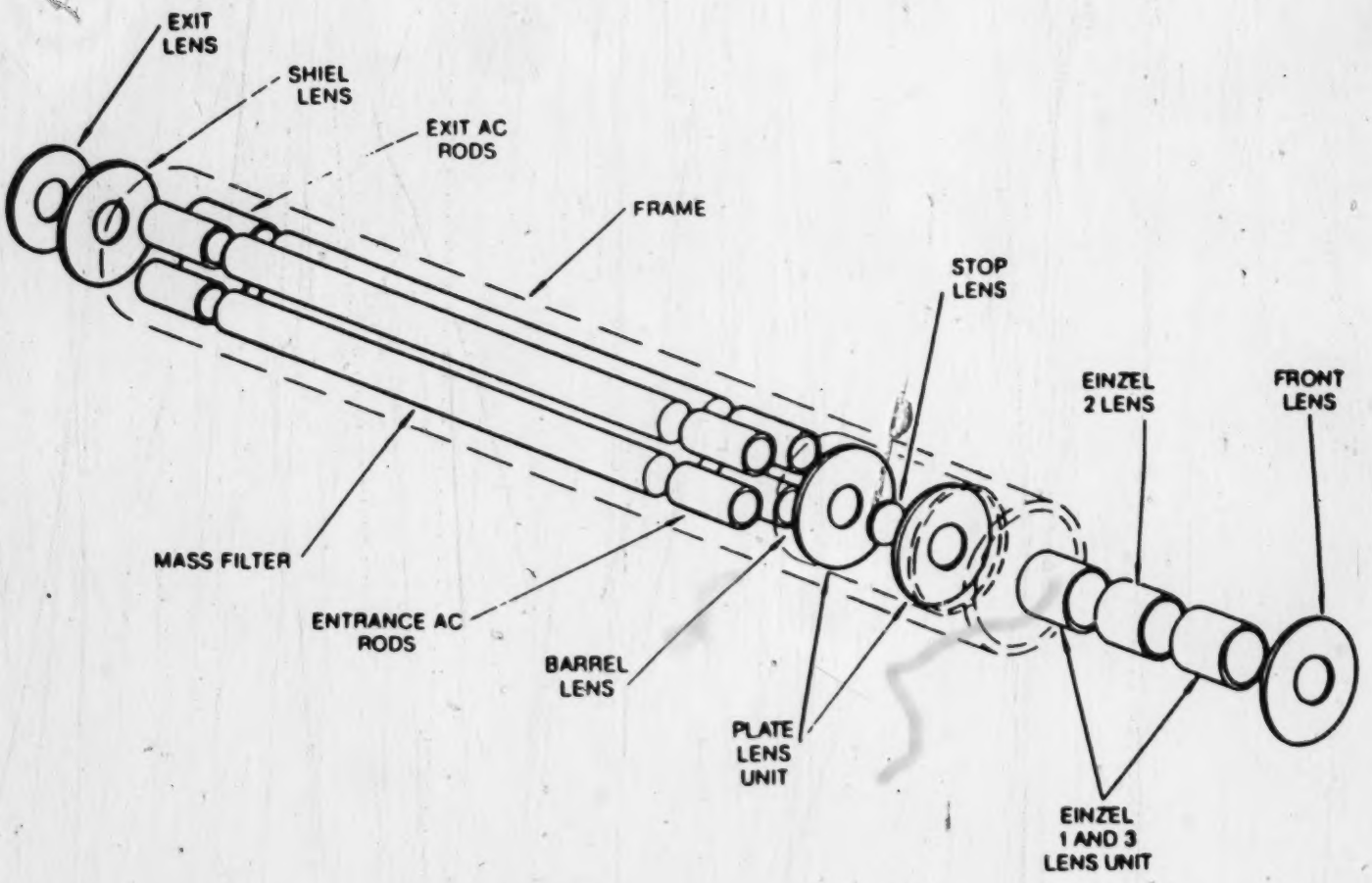

Figure 3. Schematic diagram of mass filter and lenses.

drive. This computer is in turn connected to a Macintosh computer. Raw data from the ICP-MS computer were collected with the Macintosh and were then edited, reformatted and plotted using commercially available programs like Excel, Cricket Graph and Statworks.

B. ICP-AES

All experiments for ICP-AES analysis were carried out on the Applied Research Labs (ARL) model 34000 ICP spectrometer. Details on the specification and operating conditions of this instrument are shown in Tables II & III. The instrument consists of an ICP excitation box, a 34 channel direct reading spectrometer and a PDP 11/03 DEC computer with 34K memory for data acquisition. Data acquisition and control of the instrument are computer controlled. The software used to run the computer is Applied Research labs extended basic (ARLEB). All data collected were printed on an LA36 DEC hardcopy printer terminal. The channels available on the instrument are shown on the periodic chart in Figure 4.

C. Sample Description

All 51 groundwater samples were obtained from the Geology Department of the University of Alberta. There was no information as to how the sampling was carried out but all samples were properly acidified and stored in plastic bottles to ensure stability. The colour of the solutions varied from colourless to light brown. Samples were labeled WW27 through WW77.

The elements of interest in the trace analysis were: Sr, Ba,

Table II. Specifications for the ARL 34000s ICP spectrometer

Instrumentation and Operating Conditions	
Inductively Coupled Plasma	
RF Generator	Air-cooled, 0-2.5 kW continuous rating, operating at 27.1 MHz, crystal controlled to within 2000 Hz, pre-set autotuned 1200 W output power with 0 W reflected power.
Induction coil	Silver plated 3 turn copper tube, water cooled.
Plasma torch	Quartz with three concentric tubes for coolant gas, plasma gas and aerosol gas.
Nebulizer/spray chamber	Permanently aligned coaxial pneumatic nebulizer with computer controlled tip desalting; Scott-type coaxial spray chamber with direct aerosol injection.
Gas flows	LGS system, argon coolant gas - 12 l/min plasma gas -0.8 l/min aerosol gas - 1 l/min All gas flows regulated by triple regulation pressure valves with additional restriction by capillary orifices for coolant and plasma gases.
Enclosure	Fully enclosed by Faraday cages and all interlocked system.
Viewing height	15 mm ± 1 mm, enclosure moving vertically on a 3-point mount and horizontally on a set of guides.
Spectrometer	
Mount	3 point cushioned mounting, 1.0 m Paschen-Runge, 3 section cast iron bolted vacuum spectrometer with argon purge to optics and plasma.
Optics	1080 grooves/mm interferometrically ruled quartz blank replica grating blazed at 600 nm. Range:175-800 nm. Entrance slit 20 µm; exit slits 50 µm; primary lens quartz. Photomultiplier tubes for signal detection, 1 inch diameter; cathode biasing maximum of -970 volts and referenced to -100 volt ground.
Acquisition	Simultaneous capacitively stored charges with sequential conversion by a PDP 11/03 DEC computer with 32K memory. Software system is Applied Research Labs extended basic (ARLEB). Data outputted to an LA36 DEC hardcopy printer terminal.

Table III —

Elements and their wavelengths and detection limits on the ARL 34000s ICP spectrometer

HARDWARE CONFIGURATION

SCANNING PRIMARY SLIT (SAMI)
RX02 DISK
SYSTEM SERIAL DEVICES

MAIN CONSOLE ONLY ON SYSTEM

IS THE CONFIGURATION O.K. (Y/N)? Y

(P)RINT,(M)ODIFY SYMBOL TABLE? <CR> TO PROCEED? P

CHANNEL NO.	ELEMENT	WAVELENGTH (NM)	ORDER	D.L. (PPM)
1	ZR	343.82	1	.00354
2	SR	407.78	1	.00029
3	BA	455.40	1	.00077
4	NI	231.60	2	.0071
5	AL	237.34	2	.07983
6	B	249.68	2	.00371
7	MN	257.61	2	.00179
8	FE	259.94	2	.00256
9	N	174.27	3	0
10	P	178.29	3	.0581
11	S	180.73	3	.02662
12	HG	184.95	3	.05356
13	MG	279.08	2	.01663
14	AS	189.04	3	.02153
15	SN	189.99	3	.00995
16	SI	288.16	2	.03377
17	C	193.09	3	0
18	V	292.40	2	.00348
19	NA	589.59	1	.0405
20	MO	202.03	3	.00756
21	CR	205.55	3	.00437
22	SB	206.83	3	.02727
23	GE	209.53	3	.05726
24	CA	317.93	2	.00731
25	ZN	213.86	3	.004
26	CU	324.75	2	.00854
27	AG	328.07	2	.00397
28	PB	220.35	2	.00535
29	LI	670.78	1	.00142
30	TI	337.28	3	.00097
31	CD1	226.50	3	.00298
32	CD2	228.80	3	.00424
33	IN	230.61	3	.05473
34	K	766.49	1	.09404

DETECTION LIMIT MULTIPLIER TO USE AS
LOWER ANALYTICAL LIMIT 5
INSTRUMENT GRATING NO. 1080
THIS IS A VACUUM SPECTROMETER

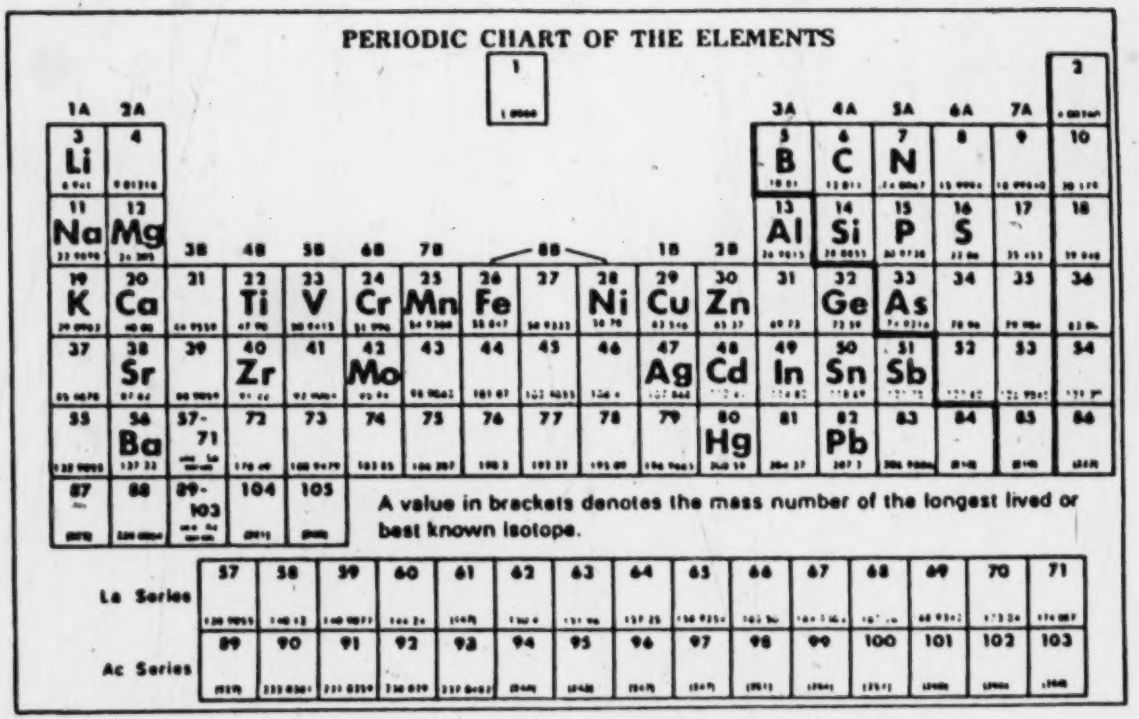

Figure 4. Periodic chart showing only the elements available on the ARL 34000S ICP spectrometer

V, Co, Cu, U, Ni, Li, and Zn. The samples also contain Na, S, Ca, Mg and Fe above the trace level and because of the ubiquitous occurrence of these elements in groundwater, they were thought to be likely major components in the samples.

CHAPTER III

Comparison of Data Display Formats for ICP-MS Parameter Studies

A. Introduction

A large number of variables affect the measured signal intensity in ICP-MS. A detailed list of these variables can be found in the paper of Horlick et al [61] In this section data on the effects of nebulizer flowrate, sampling depth and power on the measured signal intensity will be presented and a comparison of data display formats will be made. Our goal is to find the relationship between the various parameters studied and their effects on signal intensity and on one another, to select compromise conditions for ICP-MS analysis, to compare the different types of display formats as to their information content and to give possible explanations for signal variations observed.

A 0.1 ppm multielement stock solution of Cd, Zn, Y, Sr, La and Ba was used in the experiment, and data were collected after every 0.05 ℓ/min. increase in nebulizer flowrate.

B. Signal vs. Nebulizer Flow Rate

This plot format appears to be the most informative. The analyte ion-count is plotted vs. nebulizer flowrate and then on the same set of axes a family of such curves are plotted representing the ion-count nebulizer flowrate behaviour at different plasma powers or at different sampling depths.

1. Power Family At Different Sampling Depths

The plots for all the elements studied are shown in Figures 5-12. At any one particular depth the ion-count for each element goes through a maximum indicating that at a fixed depth and power there is an optimum flowrate at which the ion-count and hence sensitivity is a maximum. The position of this maximum does not vary significantly with the type of element although plots for doubly charged species tend to give a maximum at lower flowrates compared to plots for the corresponding singly charged species. Thus at 15mm and 1.3kW, Ba, La, Sr, Cd, Zn and Y all have a signal maximum close to 1.05 ℓ/min. This implies that a single set of conditions can be used for quantitative analysis of many elements with little or no sacrifice of sensitivity.

The value of the maximum ion-count is different for each species because of differences in ionization potential, differences in atomic weight which determines the number of ions in 1 litre of solution for a 0.1 ppm solution, and because of other variable effects like a different extent of oxide and other species formation. Doubly charged ions have very low ion-counts compared with their singly charged components because of the large energy required to produce them and therefore the smaller fraction produced.

For each power plot, the intensity decreases as the sampling depth is increased from 10mm to 25 mm. The position of the signal maximum is also shifted to higher flowrates. Thus for the Cd plot at 1.5kW power, increasing the sampling depth through 10, 15 and 20mm shifts the position of the peak maximum through 0.9, 1.05, and 1.15 ℓ/min

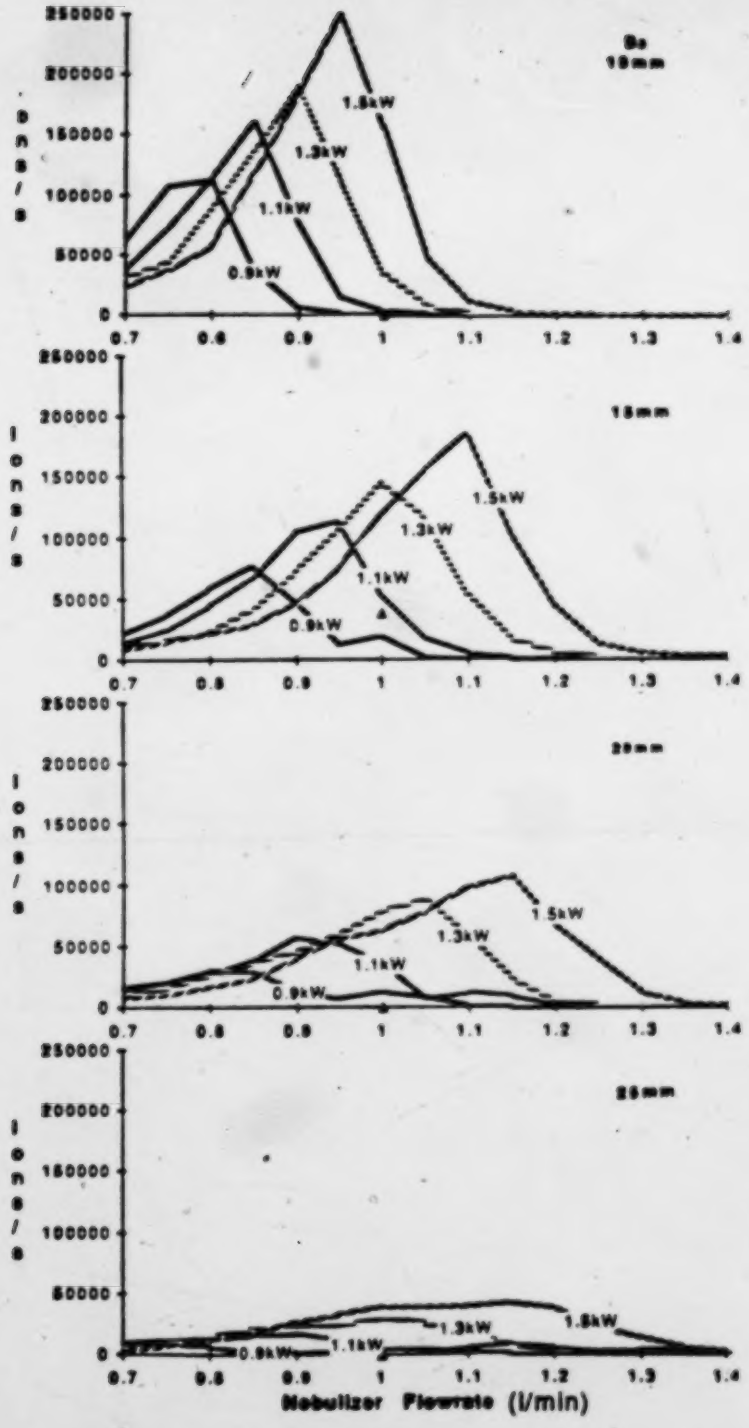

Figure 5. Nebulizer flowrate-power parameter plots for Ba at sampling depths of 10,15, 20 and 25mm from the load coil

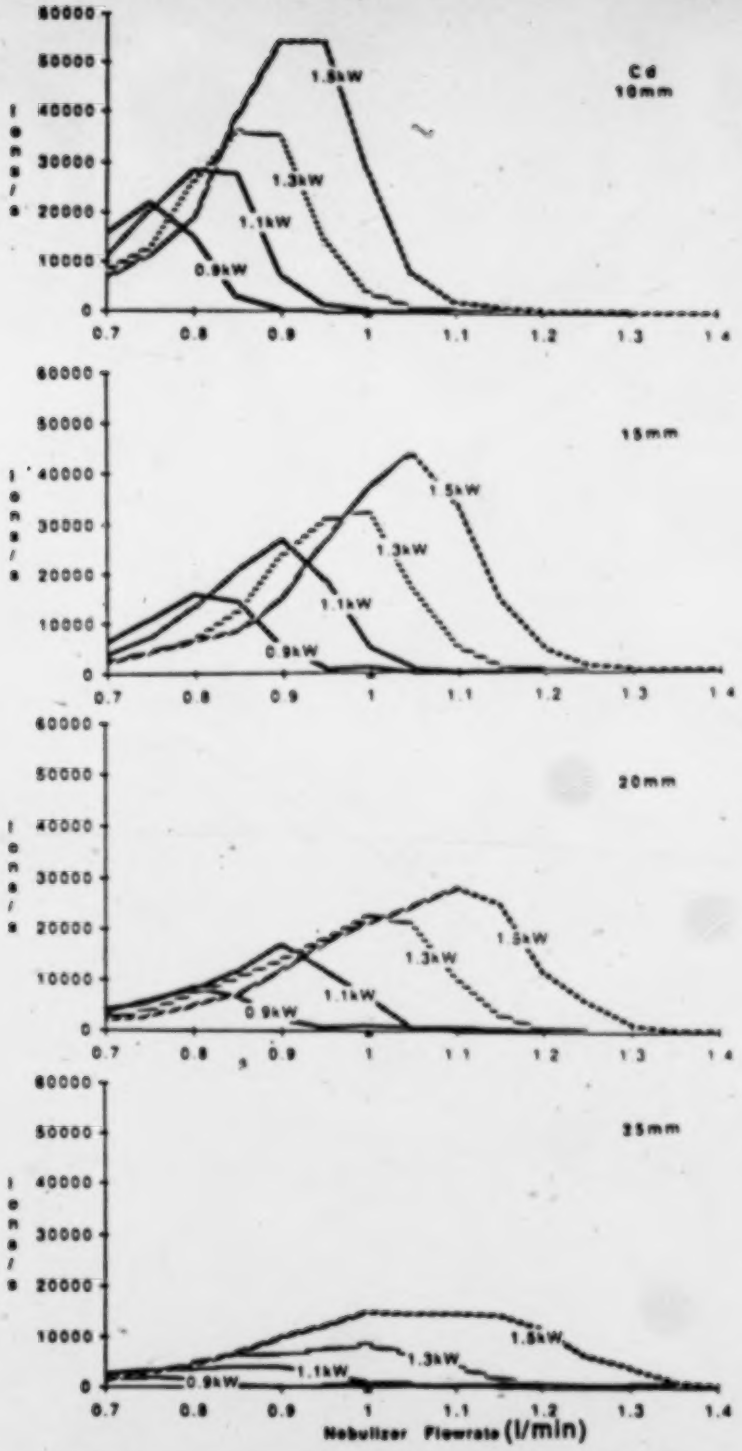

Figure 6. Nebulizer flowrate-power parameter plots for Cd at sampling depths of 10, 15, 20 and 25mm from the load coil

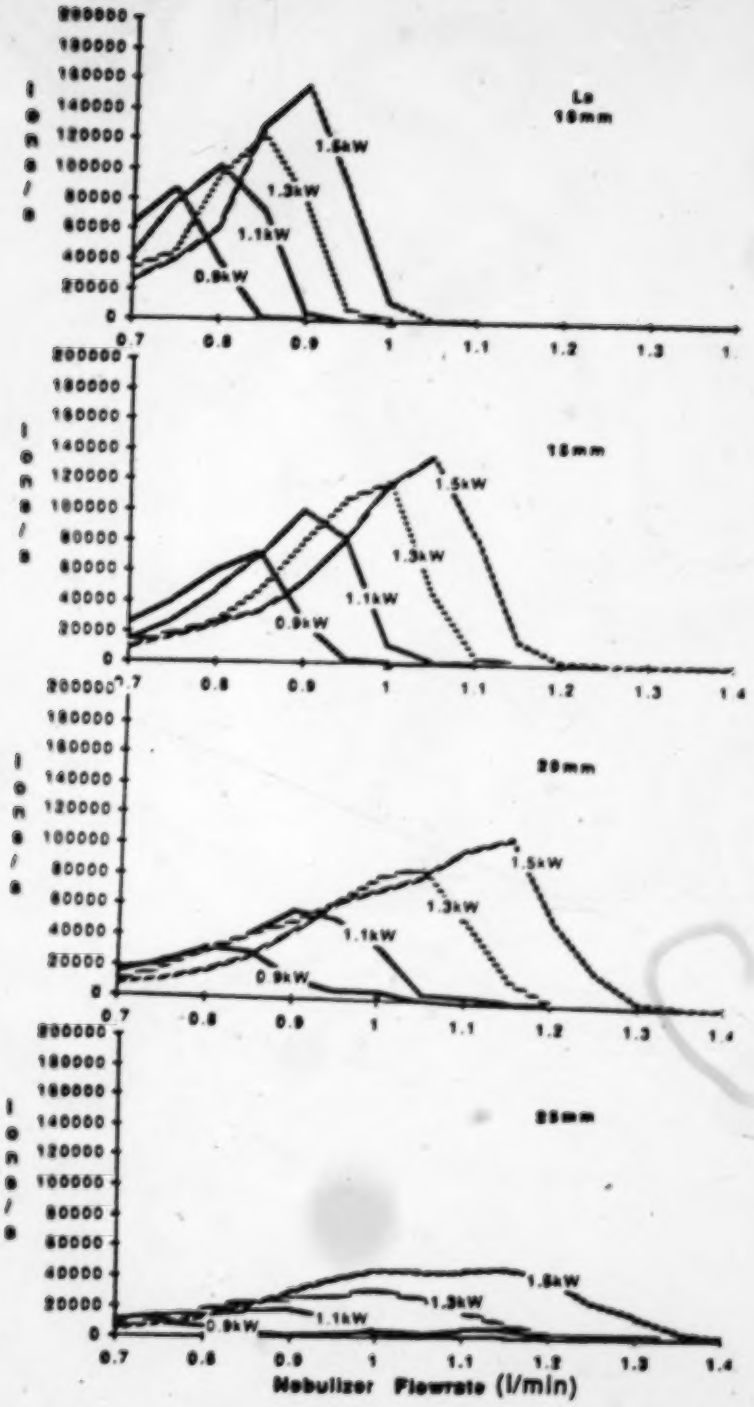

Figure 7. Nebulizer flowrate-power parameter plots for La at sampling depths of 10, 15, 20 and 25mm from the load coil

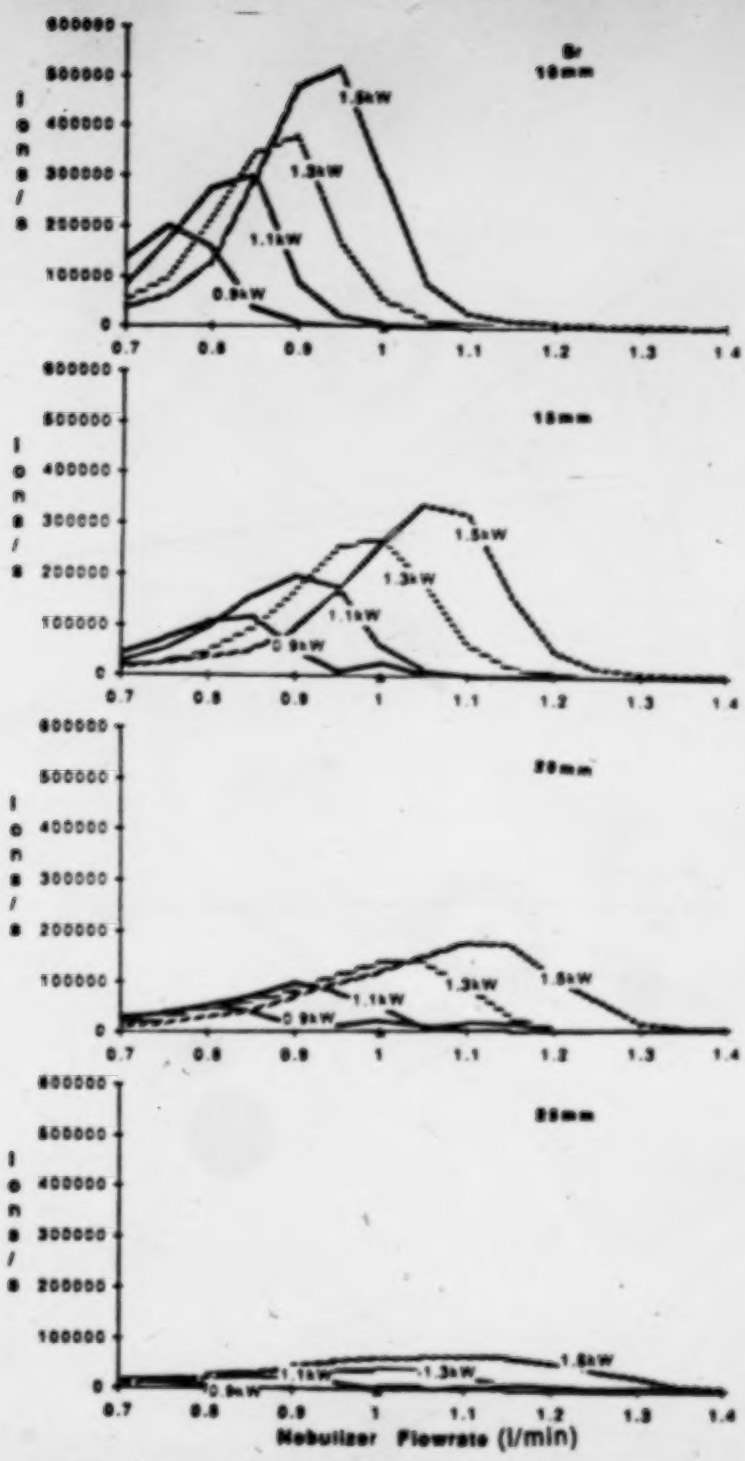

Figure 8. Nebulizer flowrate-power parameter plots for Sr at sampling depths of 10, 15, 20 and 25mm from the load coil

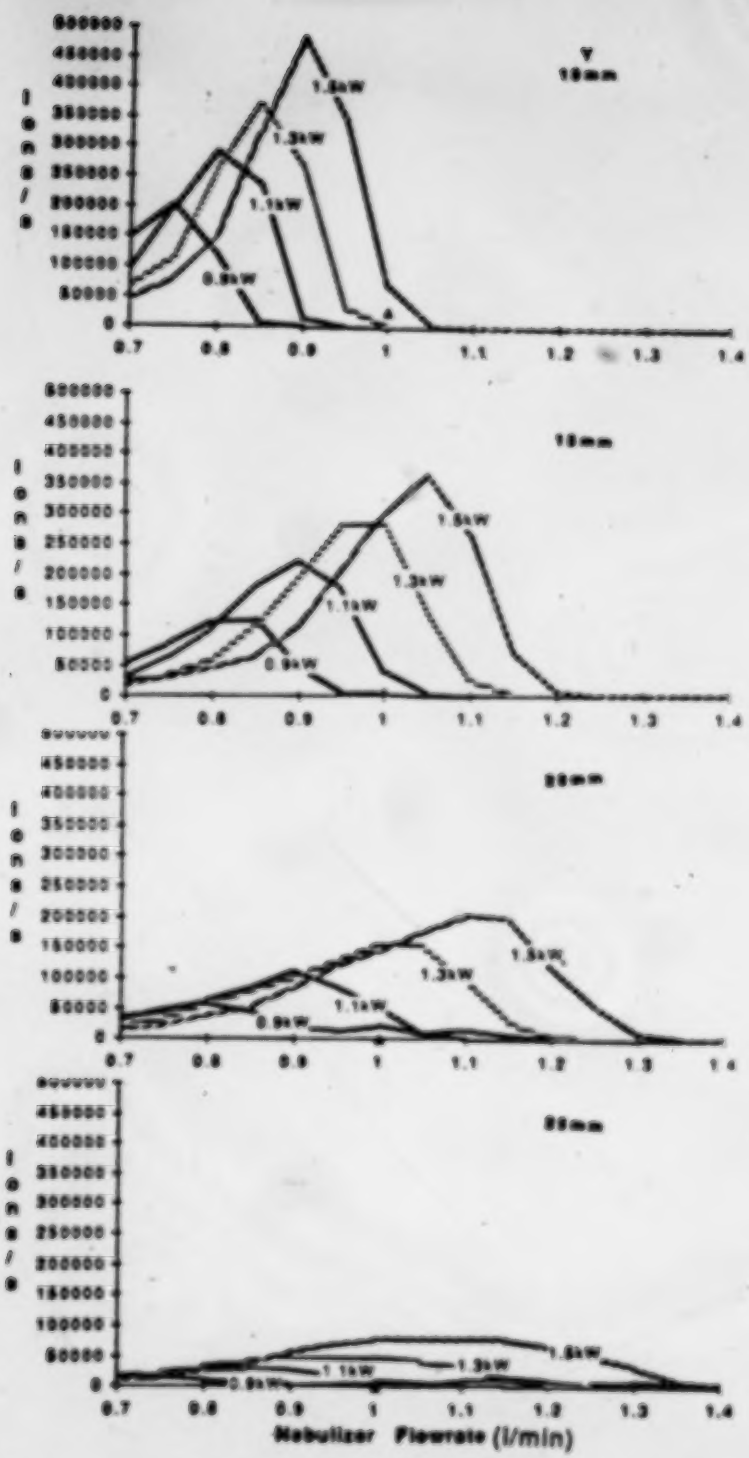

Figure 9. Nebulizer flowrate-power parameter plots for Y at sampling depths of 10, 15, 20 and 25mm from the load coil

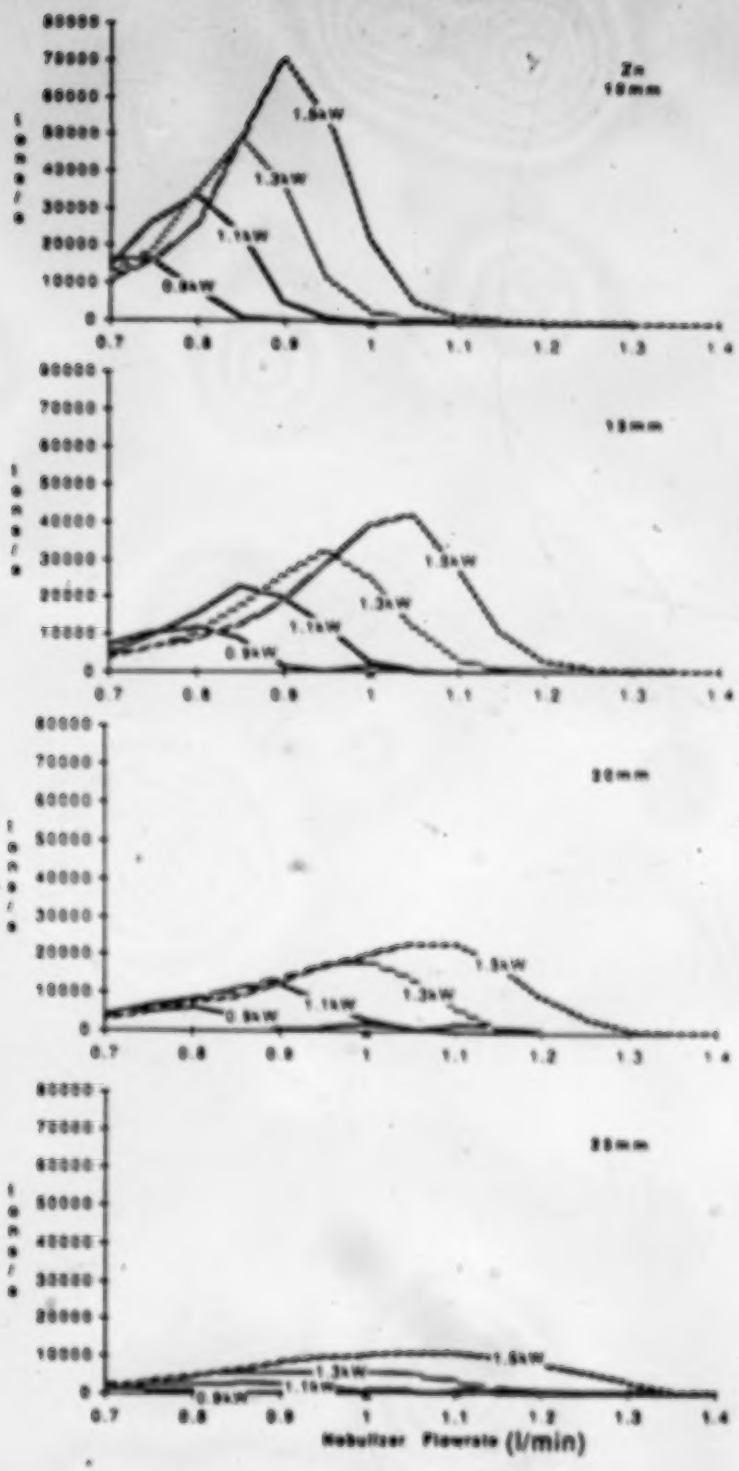

Figure 10. Nebulizer flowrate-power parameter plots for Zn at sampling depths of 10, 15, 20 and 25mm from the load coil

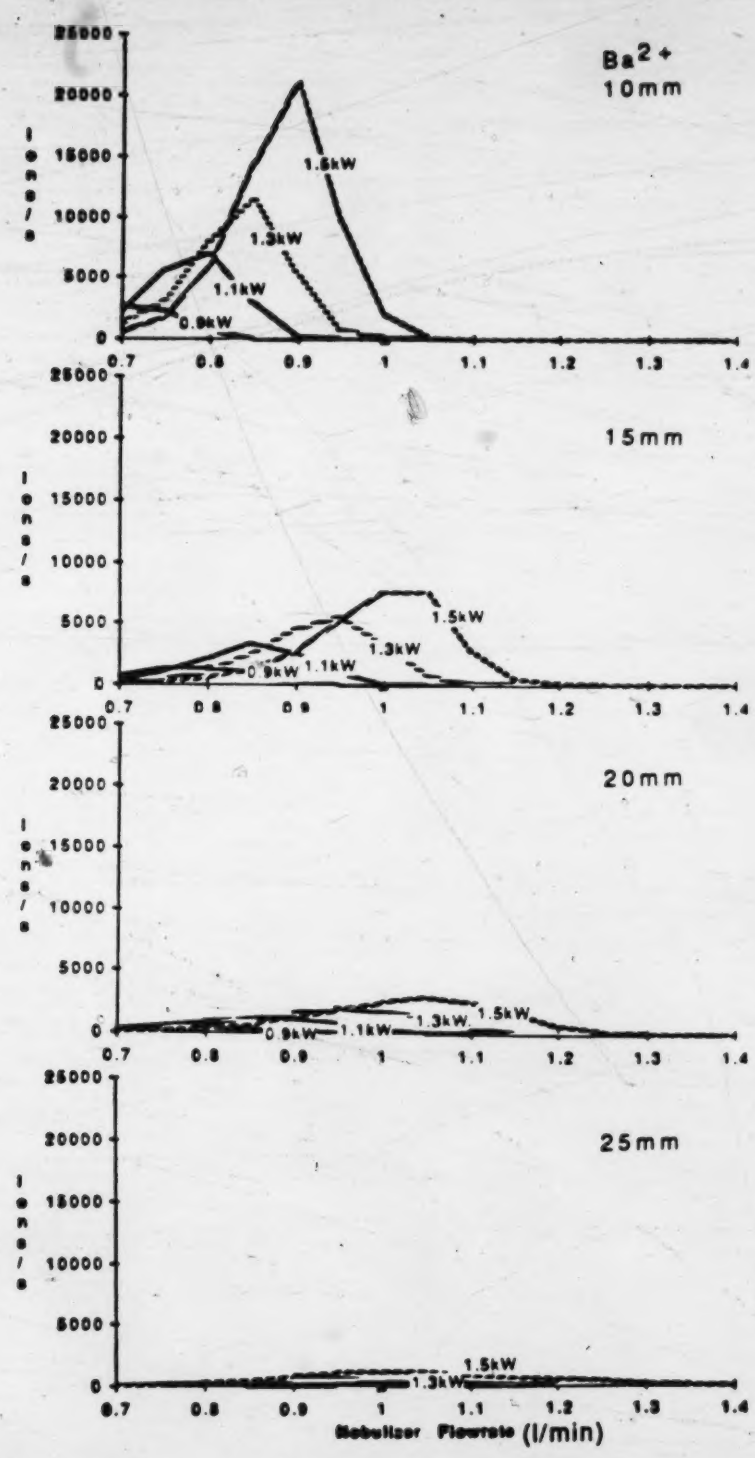

Figure 11. Nebulizer flowrate-power parameter plots for Ba^{2+} at sampling depths of 10, 15, 20 and 25mm from the load coil

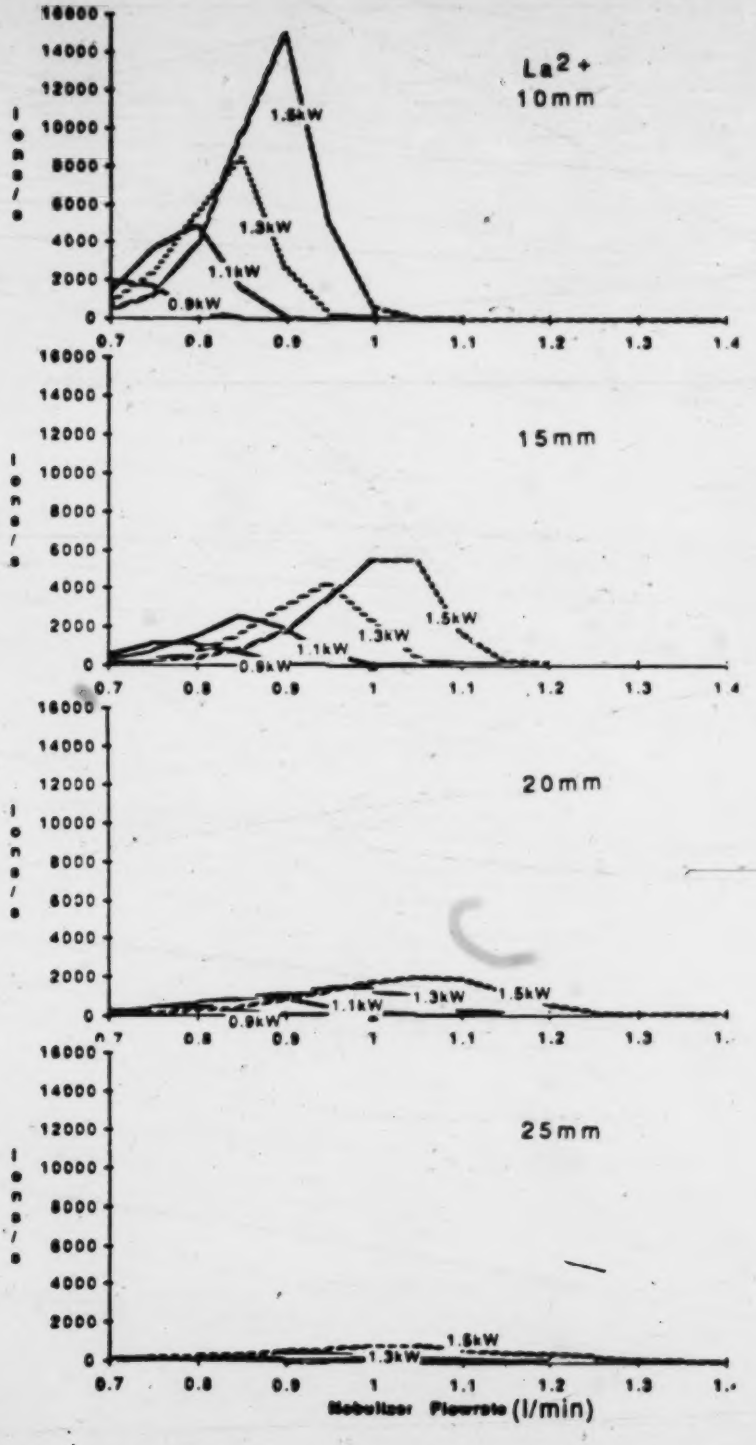

Figure 12. Nebulizer flowrate-power parameter plots for La^{2+} at sampling depths of 10, 15, 20 and 25mm from the load coil

respectively. The plots for the rest of the elements show similar behaviour. Thus for sampling depths lower than 20mm, a 5mm change in sampling depth changes the position of the peak maximum by approximately 0.12 ℓ/min. Hence an increase in sampling depth should be accompanied by an increase in nebulizer flowrate in order to obtain the maximum sensitivity possible. Above a sampling depth of 20mm, the peaks are broad and the position of the peak maximum changes very little with depth.

From these observations one can visualize a region in the plasma where the ion density is a maximum. This region will be called the Normal Analytical Zone (NAZ) [66]. The position of the NAZ varies with flowrate and other parameters that affect the temperature of the plasma. Thus the position of the NAZ would be expected to be fixed at a particular sampling depth if other parameters are constant. This would explain the existence of a peak maximum in the plots. The ion count would then be expected to decrease on changing the sampling depth from the maximum peak position because this action would move the NAZ away from the sampler of the ICP-MS.

The fact that the position of the peak maximum for each plot is linked to higher flowrates as sampling depth increases can then be explained by saying it would be necessary to push the NAZ back to its position close to the sampler by increasing the nebulizer flowrate. This increased flowrate will decrease the temperature of the plasma causing the decreasing maximum ion-count observed as depth is increased while power stays constant.

2. Sampling Depth Family At Different Powers

This display format for each element is shown in Figures 13-20. As power is increased from 0.9kW to 1.5kW, the signal maxima for each sampling depth move to higher nebulizer flowrates. Thus at a 15mm sampling depth, increasing the power through 0.9, 1.1, 1.3 and 1.5kW shifts the position of the peak maximum of Cd through 0.85, 0.90, 1.0 and 1.05 ℓ/min. Hence at 15mm a power increase of 0.2kW shifts the plots by 0.05 ℓ/min. The same behaviour is observed for the other elements. However, as stated before, the peaks are also shifted as the sampling depth increases from 10mm to 25mm. Thus at 20mm the peaks are shifted by approximately 0.1 ℓ/min. When these values are compared with those observed in the sampling depth family it becomes apparent that a power increase of 0.2kW shifts the plots by approximately the same extent as a depth increase of 2.5mm (0.2kW power increase shifts peak by approximately 0.06 ℓ/min while 5mm depth increase shifts peak by approximately 0.12 ℓ/min).

As power is increased, the maximum ion-count at each depth also increases as expected. Peaks of doubly charged species occur at lower flowrates when compared with their singly charged counterpart. This may be due to the fact that atoms have a longer residence time and experience a higher temperature in the plasma at low flowrates which increases the probability of forming doubly charged species.

At low flowrates (< 0.95 ℓ/min) a sampling depth of 10mm gives the maximum ion count, and hence maximum sensitivity. At higher flowrates, however, larger sampling depths produce higher ion counts. This observation may be accounted for as follows: as the

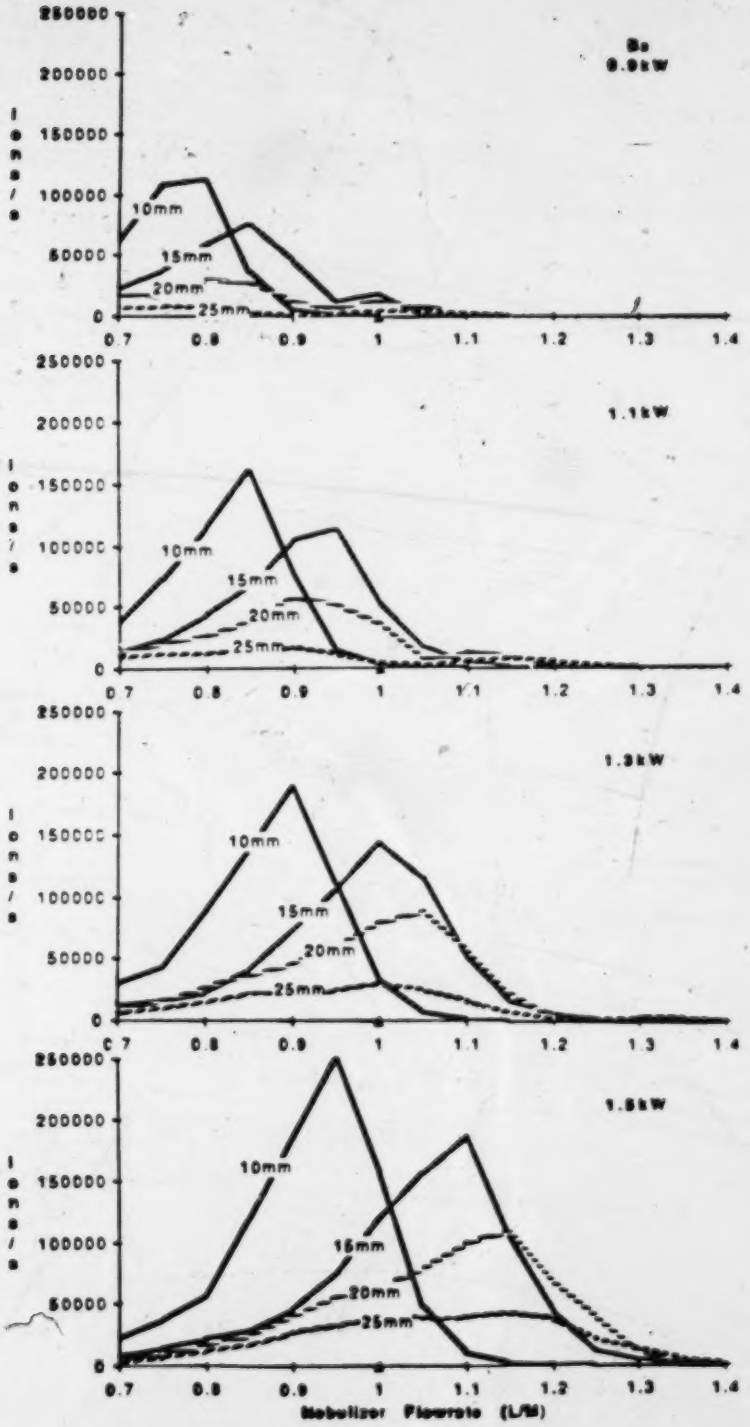

Figure 13. Nebulizer flowrate-depth parameter plots for Ba at plasma rf powers of 0.9, 1.1, 1.3 and 1.5kW

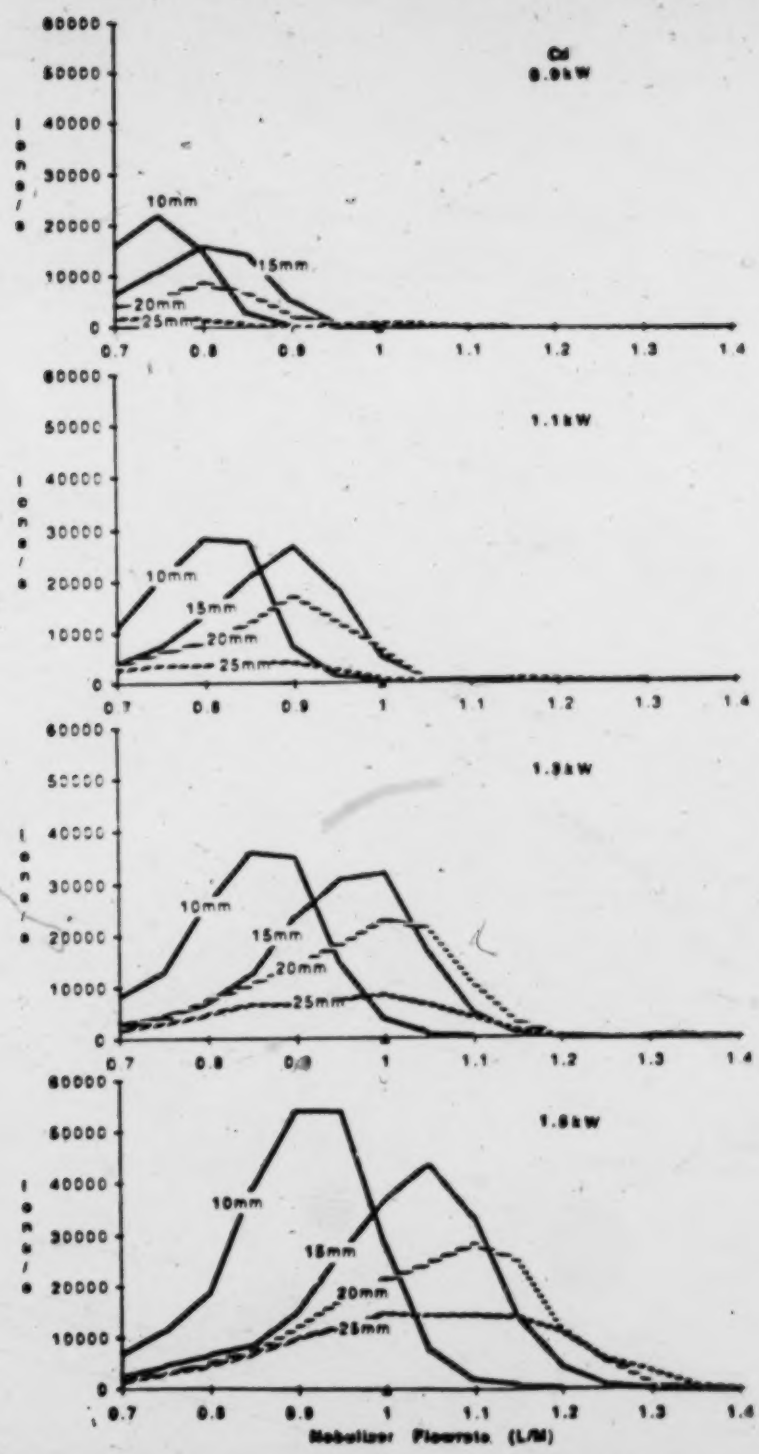

Figure 14. Nebulizer flowrate-depth parameter plots for Cd at plasma rf powers of 0.9, 1.1, 1.3 and 1.5kW

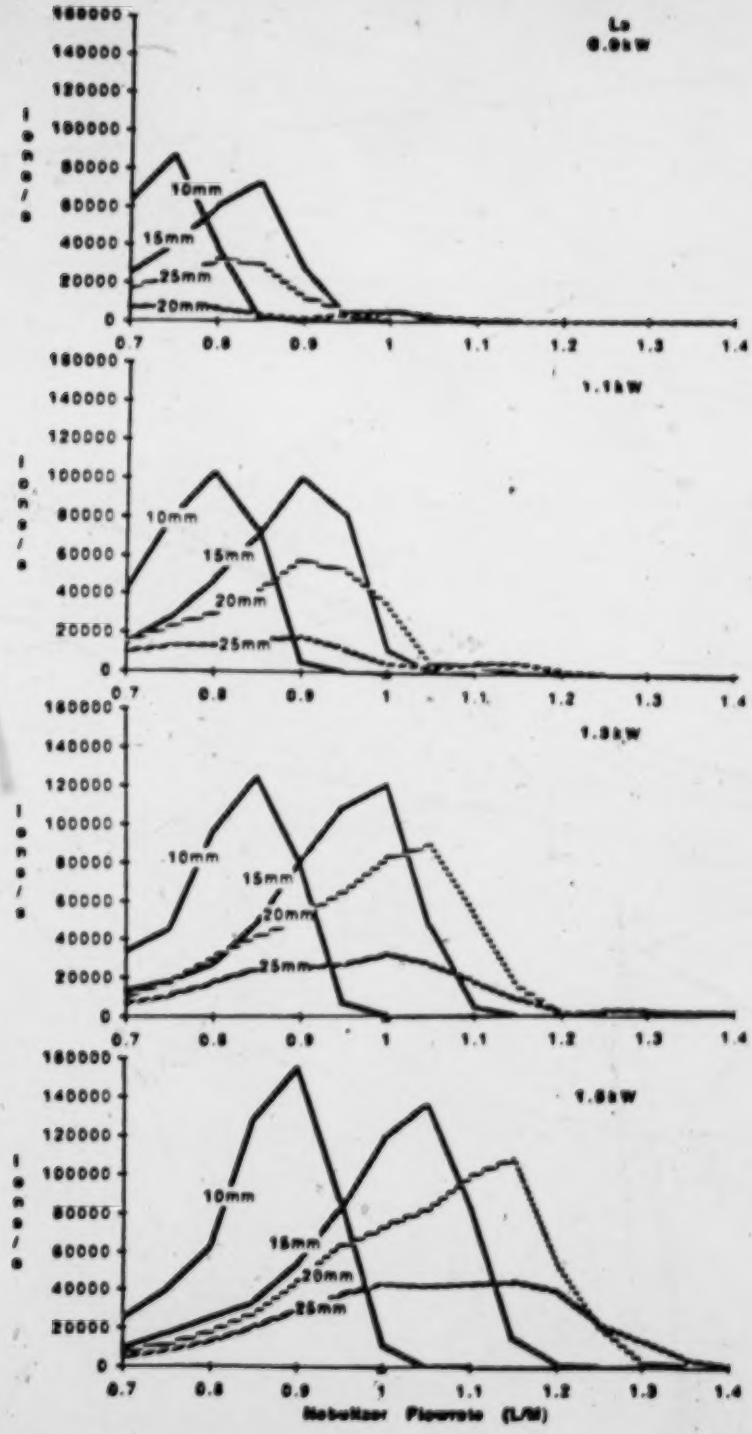

Figure 15. Nebulizer flowrate-depth parameter plots for La at plasma rf powers of 0.9, 1.1, 1.3 and 1.5kW

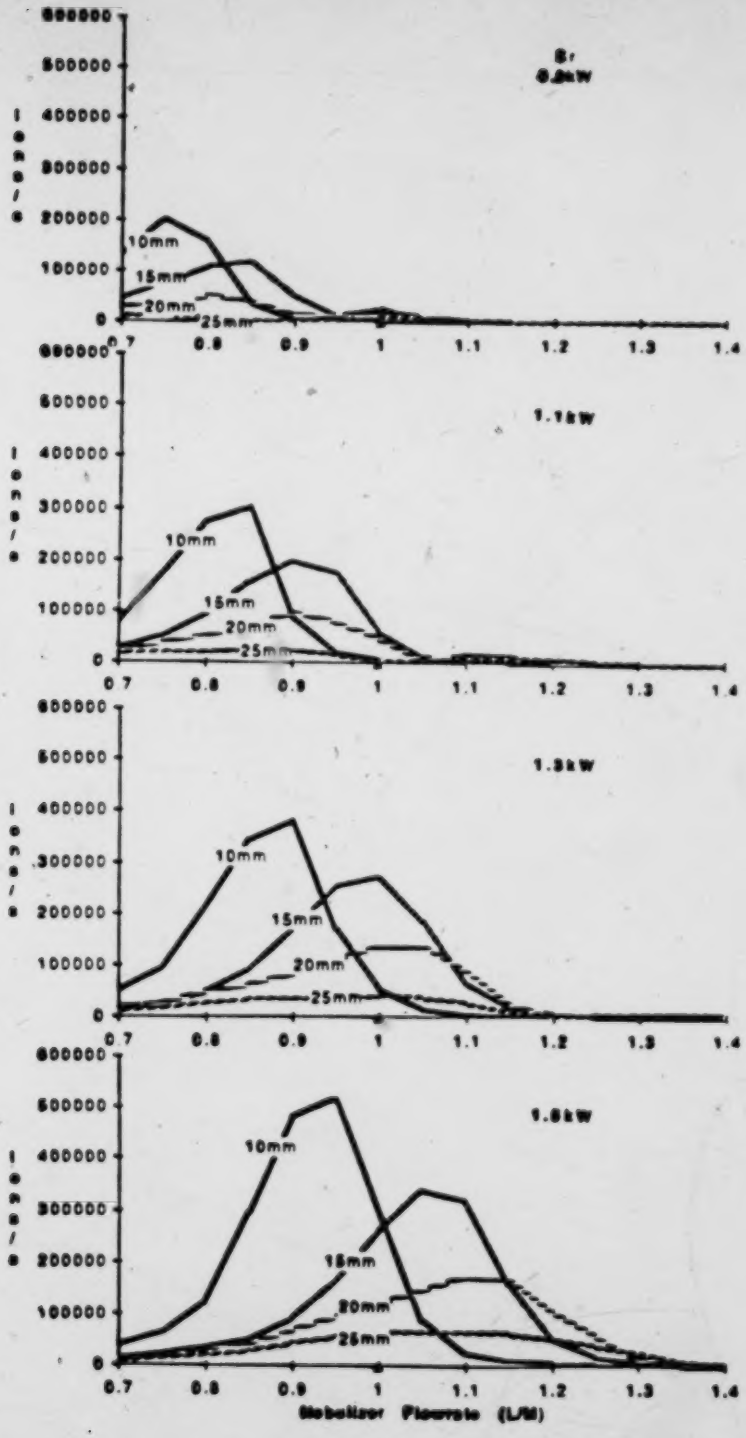

Figure 16. Nebulizer flowrate-depth parameter plots for Sr at plasma rf powers of 0.9, 1.1, 1.3 and 1.5kW

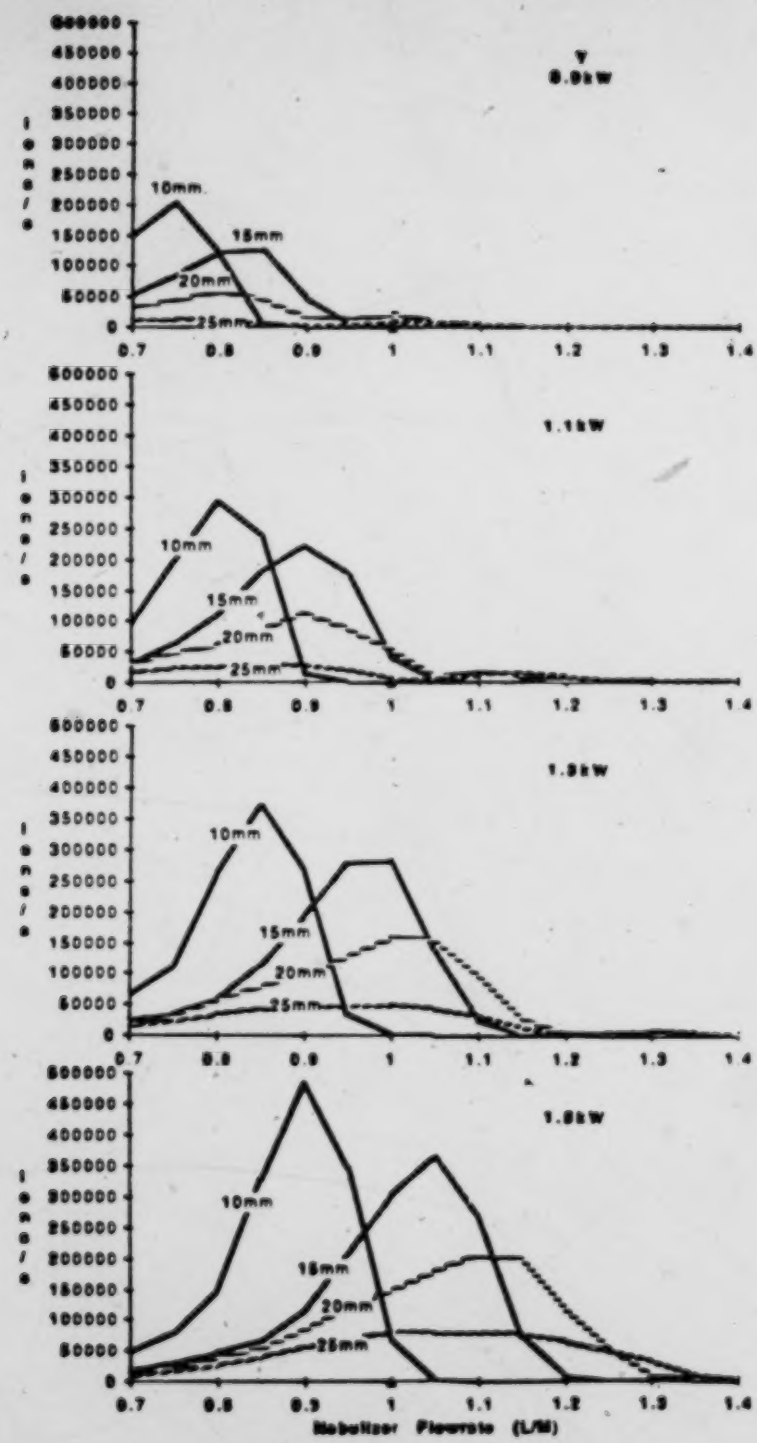

Figure 17. Nebulizer flowrate-depth parameter plots for Y at plasma rf powers of 0.9, 1.1, 1.3 and 1.5kW.

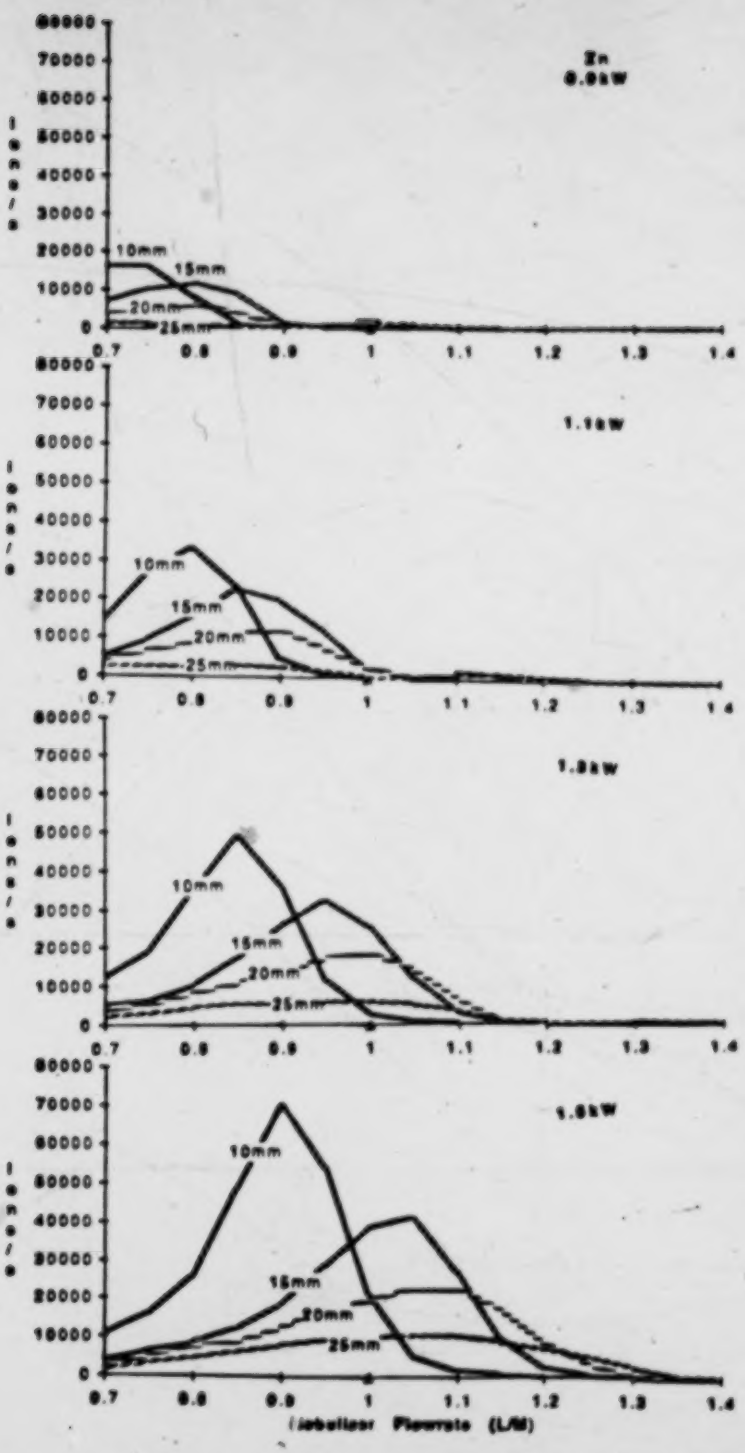

Figure 18. Nebulizer flowrate-depth parameter plots for Zn atplasma rf powers of 0.9, 1.1, 1.3 and 1.5kW.

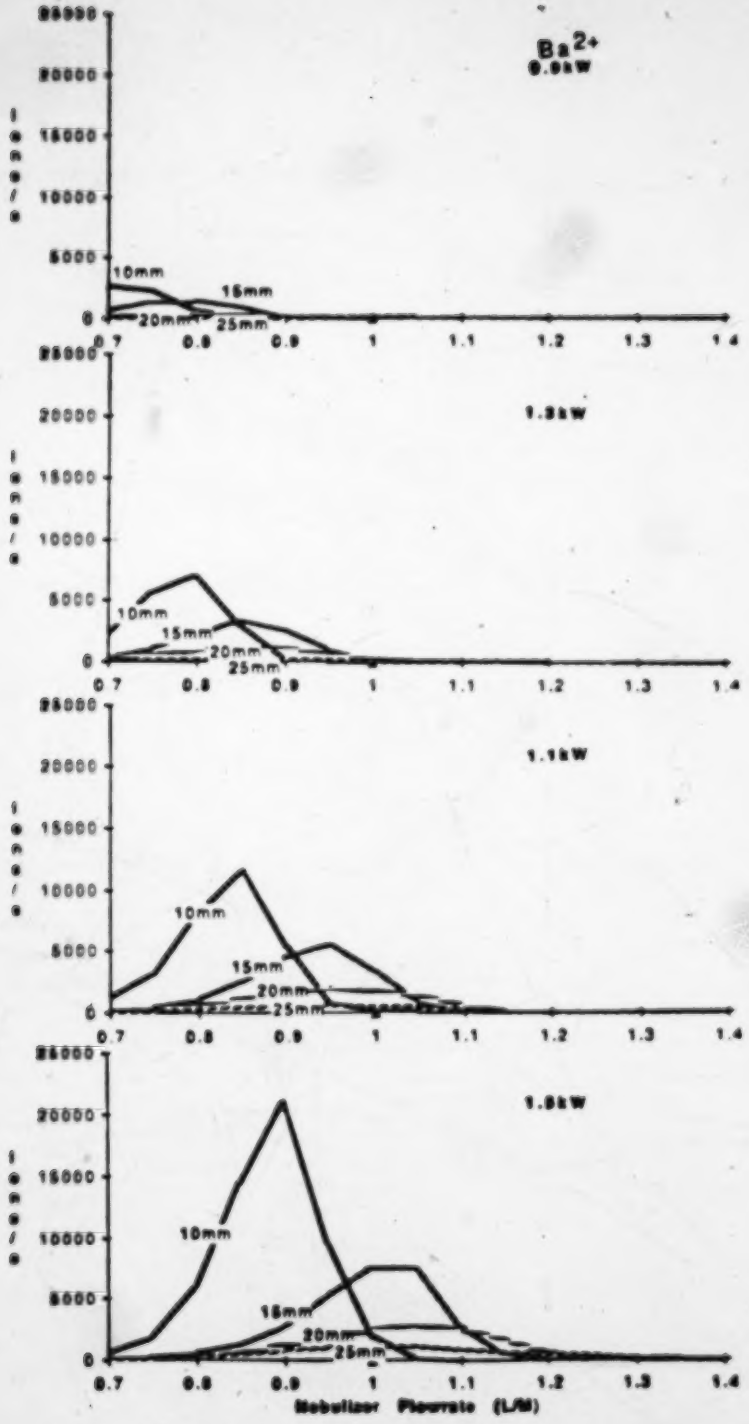

Figure 19. Nebulizer flowrate-depth parameter plots for Ba^{2+} at plasma rf powers of 0.9, 1.1, 1.3 and 1.5kW

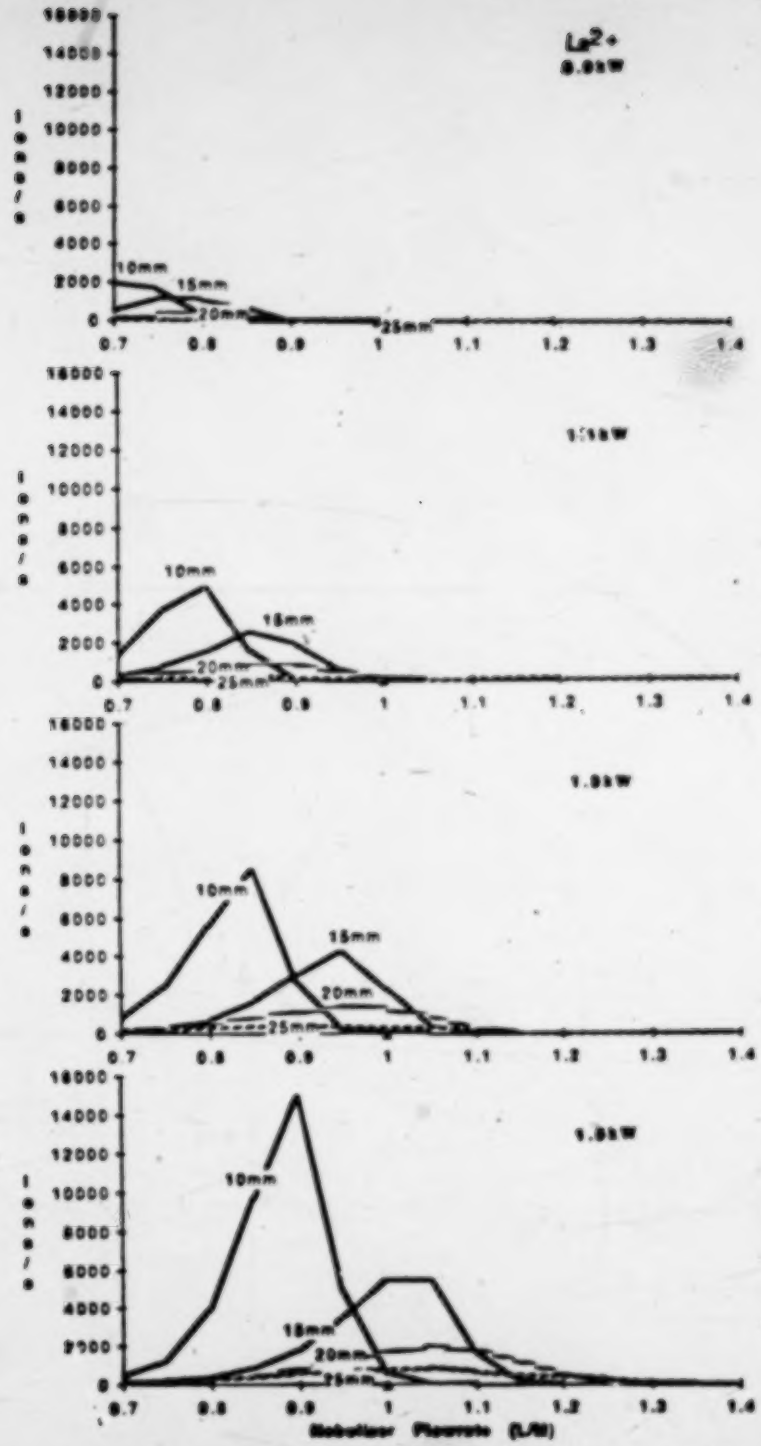

Figure 20. Nebulizer flowrate-depth parameter plots for La^{2+} at plasma rf powers of 0.9, 1.1, 1.3 and 1.5kW

flowrate increeses while sampling depth stays constant, the NAZ in the plasma is pushed closer to the sampler causing the number of ions sampled and therefore counted to increase. At a certain flowrate the region will exist just opposite the sampler and one would expect the ion count to be a maximum. Beyond this flowrate the region of the plasma next to the sampler would have a lower ion density than the NAZ and one would expect the ion count to decrease and to continue decreasing as the flowrate is further increased. Since the position of the NAZ is shifted outwards as flowrate increases, it would be expected that the maximum for succeeding depth plots will occur at higher flowrates, as is observed in these figures.

C. Signal vs. Sampling Depth

This plot format is not as informative as the nebulizer flowrate plots. The analyte ion-count is plotted vs. sampling depth and then on the same set of axes a family of such curves is plotted representing the ion-count--sampling depth behaviour at different nebulizer flowrates or at different plasma powers. Due to the broad shape of the plots, selection of compromise conditions for chemical analysis is more difficult.

1. Power Family At Different Nebulizer Flow Rates

Figures 21-28 show the plots for all the elements studied. The plot format shows clearly what power to use at a given nebulizer flow rate and sampling depth so as to achieve maximum sensitivity. Despite the fact that the plasma should be hottest at the highest power (1.5kW), this power does not always give the highest

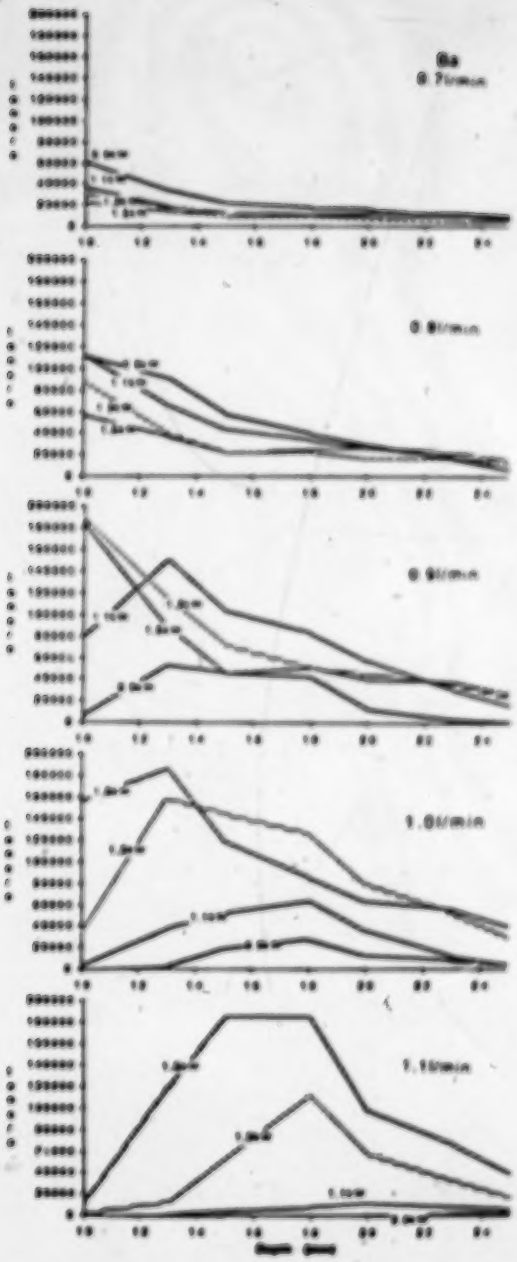

Figure 21. Sampling depth-power parameter plots for Ba at nebulizer flowrates of 0.7, 0.8, 0.9, 1.0 and 1.1l/min

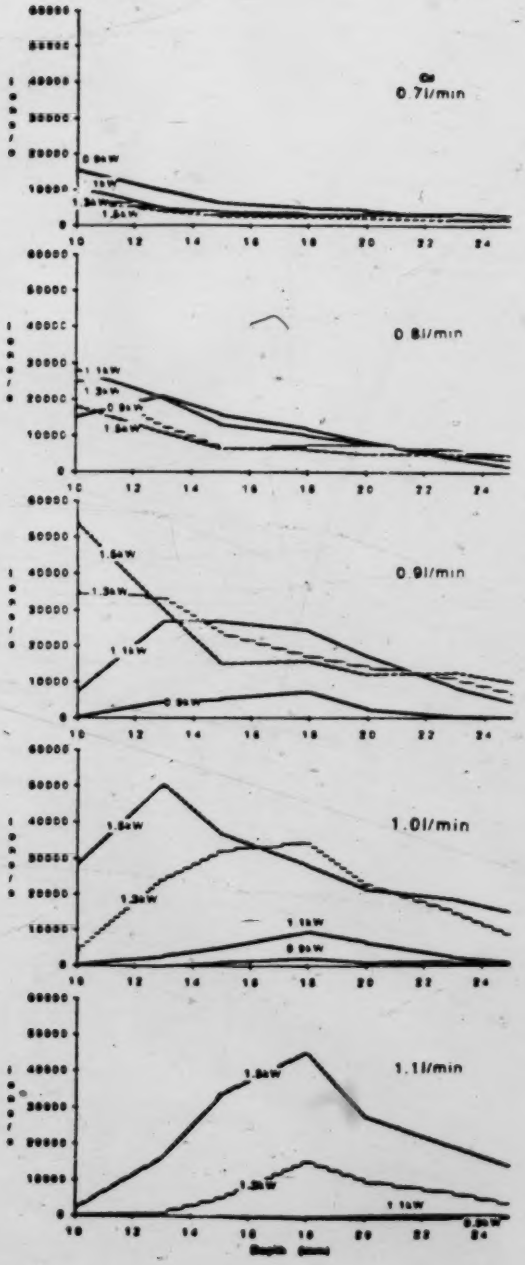

Figure 22. Sampling depth-power parameter plots for Cd at nebulizer flowrates of 0.7, 0.8, 0.9, 1.0 and 1.1l/min

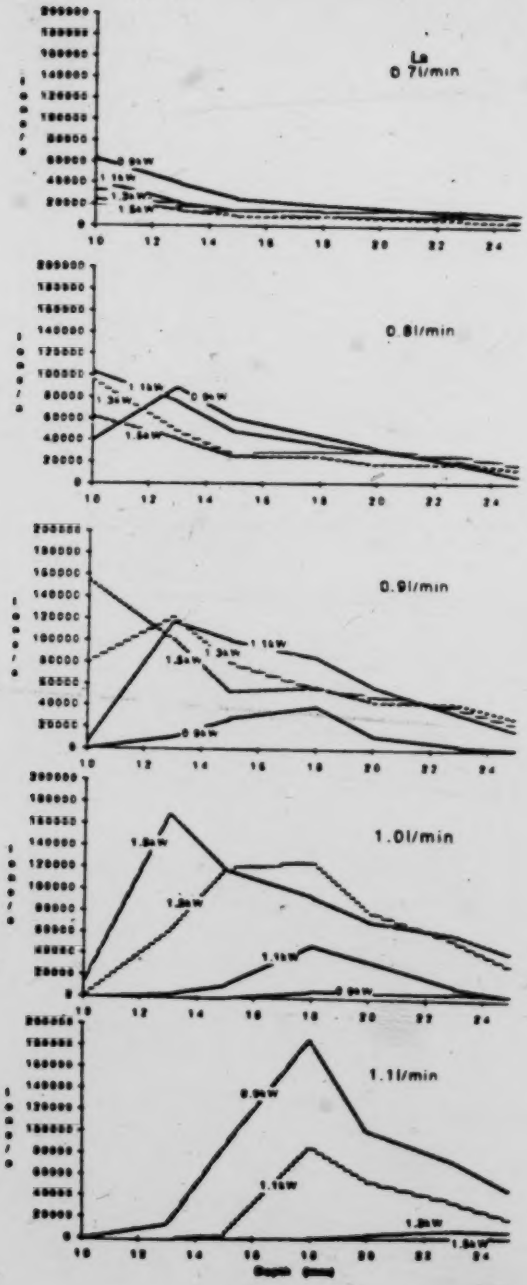

Figure 23. Sampling depth-power parameter plots for La at nebulizer flowrates of 0.7, 0.8, 0.9, 1.0 and 1.1l/min

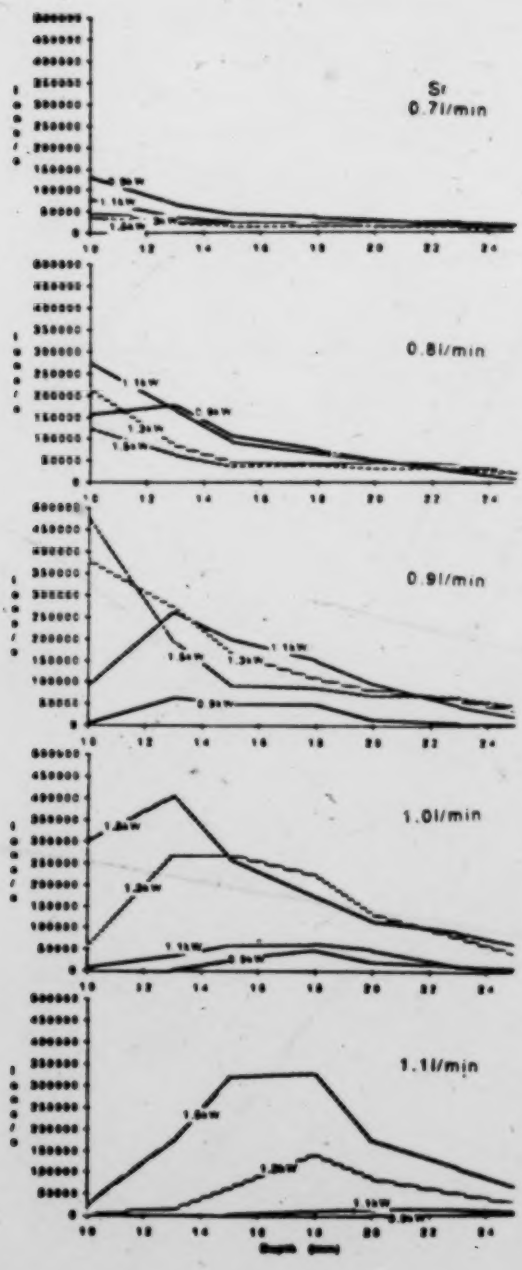

Figure 24. Sampling depth-power parameter plots for Sr at nebulizer flowrates of 0.7, 0.8, 0.9, 1.0 and 1.1l/min

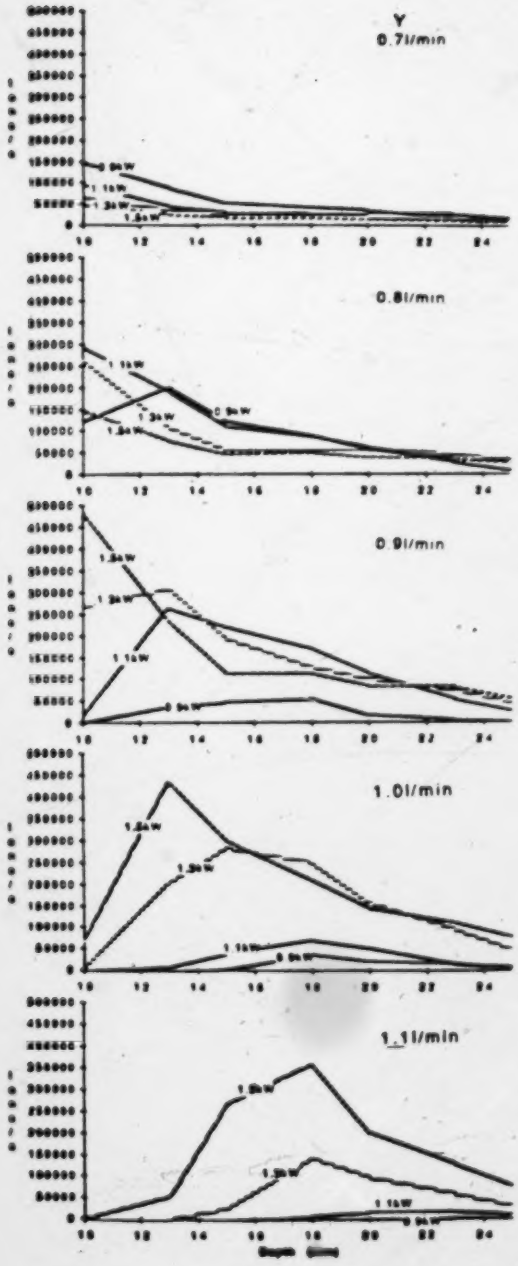

Figure 25. Sampling depth-power parameter plots for Y at nebulizer flowrates of 0.7, 0.8, 0.9, 1.0 and 1.1l/min

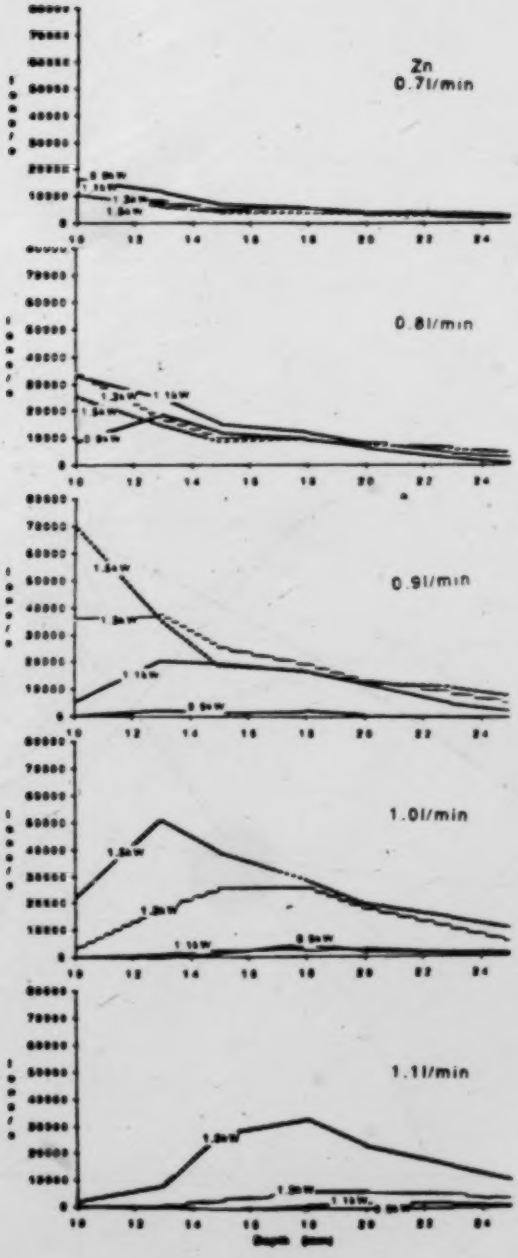

Figure 26. Sampling depth-power parameter plots for Zn at nebulizer flowrates of 0.7, 0.8, 0.9, 1.0 and 1.1l/min

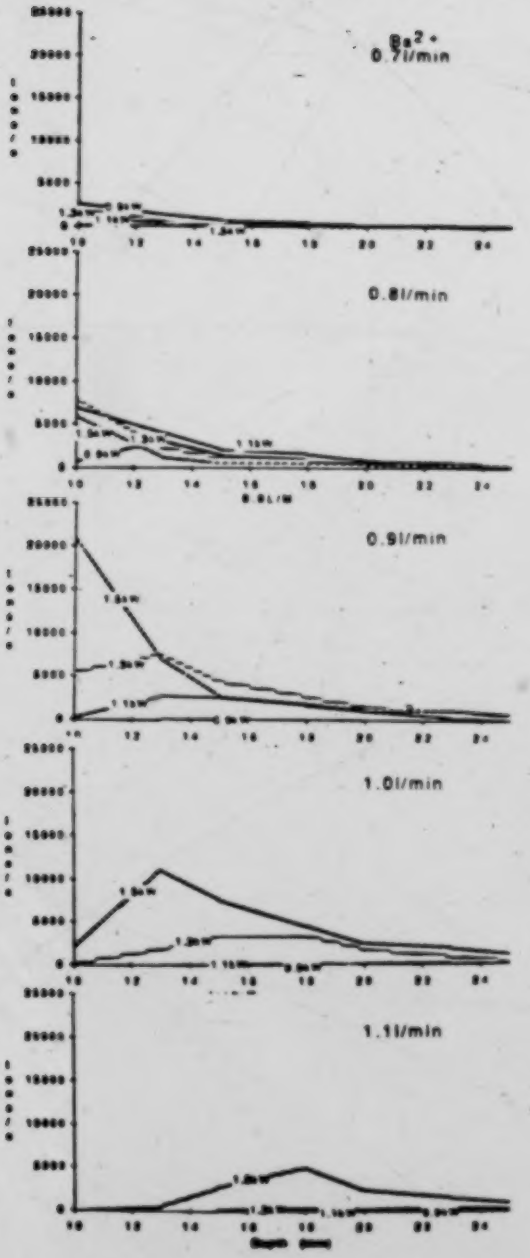

Figure 27. Sampling depth-power parameter plots for Ba^{2+} at nebulizer flowrates of 0.7, 0.8, 0.9, 1.0 and 1.1l/min

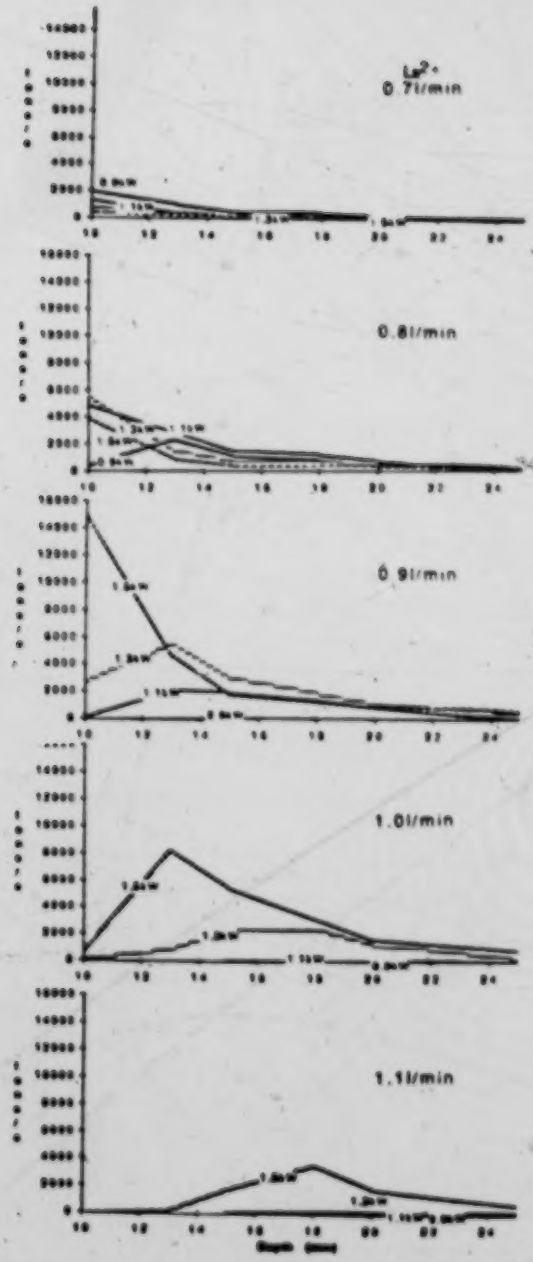

Figure 28. Sampling depth-power parameter plots for La^{2+} at nebulizer flowrates of 0.7, 0.8, 0.9, 1.0 and 1.1l/min

sensitivity. Thus at low flowrates (< 0.7 ℓ/min) the plots for the various powers show ion-count variation in the order

0.9kW > 1.1kW > 1.3kW > 1.5kW

Above 0.7 ℓ/min this order reverses gradually until at 1.0 ℓ/min and above, the order is:

1.5kW > 1.3kW > 1.1kW > 0.9kW

The peak maximum for each power plot does not appear for the 0.7 ℓ/min plots. At this flowrate the NAZ appears to be at a sampling depth that is less than 10mm. At flowrates of 0.8 ℓ/min and above, the peak maximum begins to appear.

As flowrate is increased, the position of the peak maxima shift to larger sampling depth. Thus on increasing the nebulizer flowrate from 0.8 ℓ/min to 0.9 ℓ/min, the position of the peak maximum for the 0.9kW plot of Cd moves from 14mm to 18mm. Above 0.9 ℓ/min the ion-count is very low, and the peak does not appear to be strongly affected by further increases in nebulizer flowrate. At flowrates at which the peaks appear to be very sensitive to flowrate changes, a 0.1 ℓ/min increase in flow rate appears to shift the peak maxima by about 4mm, Thus after increasing the flow rate by 0.1 ℓ/min, one would have to increase the sampling depth by about 4mm to regain maximum sensitivity. Plots for the double be charged species show similar behaviour.

The above observations can again be explained by movement of the NAZ as power and nebulizer flowrate are varied. At low flowrates the plasma has a relatively high temperature and the NAZ moves farther away from the sampler orifice as power increases. Thus a smaller

number of ions will be sampled at higher powers than at lower powers and maximum ion count will be observed at a low power. Increasing the nebulizer flowrate should lower the temperature of the plasma and the NAZ at each power will move closer to the sampler orifice. Since the NAZ at 1.5kW would have to move the longest distance to get to the sampler orifice and since the NAZ is pushed towards the orifice by increasing the nebulizer flowrate, it would be expected that the 1.5kW rf power would give the highest ion count at high nebulizer flowrate. The spatial overlap of all the power family plots in Figures 5-12 shows the same trend on moving from low to high nebulizer flowrates.

2. Flowrate Family At Different Powers

Figures 29-36 show the plots for all the elements studied. This plot format shows clearly the optimum flowrate to use at different powers and sampling depths. Thus below 1.5kW the plots show that a flowrate of 1.0 ℓ/min is optimum for all sampling depths. However at 1.5kW and a 16mm sampling depth, the Cd plot shows that a flowrate of 1.1 ℓ/min will give the maximum sensitivity.

As power is increased from 0.9kW to 1.5kW, ion counts for all plots increase and the position of the maximum for each plot moves to lower sampling depth. Thus as power is increased through 1.1kW, 1.3kW and 1.5kW the peak maximum of the Cd plot (1.0 ℓ/min) moves through 18mm, 16mm and 13mm. The same behaviour is approximately followed by the other elements. Thus a 0.2kW power increase shifts the peak maximum by approximately 2.3mm. Since a 0.1 ℓ/min increase in flowrate shifts the peak maximum by about 4mm as shown in the

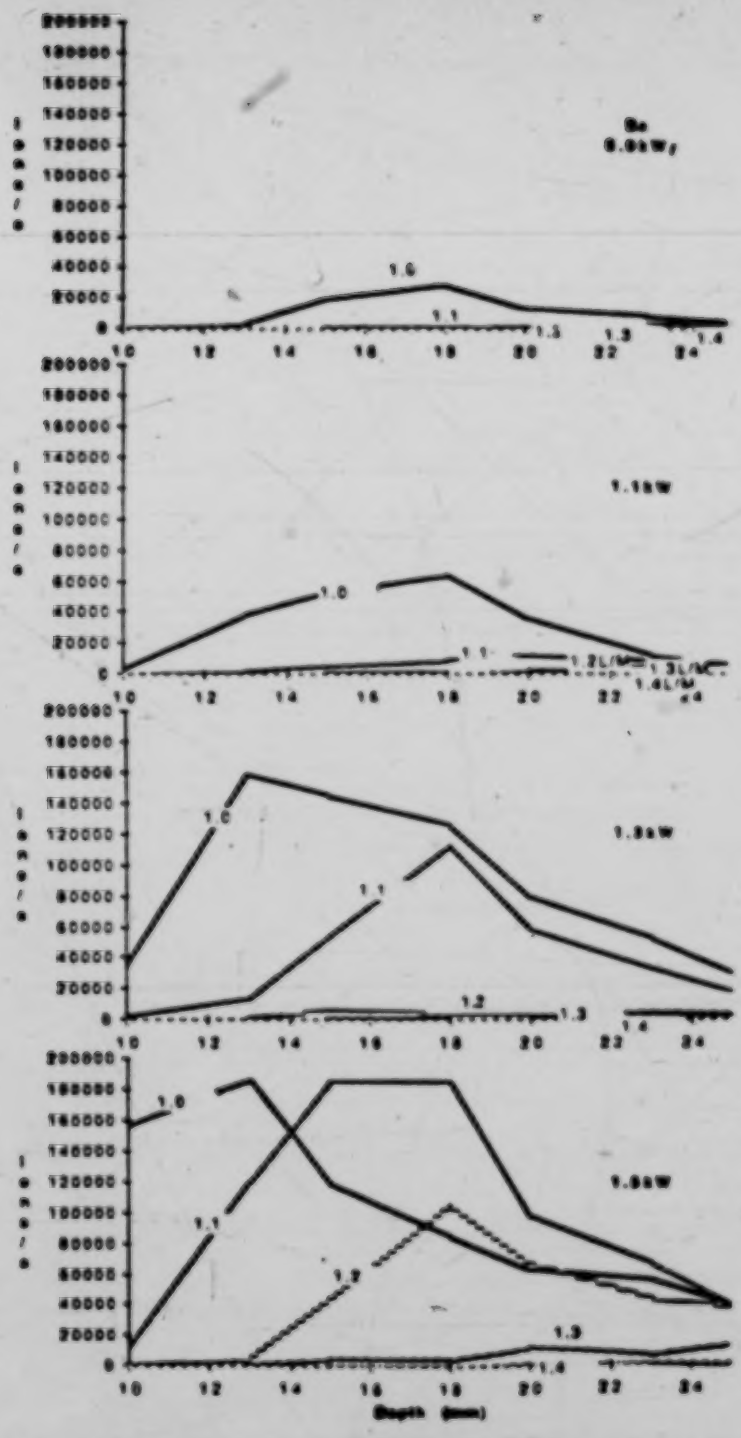

Figure 29. Sampling depth-nebulizer flowrate parameter plots for Ba at plasma rf powers of 0.9, 1.1, 1.3 and 1.5kW; Nebulizer flowrate in l/min shown on each line

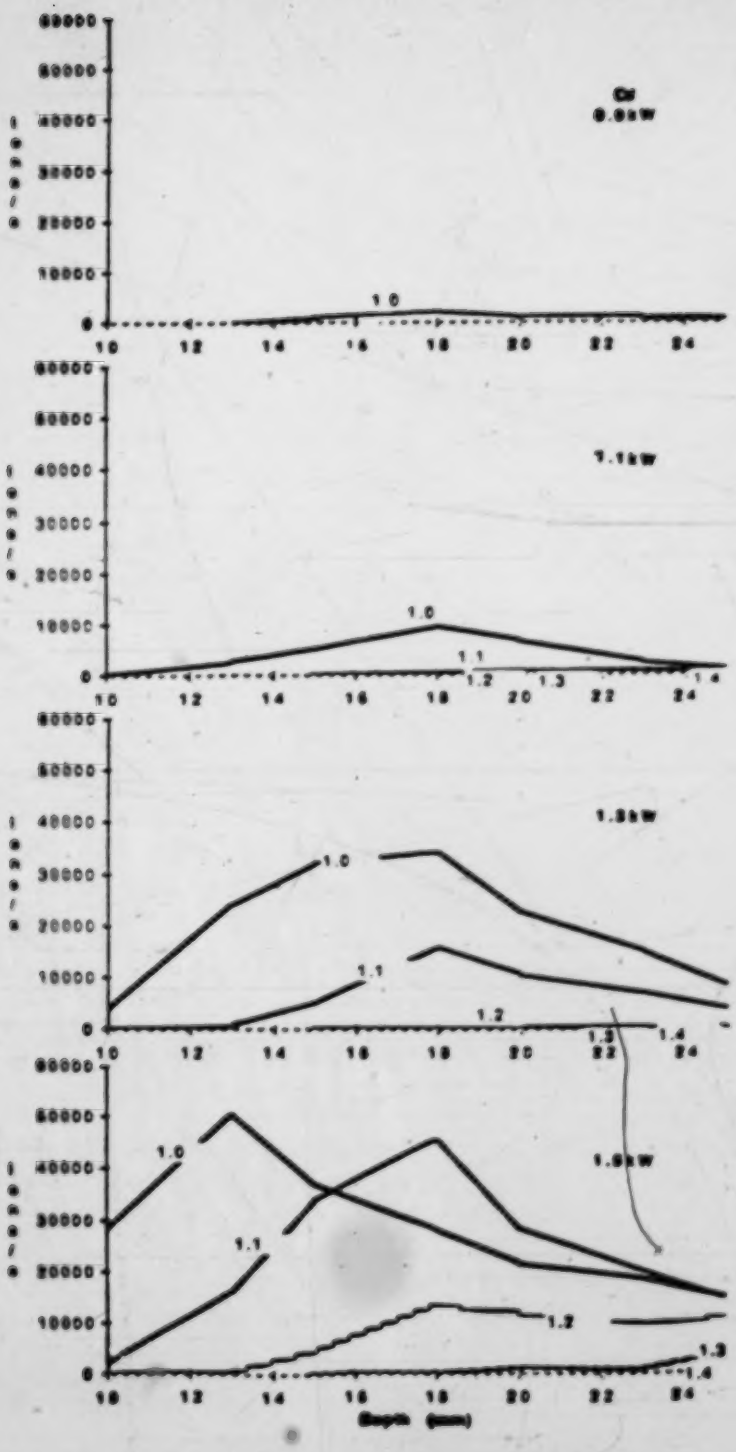

Figure 30. Sampling depth-nebulizer flowrate parameter plots for Cd at plasma rf powers of 0.9, 1.1, 1.3 and 1.5kW; nebulizer flowrate in l/min shown on each line

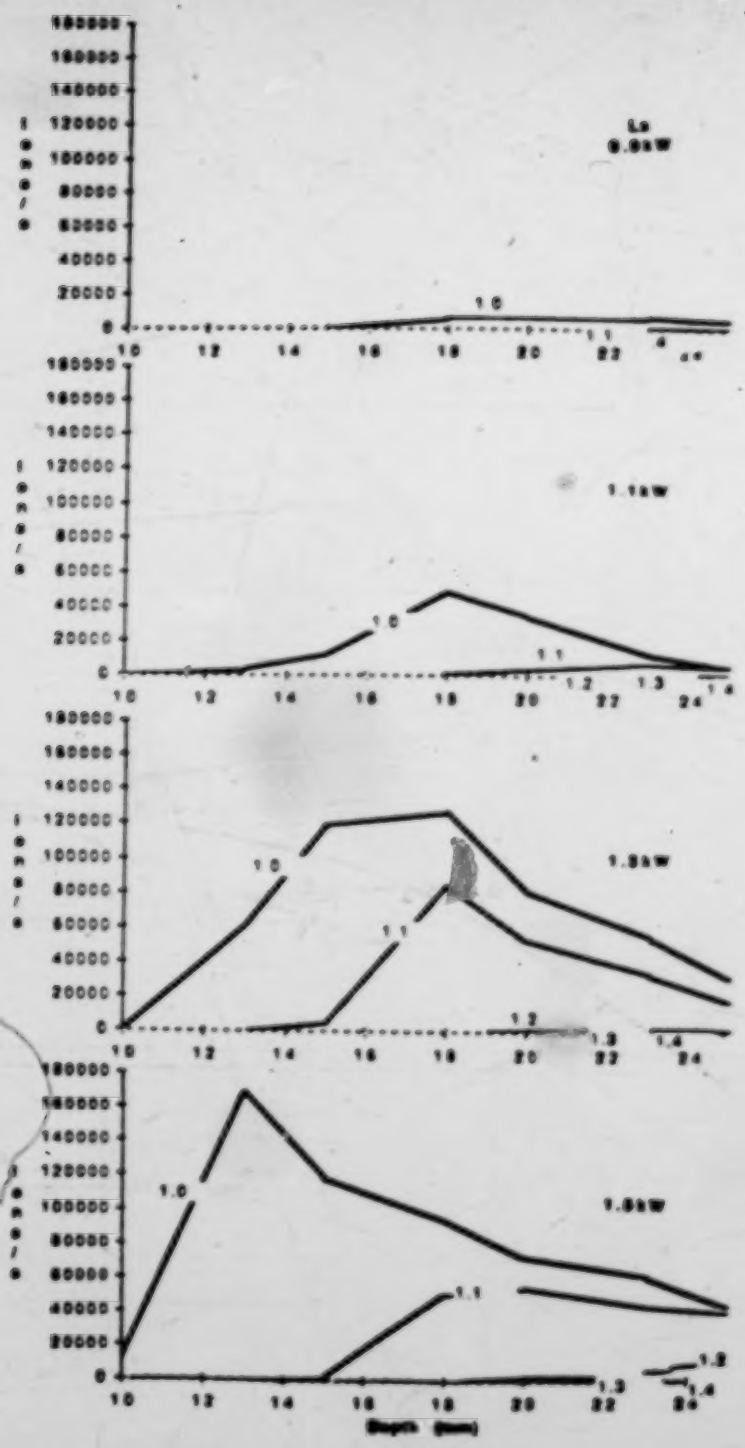

Figure 31. Sampling depth-nebulizer flowrate parameter plots for La at plasma rf powers of 0.9, 1.1, 1.3 and 1.5kW; nebulizer flowrate in l/min shown on each line

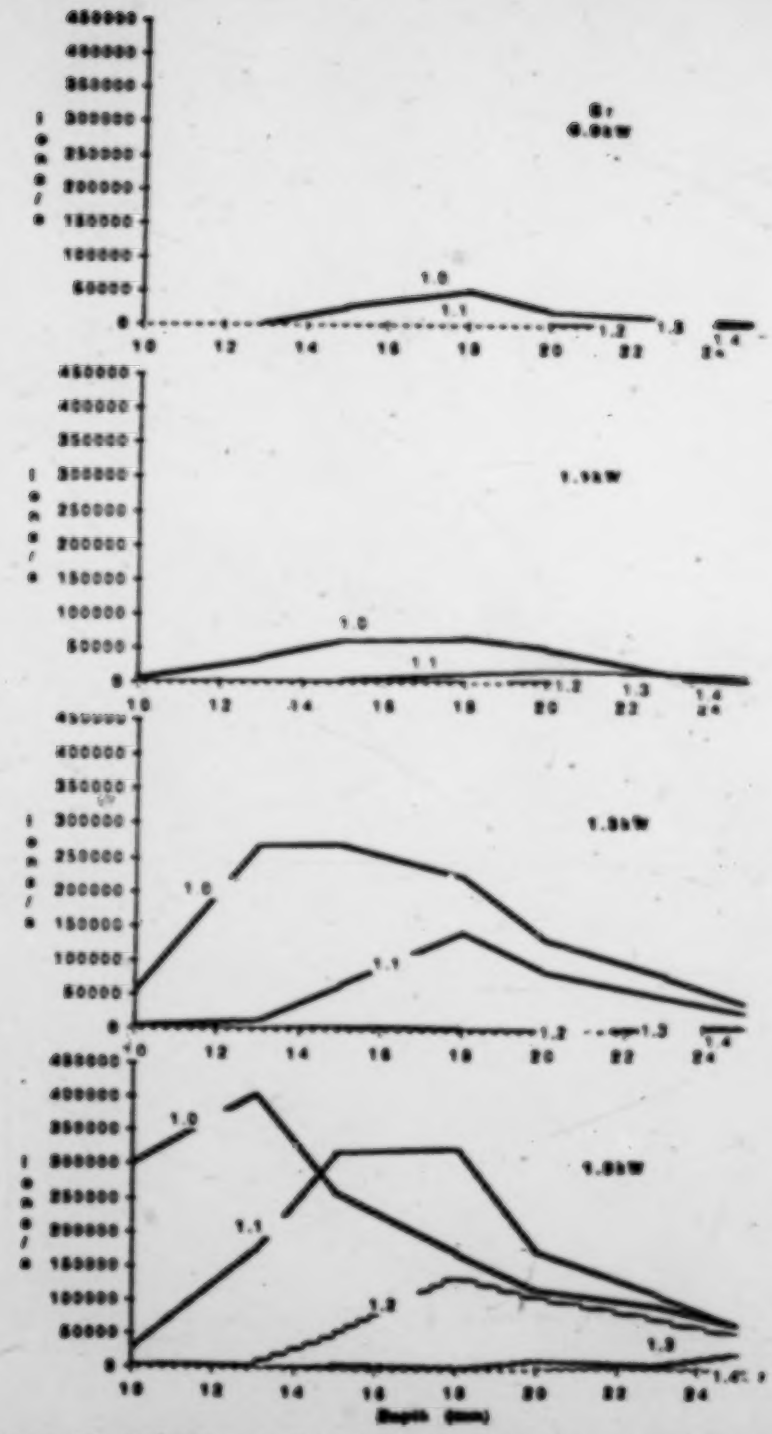

Figure 32. Sampling depth-nebulizer flowrate parameter plots for Sr at plasma rf powers of 0.9, 1.1, 1.3 and 1.5kW; nebulizer flowrate in l/min shown on each line

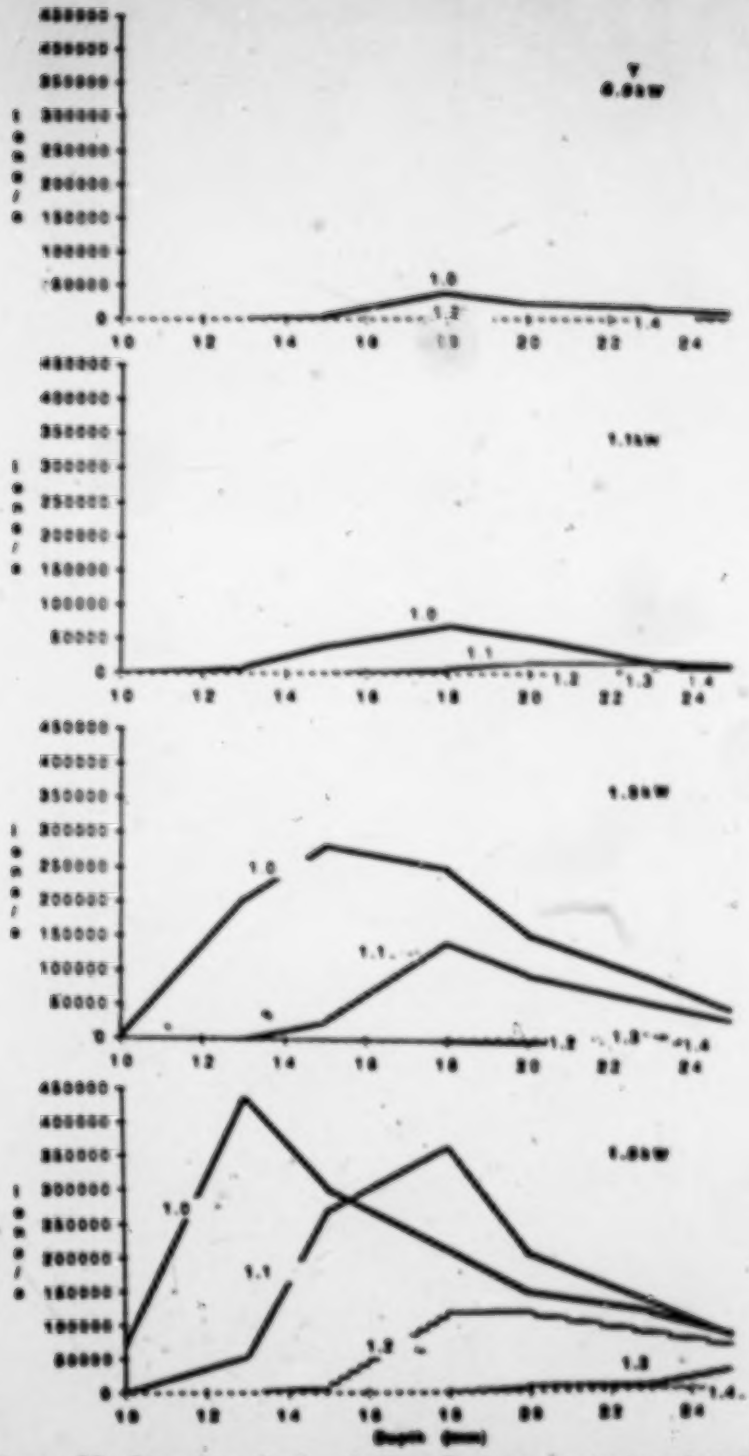

Figure 33. Sampling depth-nebulizer flowrate parameter plots for Y at plasma rf powers of 0.9, 1.1, 1.3 and 1.5kW; nebulizer flowrate in l/min shown on each line

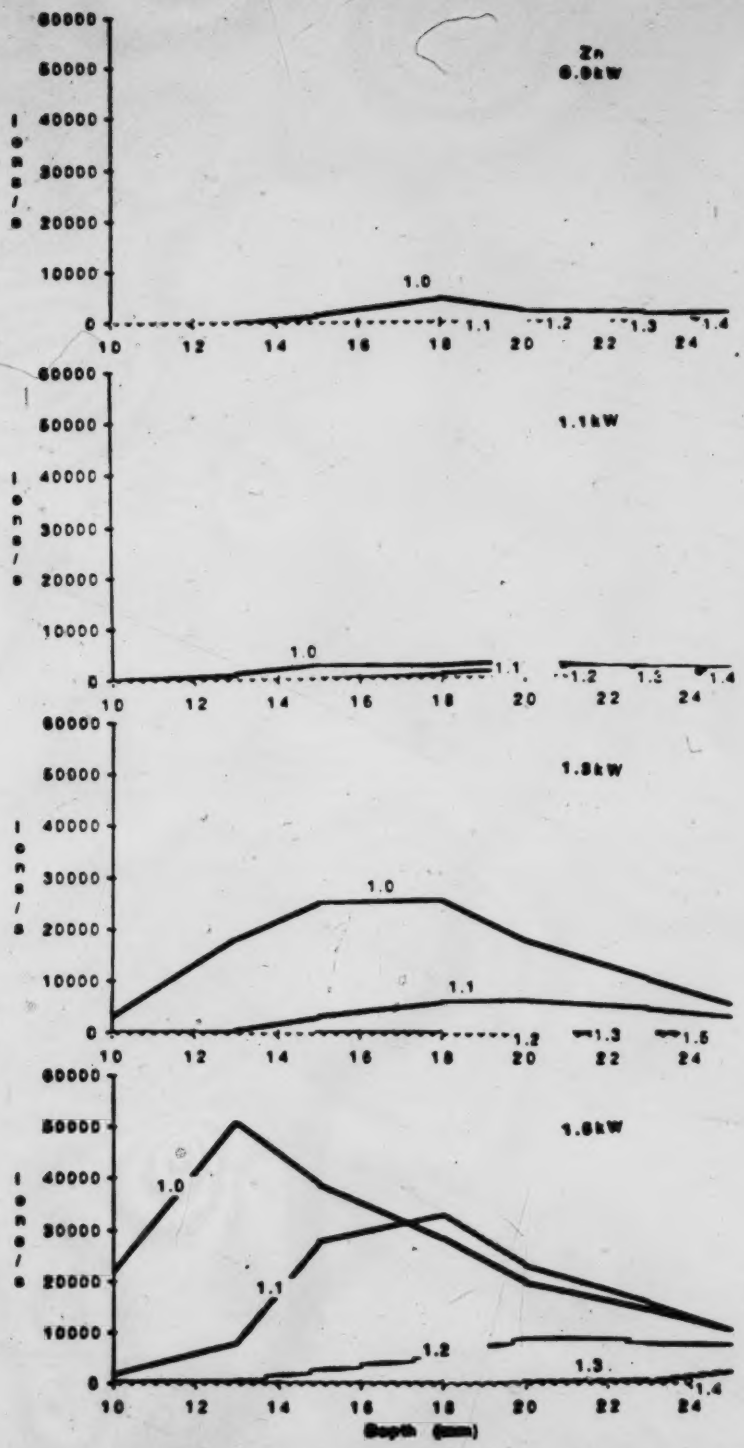

Figure 34. Sampling depth-nebulizer flowrate parameter plots for Zn at plasma rf powers of 0.9, 1.1, 1.3 and 1.5kW; nebulizer flowrate in l/min shown on each line

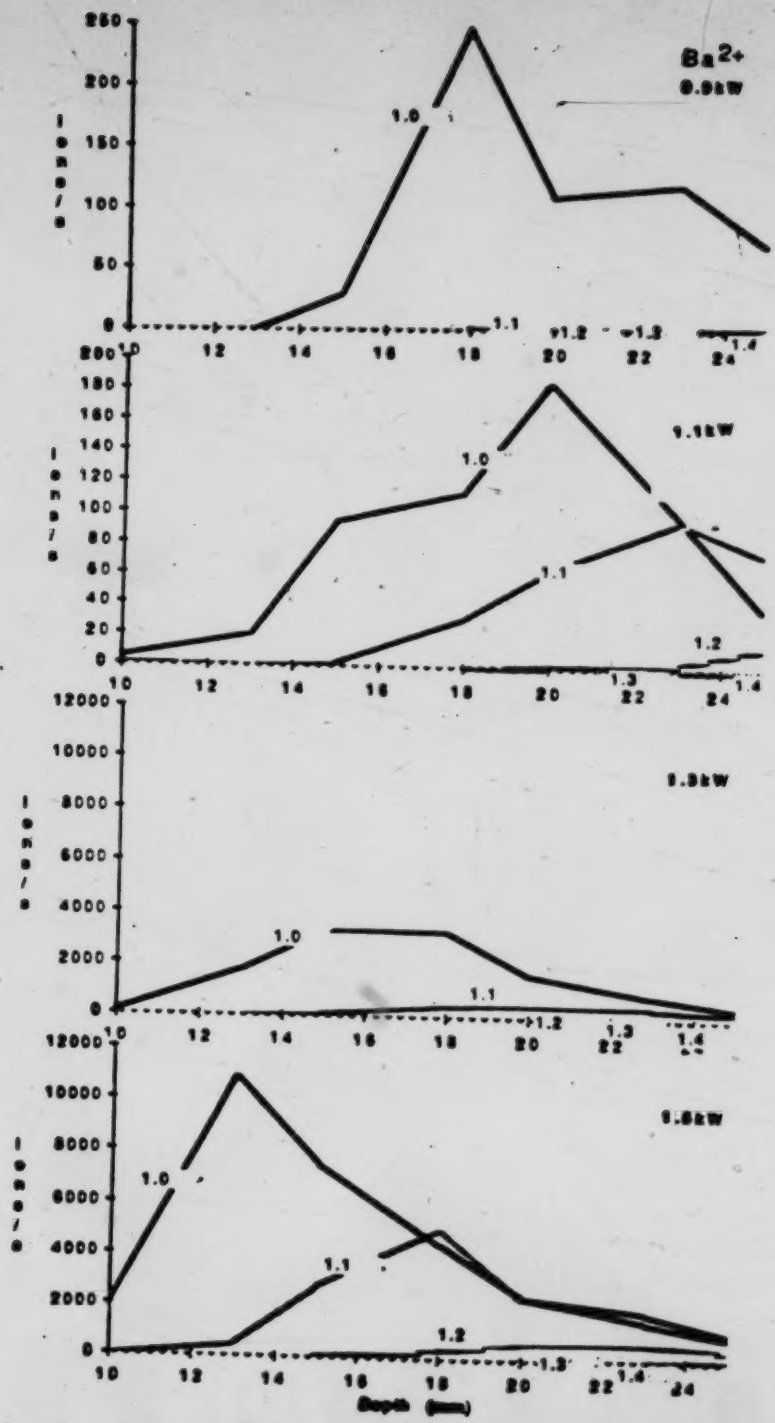

Figure 35. Sampling depth-nebulizer flowrate parameter plots for Ba^{2+} at plasma rf powers of 0.9, 1.1, 1.3 and 1.5kW; nebulizer flowrate in l/min shown on each line

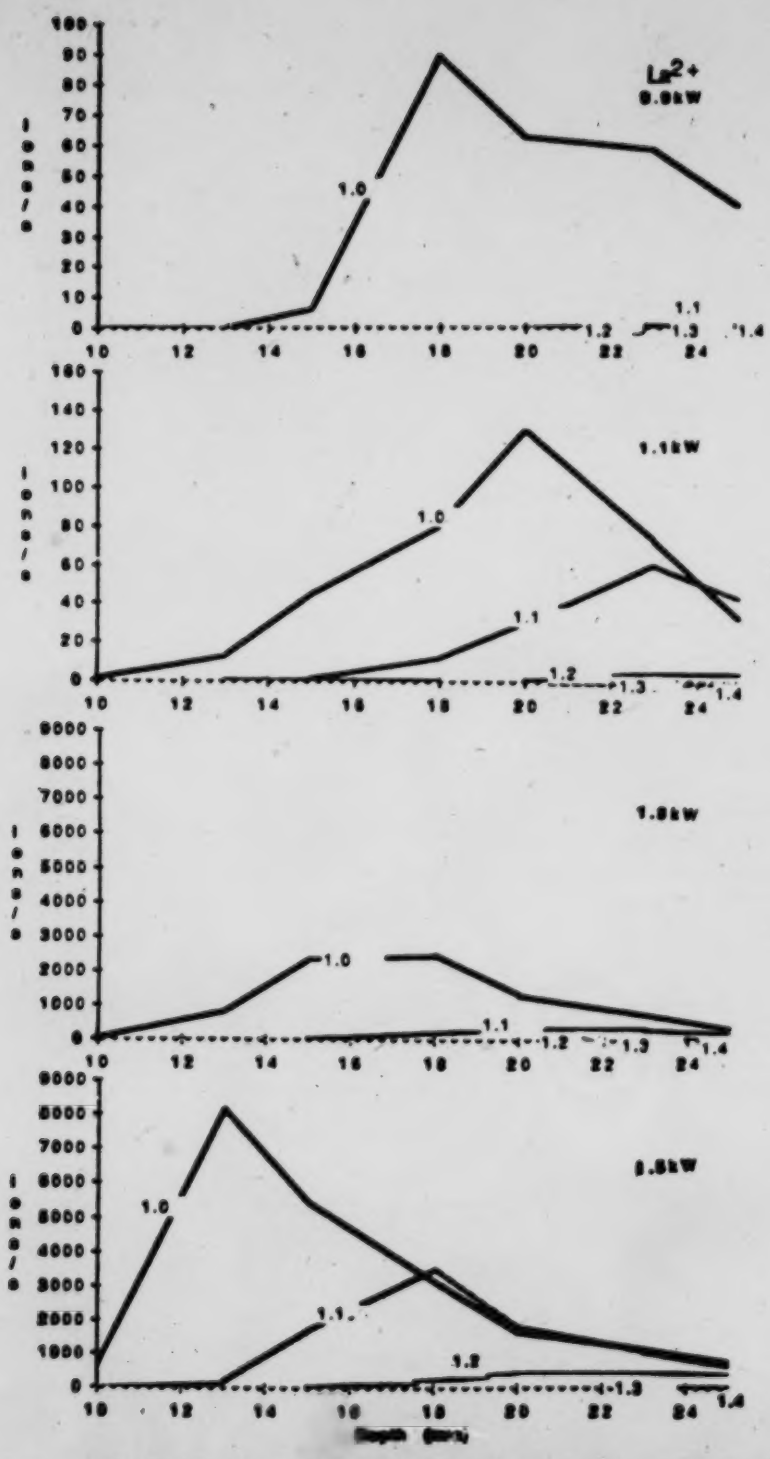

Figure 36. Sampling depth-nebulizer flowrate parameter plots for La^{2+} at plasma rf powers of 0.9, 1.1, 1.3 and 1.5kW; nebulizer flowrate in l/min shown on each line

last section, one can say that in order to achieve maximum sensitivity after increasing the nebulizer flowrate by 0.1 ℓ/min, one would have to increase the power by about 0.35kW.

Again, the observations in this display format can be explained by movements of the NAZ as the plasma power and nebulizer flowrate are varied. At a high power (1.5kW) the position of the NAZ exists close to the torch (i.e further away from the sampler) due to the high temperature of the plasma and the relatively short time that would be required for ionization to occur. Thus the NAZ would exist close to the torch, and a small sampling depth would be required for maximum sensitivity.

At high flowrates the plasma is comparatively cooler and the NAZ would exist further away from the torch end. Hence the maximum ion-count (sensitivity) would be obtained at a large sampling depth and this depth should increase as flowrate increases.

The same behaviour is observed for the doubly charged species.

D. Conclusion

The two display formats obtained by plotting ion-counts vs. nebulizer flowrate appear to be equally informative in selecting optimum analytical conditions. Both types of plots under this category show the peak positions for all depths and plasma powers. Since the peaks are clearly visible, selection of analytical conditions for maximum sensitivity is greatly facilitated.

The display formats showing the plots of ion-counts vs. depth can also aid in the selection of optimum analytical conditions but in this format some of the peak positions are not clearly shown

except at the optimum flowrate of about 1.0 ℓ/min. However the plots can be used to show very clearly the effects of varying sampling depth on the signal intensity measured. The fact that the peaks are broad would indicate that the ion-count measured is not very sensitive to small charges in sampling depth.

The display formats showing the plots of ion-counts v.s nebulizer flowrate can give an idea of the optimum conditions at a glance. Thus the conditions selected for further studies in the groundwater analysis was a sampling depth of 15mm and a plasma power of 1.3kW. Although a sampling depth of 10mm and a plasma power of 1.5kW would have resulted in higher sensitivity, the former conditions were selected so as to minimize background signal and erosion of the sampler.

CHAPTER IV

Determination of Major Elements

A. Introduction

Since all of the major elements are potential sources of isobaric interference, an estimate of their concentration should enable the analyst to recognize these interferences when they occur and should help in the selection of alternate isotopes for quantitative analysis. The concentrations were estimated by first, performing ICP-MS semi quantitative analysis on diluted samples and then performing quantitative analysis with ICP-AES, using the ARL 34000 ICP spectrometer. ICP-MS could not be used for the quantitative studies because of its high sensitivity which would require large dilutions of the sample to avoid instrument shut-down and because most of the major species suffer from interference problems in ICP-MS. Thus S overlaps with O_2 which is basic to the ICP. ^{54}Fe, ^{56}Fe, ^{57}Fe and ^{58}Fe are affected by $^{40}Ar^{14}N$, $^{40}Ar^{16}O$, $^{40}Ar^{16}OH$ and ^{58}Ni respectively. $^{35}Cl^{16}O$ overlaps with ^{51}V and $^{37}Cl^{14}N$ overlaps with ^{50}V. ^{40}Ca overlaps with ^{40}Ar which is used as the plasma gas and so cannot be measured without destroying the detector. ICP-AES on the other hand, does not have these interference problems.

B. Semiquantitative Analysis by ICP-MS

The semiquantitative analysis program (Semi-Quant) is used to determine the elements present in a sample and their approximate concentrations. Before carrying out a semi-quantitative analysis,

the instrument must be optimized by aspirating a solution containing Li, Rh and Pb and adjusting the plasma conditions and/or the lens settings until the Li and Pb peak intensities are equal and the Rh peak intensity is at a maximum.

The data acquisition and plasma operating conditions are shown in Table IV. The sampling depth was 15mm. All samples were prepared by mixing 20ml of each water sample with 20ml of 1ppm Rh solution. The 1ppm Rh stock solution contained 2% HNO_3 to prevent loss of analyte species from the samples through precipitation. Rhodium was used as the internal standard.

C. Results and Discussion

The Semi-Quant program computes the concentration of each element from its relative response factor after it has initially checked for its presence by comparing the elements isotopic abundance with its measured isotopic peak intensities. A default response table containing response factors in units of counts per second per ppm for all elements that are amenable to ICP-MS together with the normalized response factor of the internal standard and the intensity of each element is used to calculate concentrations.

Table V shows the semiquantitative report for the major elements for samples WW39-66. The detailed results for all samples can be used to obtain an approximate concentration range for each element of interest so that suitable standards can be prepared for

Table IV. ICP-MS semiquantitative analysis data acquisition and experimental parameters

Instrumental parameter	Range	Experimental value
Resolution	(High, Low, Man.)	L
Ion Multiplier HV	(25000 to 6000)	4000
Plasma RF Power (watts)	(500 to 2500)	1300
Auxiliary Flow L/min	(0 to 2.2)	1.4
Plasma Flow L/min	(0 to 22)	15.0
Nebulizer Flow L/min	(0 to 1.4)	1.0
Measurement/Peak	(1 to 20)	3
Scanning Mode	(Elem., Iso., Range)	R
Measurement Mode	(Seq, Multi, Trans)	S
Measurement Time (sec)	(0.001 to 500)	0.100
Repeats/Integration	(1 to 3200)	1
Threshold ion/sec	(1 to 50000)	50
Counting Precision %	(0.050 to 20)	0.100
Einzel lens(E1)	(00 to 99)	94
Bessel-box plates(P)	(00 to 99)	22
Bessel-box barrel(B)	(00 to 99)	45
Photon stop(S2)	(00 to 99)	25

Table V

Major elements semiquantitative analysis results for WW39-WW66

Sample #	B (ppm)	Ca (ppm)	Fe (ppm)	Mg (ppm)	S (ppm)	Sample #	Na (ppm)
WW39	3.6	N/A	5.5	158	2703	WW39	60
WW40	6.8	N/A	2.4	89	1087	WW40	78
WW41	2.4	N/A	2.4	77	1535	WW41	71
WW42	1.2	N/A	0.22	0.037	528	WW42	0.34
WW43	3.2	N/A	4.1	78	1571	WW43	63
WW44	3.3	N/A	12.9	89	1717	WW44	60
WW45	16.0	N/A	0.47	6.6	937	WW46	65
WW46	2.2	N/A	0.83	120	1260	WW48	56
WW47	13.9	N/A	0.82	8.3	839	WW49	61
WW48	3.2	N/A	0.52	17	1022	WW50	74
WW49	6.0	N/A	0.33	5.1	867	WW52	88
WW50	1.8	N/A	0.75	228	1882	WW53	57
WW52	2.1	N/A	1.7	265	2945	WW56	82
WW53	2.1	N/A	6.0	49	892	WW57	58
WW54	8.2	N/A	3.4	2.8	729	WW58	59
WW55	5.7	N/A	0.62	2.9	595	WW60	57
WW56	2.1	N/A	0.80	254	3596	WW62	54
WW57	4.5	N/A	0.71	5.3	783	WW63	49
WW58	4.9	N/A	0.34	6.5	1009	WW65	53
WW59	6.8	N/A	1.9	41	687	WW66	22
WW60	3.6	N/A	9.0	157	3091		
WW61	2.6	N/A	2.5	18	332		
WW62	2.3	N/A	9.0	67	1608		
WW63	2.4	N/A	5.4	63	1714		
WW65	1.6	N/A	0.91	201	2613		
WW66	0.94	N/A	0.71	27	617		

the quantitative analysis. Although the results are semiquantitative they can be used to predict possible interference problems that would occur in the trace element analysis. Thus the apparent large amount of sulphur in the samples means that isobaric interferences can be expected for ^{64}Zn, ^{66}Zn and ^{68}Zn due to $^{32}S^{16}O^{16}O$, $^{34}S^{16}O^{16}O$ and $^{36}S^{16}O^{16}O$ respectively. A more detailed list of the major isobaric species resulting from sulphur is shown in Table VI, [58]. The semiquantitative results for sulphur could, however, be much lower than listed in Table V because of sulphur being seriously interfered with by oxygen ($^{16}O^{16}O$) from the water solvent.

Magnesium and sodium are also shown to be present at a high concentration. The sodium concentration does not show a wide variation. The oxide and hydroxide species of Mg, shown in Table VII, interfere with Ca and K. However, since these species are not important for the trace element analysis and since Mg has not been shown to produce significant ionization interference at the concentrations reported, its effect on the trace analysis should be negligible.

Sodium, however, produces $^{23}Na^{40}Ar$ and $Na_2{}^{16}O$ which interfere with ^{63}Cu and ^{62}Ni and is also known to cause a matrix effect if present at high concentrations. The fact that the Na concentrations reported do not vary greatly from sample to sample would imply that matrix matching of sample and standards should result in a good correction for any matrix effect (normally signal suppression) caused by Na.

Table VI. Isobaric interfering species associated with S

Element	Mass	%Abund	Assoc. species	Mass	Affected Elements (% abund.)
S	32	95.02	$S^{14}N$	46	Ti(7.99), Ca(0.003)
S	33	0.75	$S^{14}N$	47	Ti(7.32)
S	34	4.21	$S^{14}N$	48	Ti(73.98), Ca(0.19)
S	36	0.02	$S^{14}N$	50	Ti(5.25), Cr(4.35), V(0.24)
S	32	95.02	$S^{16}O$	48	Ti(73.98), Ca(0.19)
S	33	0.75	$S^{16}O$	49	Ti(5.46)
S	34	4.21	$S^{16}O$	50	Ti(5.25), Cr(4.35), V(0.24)
S	36	0.02	$S^{16}O$	52	Cr(83.75)
S	32	95.02	$S^{16}O^{16}O$	64	Zn(48.9), Ni(1.16)
S	33	0.75	$S^{16}O^{16}O$	65	Cu(30.9)
S	34	4.21	$S^{16}O^{16}O$	66	Zn(4.11)
S	36	0.02	$S^{16}O^{16}O$	68	Zn(18.57)
S	32	95.02	$S^{32}S$	64	Zn(48.89), Ni(1.16)
S	33	0.75	$S^{32}S$	65	Cu(30.9)
S	34	4.21	$S^{32}S$	66	Zn(27.81),
S	36	0.02	$S^{32}S$	68	Zn(18.75)
S	32	95.02	^{40}ArS	72	Ge(27.4)
S	33	0.75	^{40}ArS	73	Ge(7.76)
S	34	4.21	^{40}ArS	74	Ge(36.56), Se(0.87)
S	36	0.02	^{40}ArS	76	Ge(7.77), Se(9.02)
S	32	95.02	$S^{16}O^{16}O^{16}O$	80	Se(49.82), Kr(2.27)
S	33	0.75	$S^{16}O^{16}O^{16}O$	81	Br(49.46)
S	34	4.21	$S^{16}O^{16}O^{16}O$	82	Kr(11.56), Se(9.19)
S	36	0.02	$S^{16}O^{16}O^{16}O$	84	Kr(56.9), Sr(0.56)
S	32	95.02	$S^{16}O^{16}O^{16}OH$	81	Br(49.46)
S	33	0.75	$S^{16}O^{16}O^{16}OH$	82	Kr(11.56), Se(9.19)
S	34	4.21	$S^{16}O^{16}O^{16}OH$	83	Kr(11.55)
S	36	0.02	$S^{16}O^{16}O^{16}OH$	85	Rb(72.2)

Table VII. Isobaric interfering species associated with Ca, Mg, Fe, Na and Al

Element	Mass	%Abund.	Assoc. species	Mass	Affected elements (%abund.)
Ca	40	96.97	$Ca^{16}O$	56	Fe(91.7)
Ca	42	0.64	$Ca^{16}O$	58	Ni(67.7),Fe(0.33)
Ca	43	0.145	$Ca^{16}O$	59	Co(100)
Ca	44	2.06	$Ca^{16}O$	60	Ni(26.2)
Ca	46	0.003	$Ca^{16}O$	62	Ni(3.66)
Ca	48	0.185	$Ca^{16}O$	64	Zn(48.9),Ni(1.16)
Ca	40	96.97	$Ca^{16}OH$	57	Fe(2.19)
Ca	42	0.64	$Ca^{16}OH$	59	Co(100)
Ca	43	0.145	$Ca^{16}OH$	60	Ni(26.2)
Ca	44	2.06	$Ca^{16}OH$	61	Ni(1.25)
Ca	46	0.003	$Ca^{16}OH$	63	Cu(69.1)
Ca	48	0.185	$Ca^{16}OH$	65	Cu(30.9)
Mg	24	78.80	$Mg^{16}O$	40	Ar(99.6),Ca(96.97),K(0.01)
Mg	25	10.15	$Mg^{16}O$	41	K(6.91)
Mg	26	11.05	$Mg^{16}O$	42	Ca(0.64)
Mg	24	78.80	$Mg^{16}OH$	41	K(6.91)
Mg	25	10.15	$Mg^{16}OH$	42	Ca(0.64)
Mg	26	11.05	$Mg^{16}OH$	43	Ca(0.14)
Fe	54	5.82	$Fe^{16}O$	70	Ge(20.5),Zn(0.62)
Fe	56	91.66	$Fe^{16}O$	72	Ge(27.4)
Fe	57	2.19	$Fe^{16}O$	73	Ge(7.76)
Fe	58	0.33	$Fe^{16}O$	74	Ge(36.6),Ge(7.77)
Fe	54	5.82	$Fe^{16}OH$	71	Ga(39.8)
Fe	56	91.66	$Fe^{16}OH$	73	Ge(7.76)
Fe	57	2.19	$Fe^{16}OH$	74	Ge(36.6),Ge(7.77)
Fe	58	0.33	$Fe^{16}OH$	75	As(100)
Na	23	100	NaNa	46	Ca(0.003),Ti(7.99)
Na	23	100	$Na_2{}^{16}O$	62	Ni(3.66)
Na	23	100	$Na_2{}^{16}OH$	63	Cu(69.1)
Na	23	100	$Na^{40}Ar$	63	Cu(69.1)
Al	27	100	$Al^{16}O$	43	Ca(0.14)
Al	27	100	$Al^{16}OH$	44	Ca(2.06)
Al	27	100	$Al_2{}^{16}O_3$	102	Ru(31.6),Pd(0.96)
Al	27	100	$Al_2{}^{16}O_3H$	103	Rh(100)

Iron and boron are not present at high concentrations and should not cause interference problems with the analytes of interest.

No results were obtained for Calcium because of ^{40}Ar overlapping with ^{40}Ca making measurement at this mass impossible.

D. Quantitative Determination of Major Elements by ICP-AES

Spex industries single element standards were used for all standard preparation. Preparation of multi-element standards for ICP-AES involves grouping elements together so as to avoid spectral overlap problems, to obtain standards that would be stable over a long period of time and to prepare standards that would bracket the concentration range of the unknowns. Previous work done in our lab indicated the required element grouping. Table VIII shows the composition of the standards used. All standards were prepared to contain 2% HNO_3 to avoid precipitation of metals from solution and were stored in clean plastic bottles.

Samples were prepared by diluting equal volumes of the unknown and 2% HNO_3 so that each resulting solution was of the same acidity. All samples were stored in clean plastic bottles.

Prior to analysis with the ARL 34000S ICP spectrometer, a Task file and a Calibration (Cal) file must be created. The Task file contains the data acquisition parameters and description of the standards. Table VIII also shows the content of the Task file used for the analysis.

The Cal file contains information on the intensity data for

Table VIII

Calibration scheme for ICP-AES: major element analysis

TASK FILE FOR ICP-AES MAJOR ELEMENT ANALYSIS

PRE-FLUSH TIME (SECONDS) 20
INTEGRATION TIME (SECONDS) 10
NUMBER OF INTEGRATIONS 3

ELEMENT	CONCENTRATION IN STANDARDS (ppm)						
	1	2	3	4	5	6	7
B	0	1	10	100			
Ba	0	1	10	100			
Fe	0	1	10	100			
Li	0	1	10	100			
Ca					1	10	100
Mg					1	10	100
Na					10	100	1000
S					1	10	100

each standard and the regression analysis curves for each element. The file is built after the instrument has been calibrated by running the program 'Cal'.

Throughout the time of analysis the instrument was frequently checked for instrumental drift by analyzing one of the multielement standard solutions. If a significant drift was evident, the instrument was recalibrated and the samples that were run prior to that check re-analyzed.

E. Results and Discussion

The calibration curves of all the elements studied are shown in Figure 37. They are all log-log plots and are linear over the concentration range studied. The slopes of all the plots are essentially unity.

The concentrations obtained for the elements are shown in Tables IX and X. The precision (relative standard deviation) of each measurement is also shown. The average concentration for each element in all the water samples is shown in the last row.

Sodium has the highest average concentration (245ppm) followed by sulphur (50ppm), calcium (48ppm), and magnesium (18ppm). Boron and Iron have an average concentration of less than 1ppm.

Most of the results obtained in the ICP-MS Semiquantitative results (Table V) are higher than their corresponding quantitative results by an order of magnitude or less. The difference between the semiquantitative results for sulphur, however, is more than an

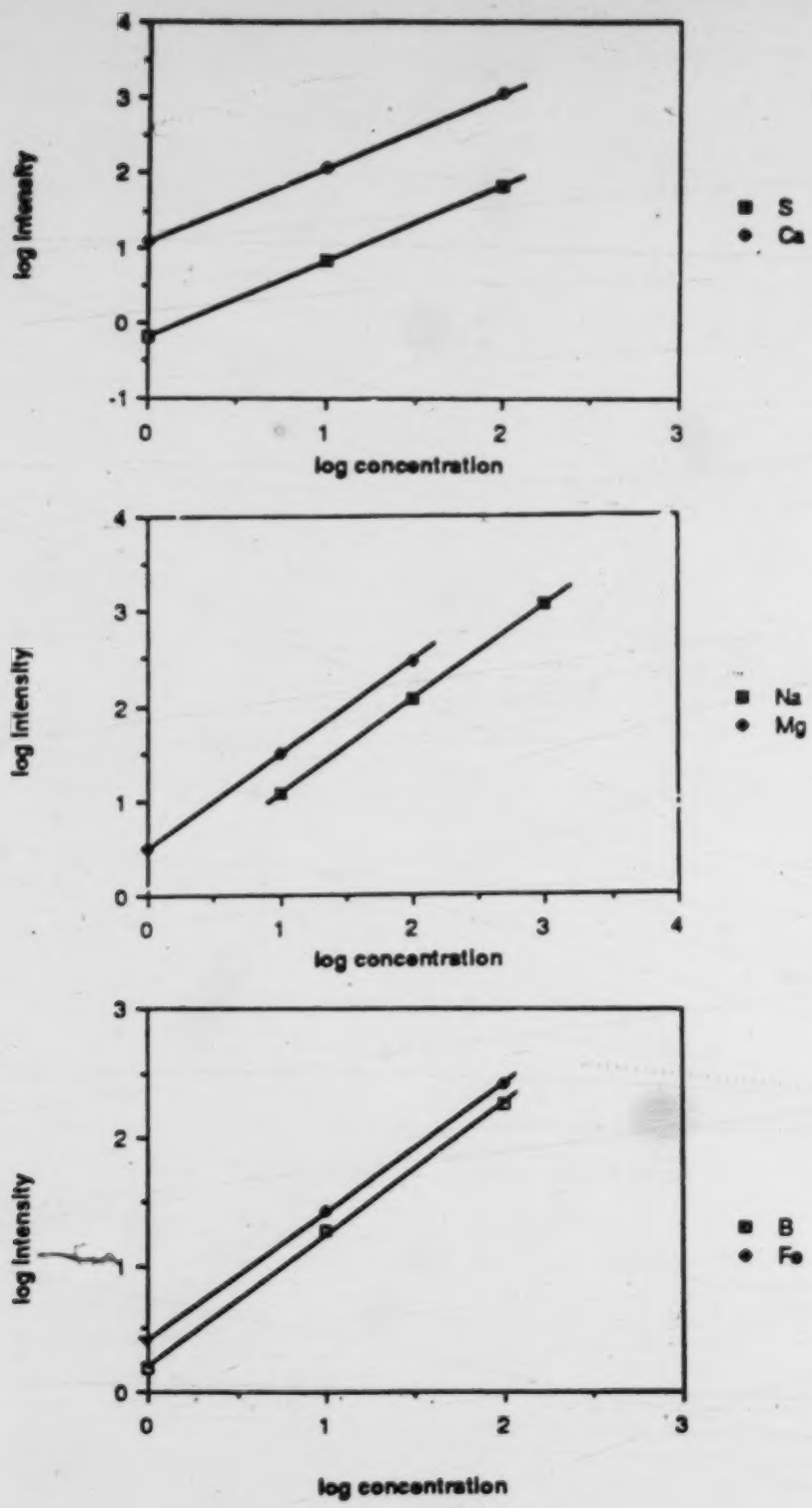

Figure 37. ICP-AES Calibration Curves for S, Ca, Na, Mg, B and Fe

Table IX

Major element analysis report; WW27-WW52

SAMPLE NO.	B (ppm)	RSD	Fe(ppm)	RSD	Ca(ppm)	RSD	Mg(ppm)	RSD	Na(ppm)	RSD	S(ppm)	RSD
WW27	0.17	1.2	2.1	0.2	99.0	0.2	49	0.2	106.3	0.3	100.5	0.4
WW28	0.29	2.2	3.2	0.4	61.6	0.4	30	0.5	208.2	0.4	84.3	0.4
WW29	0.060	1	<0.013		95.7	0.2	35	0.2	19.0	0.3	23.0	0.8
WW30	0.78	1	0.10	2.9	5.0	0.3	1.5	1	261.5	0.1	33.4	0.4
WW31	0.51	0.7	0.035	4.4	7.5	0.9	2.3	0.7	341.8	0.1	84.2	0.7
WW32	1.2	0.4	0.033	4.8	3.2	0.3	0.6	2.4	354.1	0.5	62.1	1.2
WW33	0.36	0.5	0.23	0.1	6.5	0.4	1.7	0.4	174.9	4	25.5	0.1
WW34	0.92	0.5	0.22	0.2	5.5	0.2	1.3	0.4	263.6	0.3	39.4	0.3
WW35	0.80	1.9	0.21	2.1	21.5	0.6	4.2	1	402.8	0.4	137.7	0.5
WW36	0.026	16	0.15	1.4	59.4	0.1	15	0.5	9.2	0.4	13.9	2.1
WW37	1.4	0.6	0.31	0.3	10.1	0	2.4	0.2	839.3	0.2	0.4	9.4
WW38	0.59	1.2	0.024	5.3	32.7	0.1	16	0.3	218.3	0.2	52.4	0.2
WW39	0.35	1.1	1.9	0	98.2	0.1	38	0.1	144.8	0.2	119.3	0.4
WW40	0.44	1.3	0.59	0.4	50.3	0.3	19	0.4	734.8	0.3	8.3	2.5
WW41	0.19	1.2	0.76	0.5	71.8	0.4	28	0.5	122.3	0.5	60.9	0.6
WW42	0.33	1.8	2.8	0.2	40.0	0.2	18	0.2	214.8	0.2	66.0	0.2
WW43	0.25	1	1.5	0.6	61.8	0.2	26	0.6	133.4	0.6	52.5	1.3
WW44	0.33	2.4	4.7	0.3	67.5	0.2	29	0.3	148.6	0.3	63.4	0.3
WW45	1.5	1	0.019	3.2	5.7	0.5	1.3	1	612.6	0.2	0.4	21.5
WW46	0.20	2.9	0.073	1.9	80.3	0.3	32	0.4	97.0	0.5	49.4	0.6
WW47	1.4	0.5	0.18	0.2	8.1	0.4	2.1	1	742.0	0.4	0.4	11
WW48	0.37	0.7	0.080	1	27.5	0.3	6.1	0.3	217.8	0.5	30.1	2
WW49	0.87	0.4	0.036	6	7.5	0.3	1.9	1.5	200.2	0.1	16.1	0.7
WW50	0.092	3.5	0.050	5.4	107.8	0.1	61	0.1	33.9	0.4	53.6	0.4
WW51	0.32	1	0.82	0.1	16.8	0.4	4.4	0.3	217.6	0.5	29.7	0.3
WW52	0.081	3.8	0.28	1.3	170.8	0.1	59	0.1	36.9	0.1	130.1	0.3

Table X

Major element analysis report; WW53-WW76

SAMPLE NO.	B (ppm)	RSD	Fe(ppm)	RSD	Ca(ppm)	RSD	Mg(ppm)	RSD	Na(ppm)	RSD	S(ppm)	RSD
WW53	0.31	1.2	2.1	0.3	69.5	0.2	18	0.3	93.0	0.2	26.3	0.2
WW54	1.1	0.4	1.1	0.4	3.7	0.4	0.9	1.8	426.9	0.4	0.5	21.1
WW55	0.80	0.6	0.15	0	4.7	0.4	1.1	0.9	462.0	0.6	0.5	17.8
WW56	0.21	1.4	0.049	3.7	199.5	0.4	74	0.4	124.6	0.5	243.8	0.8
WW57	0.83	1.1	0.18	1	9.2	0.3	2.3	1.2	378.6	0.3	15.4	0.4
WW58	0.70	0.3	0.020	4.2	8.4	0.4	2.3	1.4	346.5	0.4	26.7	0.1
WW59	1.0	0.2	0.59	0.5	35.5	0.4	16	0.4	517.2	0.4	1.0	5.4
WW60	0.43	2.7	3.3	0.3	117.9	0.3	45	0.3	224.2	0.3	165.6	1.3
WW61	0.91	0.6	2.0	0.3	35.2	0.4	15	0.3	366.2	0.5	0.8	5.2
WW62	0.30	0.9	3.5	0.2	77.3	0.1	28	0.2	111.2	0.1	64.1	0.3
WW63	0.38	1.2	2.3	0.2	73.0	0.2	30	0.2	117.7	0.1	98.6	0.7
WW64	0.27	0.5	0.014	2	0.6	0.3	0.1	4.4	287.1	0.2	65.8	0.5
WW65	0.16	1.5	0.11	0.5	154.0	0.3	65	0.3	74.5	0.4	145.5	0.3
WW66	0.056	3.2	0.058	1.5	83.4	0.2	14	0.3	16.5	0.2	11.0	1.1
WW67	0.55	0.8	0.36	0.4	6.8	0.2	3.4	0.5	183.2	0.2	9.5	1.7
WW68	1.2	0.3	0.26	0.7	3.4	0.2	1.8	1.7	227.8	0.1	0.4	16
WW69	0.055	7.5	0.019	0.8	98.0	0.4	30	0.4	14.1	0.7	19.5	0.6
WW70	0.73	0.4	0.51	0.2	13.2	0.2	5.7	0.3	183.7	0.2	0.5	17.1
WW71	0.60	0.7	1.1	0.1	3.7	0	1.1	1.5	399.5	0.2	107.6	0.3
WW72	0.76	0.6	0.19	0.6	18.8	0.1	6.2	0.2	162.2	0.2	0.6	19.8
WW73	0.20	0.7	4.2	0.3	72.5	0.2	36	0.1	109.4	0.2	71.9	0.9
WW74	0.19	1	4.3	0.2	72.8	0.2	36	0.1	109.8	0.2	71.6	1.2
WW75	0.94	0.2	0.18	0.2	14.9	0.3	7.4	0.3	226.3	0.4	7.4	2
WW76	0.93	0.4	0.067	1.8	2.0	0.5	0.7	0.8	224.8	0.5	3.5	2.8
AVERAGE	0.55		0.96		48.0		18.4		244.8		49.9	

order of magnitude in most cases. This large difference may be due to O_2 interference in sulphur analysis by ICP-MS.

The high concentration of Mg, Ca, S and Na would indicate that their isotopes, oxides and other species are potential causes of isobaric interference in ICP-MS trace element analysis, for elements with which they overlap. The high concentration of Na could also result in matrix induced signal suppression interference in samples with high Na Concentration. Ca and S with much lower concentration may only cause negligible signal changes. Since the presence of sodium at a high concentration in a matrix can cause signal intensity changes in ICP-MS [60] a study of the effect of sodium on ICP-MS signals of the elements of interest was conducted and the effectiveness of rhodium as an internal standard for this interference correction was also studied. This is reported in the next chapter.

Rhodium was selected because it had been extensively used in our lab for previous ICP-MS analysis studies and has been shown to compensate for instrumental drift in steel analysis [67]. It meets most of the requirements for an internal standard for ICP-MS analysis: it is not present in the groundwater sample at significant levels, it is monoisotopic and is not a strong oxide former which means it is not a major source of oxide and other species that could cause isobaric spectral overlap. It is also in the mid-mass range-103, and so would have a compromise response for any mass effects.

CHAPTER V

Determination of Trace Elements

A. Introduction

In order to develop a method for quantitative analysis of trace elements in ground-water it is essential to assess the effects of matrix induced signal intensity changes that could affect the analytical results obtained. It is also important to find out how the use of an internal standard could reduce such matrix effects. Data presented in the previous chapter showed that sodium is present in some of the samples at a level that could result in matrix induced signal intensity changes. Studies done on this aspect with respect to groundwater analysis will be presented in this chapter and the degree of effectiveness of rhodium as an internal standard in correcting this interference will be presented. Then an analysis of the trace elements will be carried out using both the ICP-MS and ICP-AES techniques. Results obtained from both techniques will be used to check the accuracy of the analytical results. Finally, spectral overlap interferences in the ICP-MS analysis of groundwater will be assessed.

Our goal is to show the analytical considerations in ICP-MS groundwater analysis and to evaluate the significance of isobaric spectral overlap interferences.

B. Na Matrix Effect and Internal Standardization

1. EXPERIMENTAL:

Spex industries single element standard solutions, analytical reagent grade NaF and HNO_3 were used to prepare the following stock solutions: 1ppm Ba, Sr, Co, Ca, Ni, V, U, Zn in 2% HNO_3, 1ppm Rh in 2% HNO_3 and 2000ppm NaF in 2% HNO_3. The solutions were then used to prepare four stock solutions each with 0.1ppm Ba, Sr, Co, Cu, Ni, V, U, Zn, Rh but with varying amounts of Na. The concentration of Na in the solutions was Oppm, 10ppm, 100ppm to 1000ppm. These four solutions were used for the experiment.

The data acquisition and instrument parameters used are shown in Table XI. All measurements were carried out at a sampling depth of 15mm and an rf power of 1.3kW. Each of the four stock solutions were nebulized in turn while the nebulizer flowrate was varied from 0.7 /min to 1.2 /min. The nebulizer flowrate was controlled by a Matheson model 8240-0423 mass flow controller.

2. Results and Discussions

The effect of varying nebulizer flowrate and varying sodium matrix concentration on the ion signal of the elements studied are shown in Figures 38-45. The bottom plot of each figure is a plot of the ratio of the ion count of the element to that of rhodium, the element used as the internal standard.

It should be noted from the figures that although the elements studied are in different groups of the periodic table: alkali

Table XI. Data acquisition and instrumental parameters for ICP-MS optimization studies

Instrumental parameter	Range (High, Low, Man.)	Experimental value
Resolution		L
Ion Multiplier HV	(25000 to 6000)	4000
Plasma RF Power (watts)	(500 to 2500)	1300
Auxiliary Flow L/min	(0 to 2.2)	1.4
Plasma Flow L/min	(0 to 22)	15.0
Nebulizer Flow L/min	(0 to 1.4)	varied in steps of 0.05l/min
Measurement/Peak	(1 to 20)	3
Scanning Mode	(Elem., Iso., Range)	E
Measurement Mode	(Seq, Multi, Trans)	S
Measurement Time Sec	(0.001 to 500)	0.100
Repeats/Integration	(1 to 3200)	3
Threshold ion/sec	(1 to 50000)	50
Counting Precision %	(0.050 to 20)	0.100
Einzel lens(E1)	(00 to 99)	94
Bessel-box plates(P)	(00 to 99)	22
Bessel-box barrel(B)	(00 to 99)	45
Photon stop(S2)	(00 to 99)	25

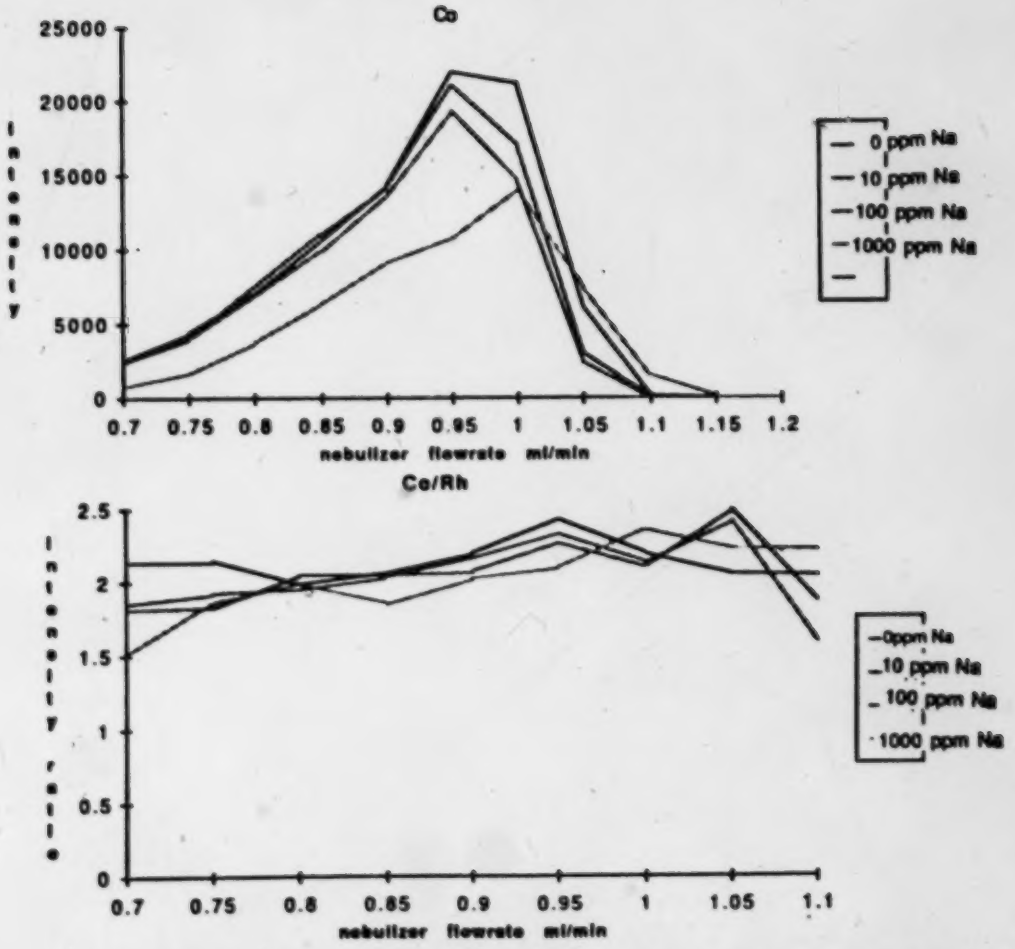

Figure 38. Effects of varying nebulizer flowrate and Na concentration on the Co signal

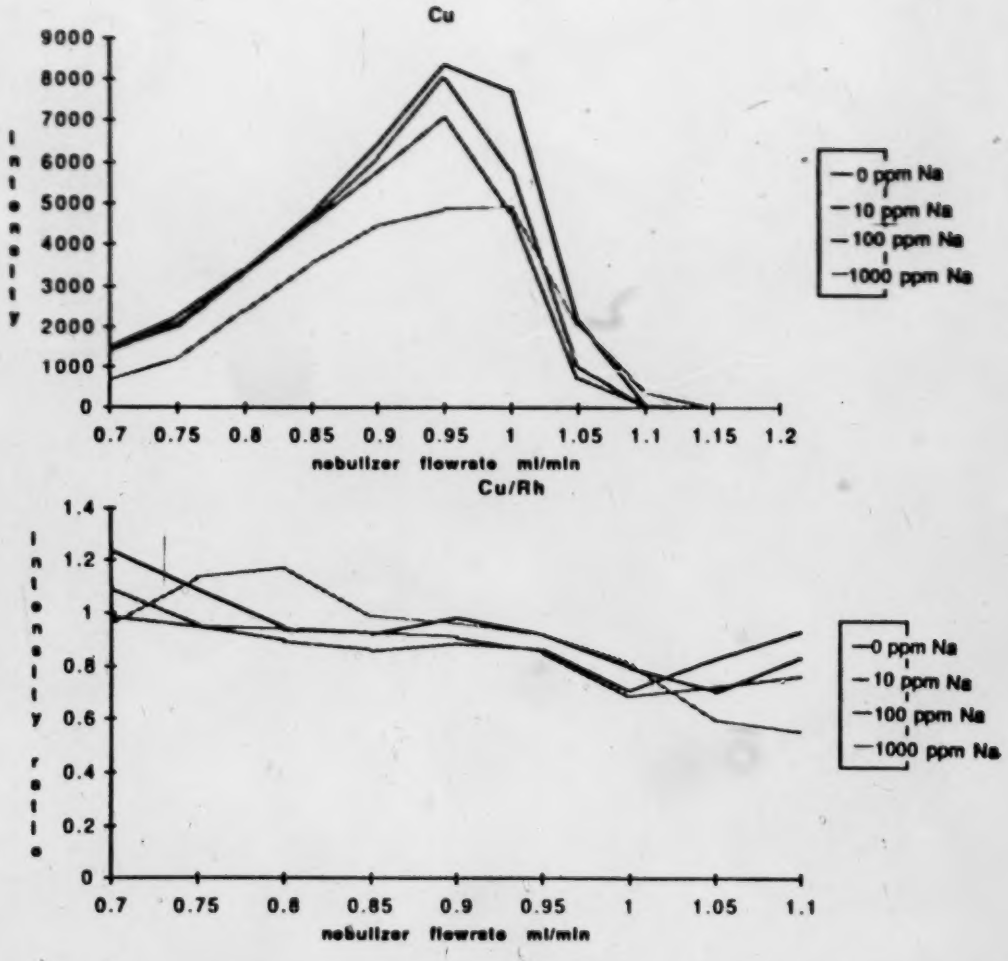

Figure 39. Effects of varying nebulizer flowrate and Na concentration on the Cu signal

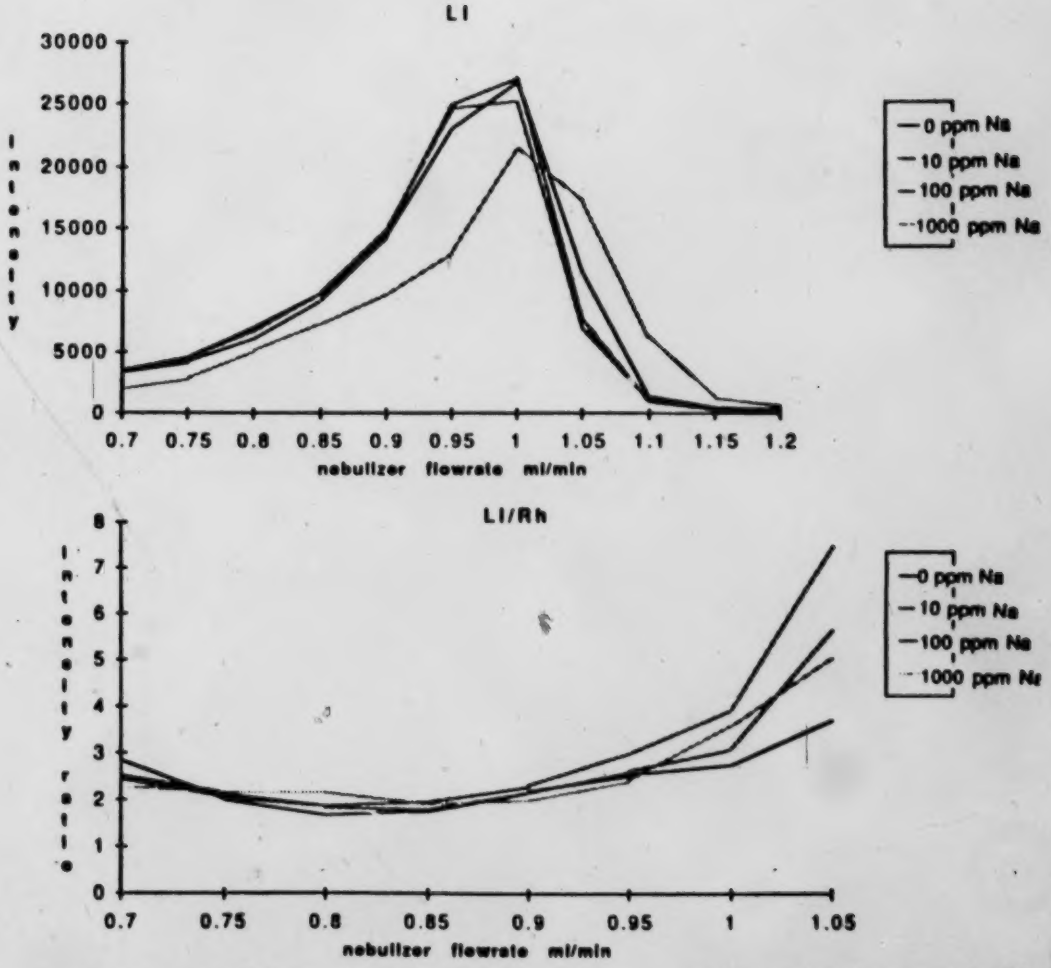

Figure 40. Effects of varying nebulizer flowrate and Na concentration on the Li signal

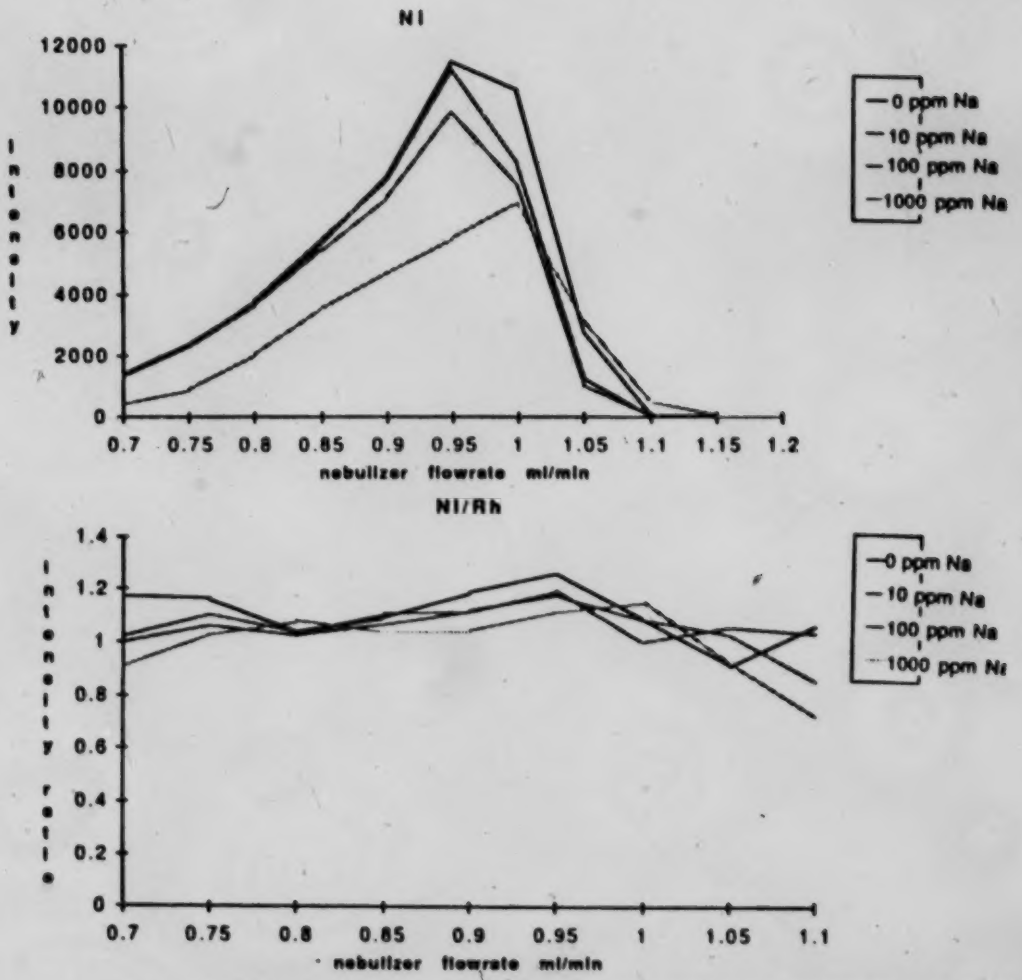

Figure 41. Effects of varying nebulizer flowrate and Na concentration on the Ni signal

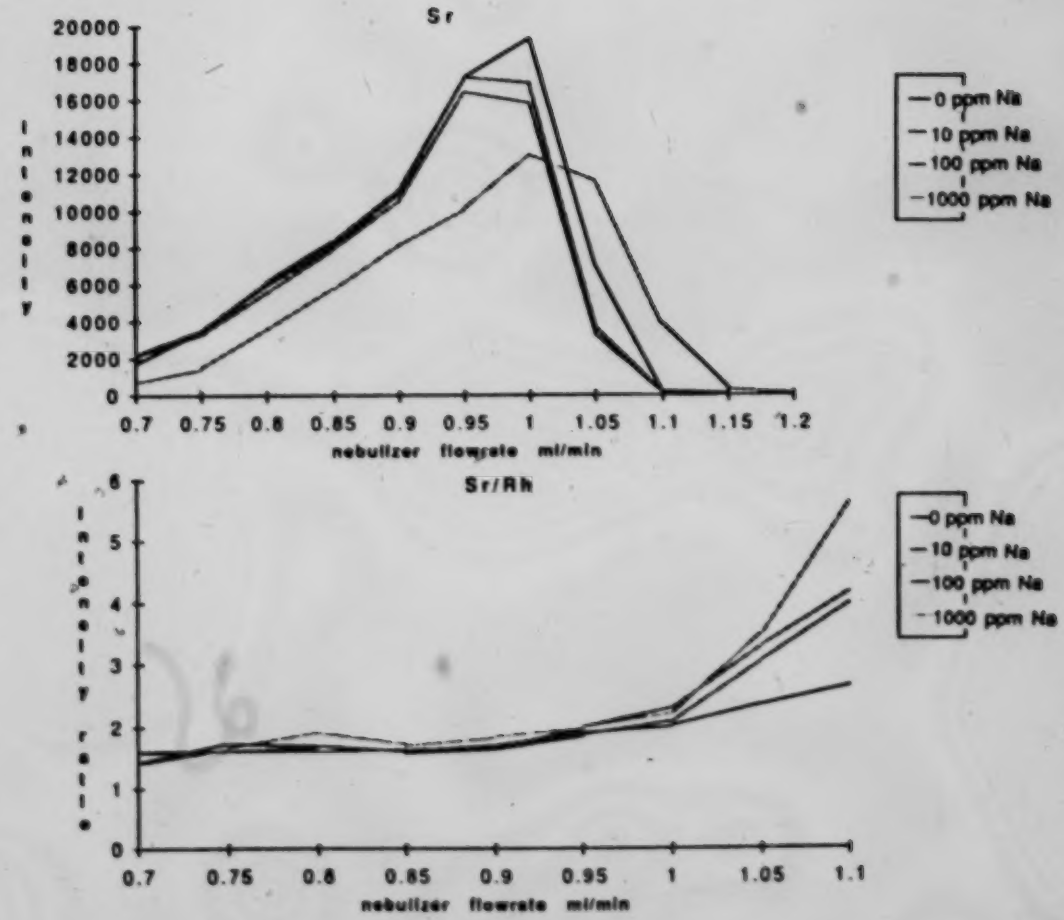

Figure 42. Effects of varying nebulizer flowrate and Na concentration on the Sr signal

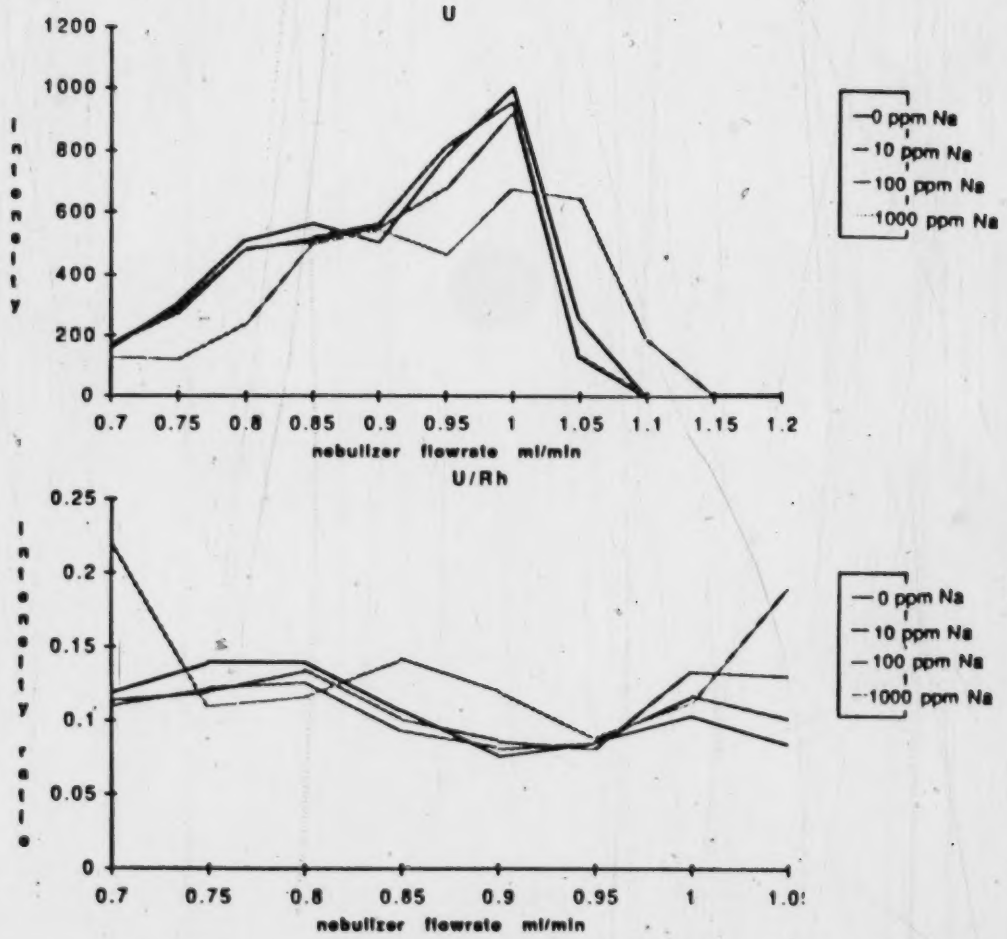

Figure 43. Effects of varying nebulizer flowrate and Na concentration on the U signal

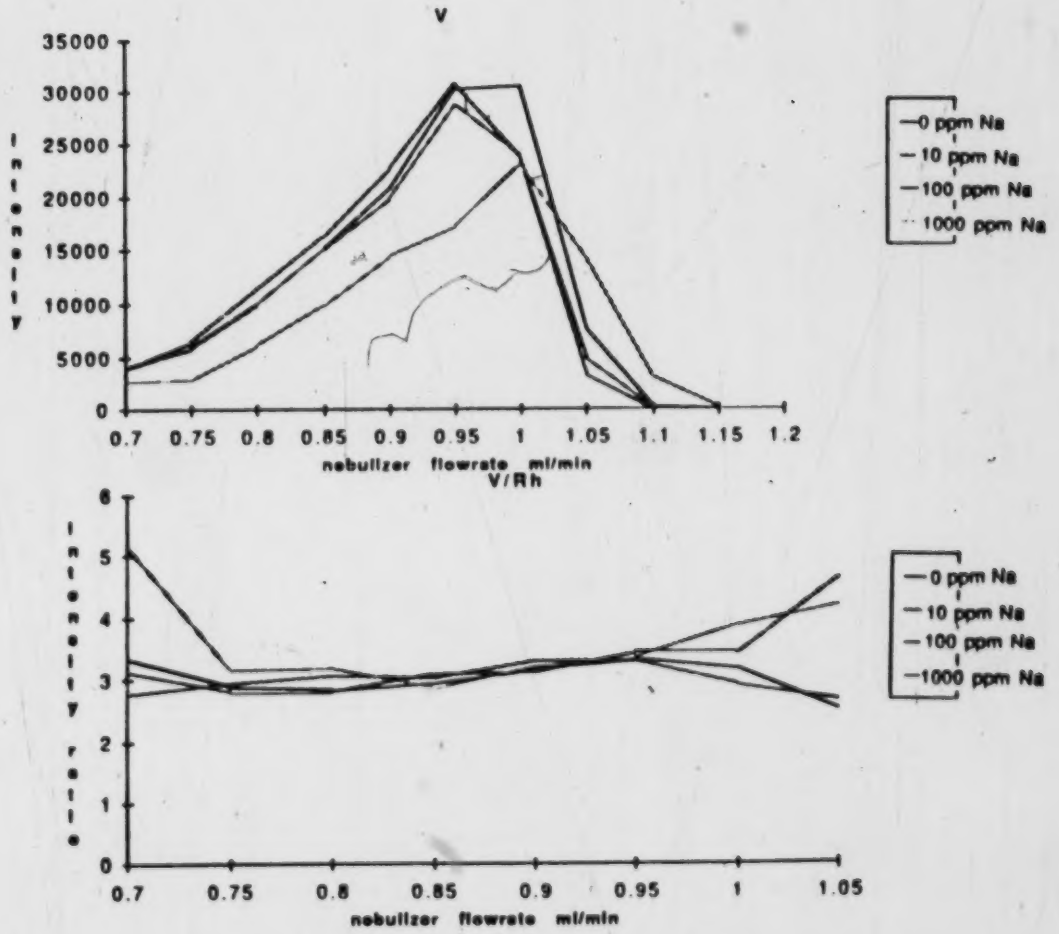

Figure 44. Effects of varying nebulizer flowrate and Na concentration on the V signal

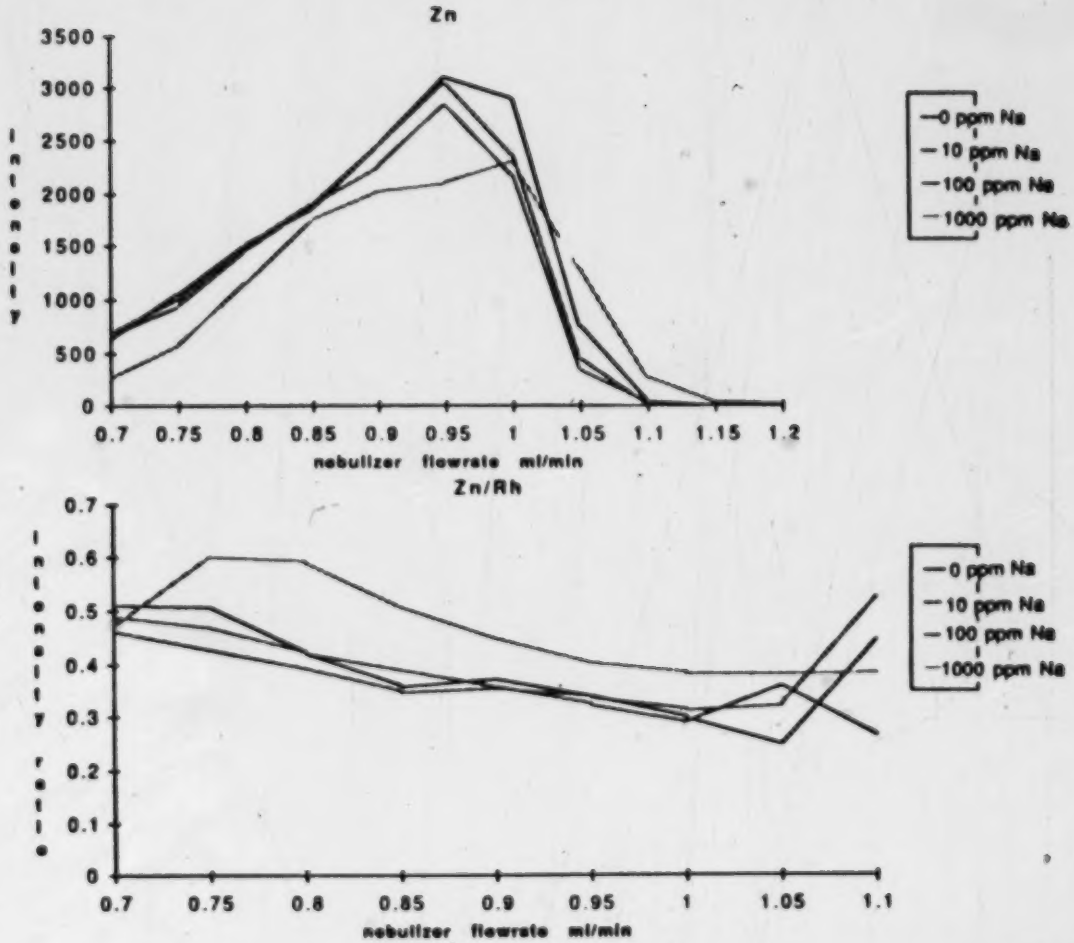

Figure 45. Effects of varying nebulizer flowrate and Na concentration on the Zn signal

metals, alkaline earth metals, transition metals and rare earth metals, they all gave an ion signal peak close to 0.95 ℓ/min. The signal intensity is strongly dependent on nebulizer flowrate, dropping off quickly on either side of the peak maximum. Thus to improve precision in analytical results, it is very important to avoid large fluctuations in nebulizer flowrate by using a mass flow controller, and using an internal standard to correct for very small fluctuations.

Signal suppression at the peak maximum was observed for all elements as the concentration of sodium in the matrix increased. At flowrates to the left of this peak maximum, a suppression is indicated, especially for the 1000ppm Na matrix, however, at flowrates to the right of the maximum an enhancement is indicated. Thus, the type of matrix effect observed depends on the nebulizer flowrate at which the measurement is taken. For a Na matrix concentration of less than 100ppm, the data show that signal suppression can be reduced by using a low flowrate, but this can only be done by sacrificing sensitivity. Increasing the sodium concentration from 0 to 100ppm does not seem to have any significant effect on the position of the peak maximum. However, a small shift from 0.95 ℓ/min to 1 ℓ/min occurs with 1000ppm Na.

The bottom plots of each figure show that rhodium is a fairly good selection for the internal standard. Ideally, the plots for each sodium concentration for each element should be horizontal, and should overlap each other. Most of the plots approximate this ideal situation between 0.8 ℓ/min and 1.0 ℓ/min. On either side of this range the internal standard does not correct properly. This is probably due to the low signal intensities at these flowrates. Such low signal intensities have large noise components making measurement precision poor. The zinc plot does not show effective correction for the 1000ppm Na matrix. No explanation could be given for this behaviour.

Since Rh appeared to be a suitable internal standard it was used for the ICP MS quantitative analysis, and a flowrate of 0.95 ℓ/min was used for maximum sensitivity.

C. ICP-MS and ICP-AES Quantitative Analysis

1. Standard Preparation

Spex industries single element standard solutions and analytical reagent grade NaF were used to prepare the following stock solutions

(a) 10ppm Ba, Sr, Zn, Co, Cu, Li, U

(b) 1ppm Rh, In

(c) 2000ppm Na

(d) 2% HNO_3

Multielement stock solutions of Ba, Sr, Zn, Co, Cu, Li, U with concentrations ranging from 0.05-2ppm were then prepared by

appropriate dilutions. All solutions were prepared in 2% HNO_3 and were matrix matched with the samples by adding enough of the 2000ppm sodium stock to give 250ppm Na in all standards. Finally each standard was diluted with the 1ppm Rh, In stock solution. A dilution factor of 2 was used.

The same standards were used for both ICP-MS and ICP-AES calibration. Rhodium was used as the internal standard for the ICP-MS analysis and In was used for the ICP-AES analysis as there is no rhodium channel on the ARL 34000 ICP spectrometer.

A solution of 250ppm Na in 2% HNO_3 was used as the blank. All solutions used for calibration are shown in Table XII.

2. Experimental

The data acquisition and plasma operating conditions stored in the parameter file for ICP-MS analysis are shown in Table XIII and those of the Task file for the ICP-AES analysis are shown in Table XIV.

For the ICP-MS analysis, a sampling depth of 15mm and an rf power of 1.3kW were used. A Matheson model 8240--423 mass flow controller was used to control the nebulizer flowrate. Sample introduction was by a Meinhard nebulizer and a Scott type spray chamber. A peristaltic pump was used to ensure even delivery of sample solution to the nebulizer. Data were acquired with the mass spectrometer running in the low resolution mode and multielement mode. A measurement time of 0.5 Sec was used for each mass peak,

Table XII

Calibration Scheme for ICP-MS trace element analysis

ELEMENT	CONCENTRATION IN STANDARD(ppm)						
STANDARD #	1	2	3	4	5	6	7
Sr	0	0.05	0.08	0.1	0.2	0.5	1
Ba	0	0.05	0.08	0.1	0.2	0.5	1
V	0	0.05	0.08	0.1	0.2	0.5	1
Cb	0	0.05	0.08	0.1	0.2	0.5	1
U	0	0.05	0.08	0.1	0.2	0.5	1
NI	0	0.05	0.08	0.1	0.2	0.5	1
Cu	0	0.05	0.08	0.1	0.2	0.5	1
LI	0	0.05	0.08	0.1	0.2	0.5	1
Zn	0	0.05	0.08	0.1	0.2	0.5	1
Rh	0	0.1	0.1	0.1	0.1	0.1	0.1
In	0	0.1	0.1	0.1	0.1	0.1	0.1

Table XIII. Data acquisition and instrumental parameters for ICP-MS trace element analysis.

Instrumental parameter	Range	Experimental value
Resolution	(High, Low, Man.)	L
Ion Multiplier HV	(25000 to 6000)	4000
Plasma RF Power (watts)	(500 to 2500)	1300
Auxiliary Flow L/min	(0 to 2.2)	1.4
Plasma Flow L/min	(0 to 22)	15.0
Nebulizer Flow L/min	(0 to 1.4)	0.95
Measurement/**Peak**	(1 to 20)	5
Scanning mode	(Elem., Iso., Range)	E
Measurement Mode	(Seq, Multi, Trans)	M
Measurement Time Sec	(0.001 to 500)	0.500
Repeats/Integration	(1 to 3200)	5
Dwell Time ms	(1 to 500000)	50
Cycle Time Sec	(0.001 to 10)	0.100
Einzel lens(E1)	(00 to 99)	4
Bessel-box plates(P)	(00 to 99)	22
Bessel-box barrel(B)	(00 to 99)	45
Photon stop(S2)	(00 to 99)	25

Table XIV. Data acquisition and instrumental parameters for ICP-AES trace element analysis

PRE-FLUSH TIME (SECONDS) 20							
INTEGRATION TIME (SECONDS) 10							
NUMBER OF INTEGRATIONS 3							
SAMPLING HEIGHT 15mm							
NEBULIZER FLOWRATE 0.7L/min							
ELEMENT		CONCENTRATION IN STANDARDS (ppm)					
	1	2	3	4	5	6	7
Sr	0	0.05	0.08	0.1	0.2	0.5	1
Ba	0	0.05	0.08	0.1	0.2	0.5	1
V	0	0.05	0.08	0.1	0.2	0.5	1
Co	0	0.05	0.08	0.1	0.2	0.5	1
U	0	0.05	0.08	0.1	0.2	0.5	1
Ni	0	0.05	0.08	0.1	0.2	0.5	1
Cu	0	0.05	0.08	0.1	0.2	0.5	1
Li	0	0.05	0.08	0.1	0.2	0.5	1
Zn	0	0.05	0.08	0.1	0.2	0.5	1
Rh	0	0.1	0.1	0.1	0.1	0.1	0.1
In	0	0.1	0.1	0.1	0.1	0.1	0.1

and all intensity data acquired were an average of five repetitive measurements at each mass. All data were dumped from the Elan computer to a Macintosh computer and processed with the Microsoft Excel Spreadsheet and Cricket Graph applications Software.

The ICP-AES analysis was carried out at a viewing height of 15mm and an rf power of 1.2kW. A Meinhard nebulizer and Scott type spray chamber with direct aerosol injection were used for sample introduction. A 10 second integration time was used with three repeats of each integration. Data were acquired by the PDP 11/03 DEC computer and outputted to an LA36DEC hardcopy printer terminal.

For both ICP-MS and ICP-AES analysis, quality control was done by frequent analysis of the multielement standards. If a large deviation was obtained, the instruments were recalibrated, and all samples before that check, re-analyzed.

3. Results and Discussion

The ICP-MS and ICP-AES calibration curves are shown in Figures 46-47 and Figure 48 respectively. All plots are log-log plots with six calibration points. The slopes obtained for all the ICP-MS and ICP-AES calibration curves are shown in Table XV. All the plots are linear, and with the exception of the ^{6}Li plot, have a slope close to unity. The reason for the ^{6}Li deviation is not apparent but the slope (log c vs. log i) indicates a positive error in the concentration for the standards and since ^{7}Li does not show the same error, the problem cannot have been due to contamination. The small isotopic abundance of this isotope and a small memory effect could be

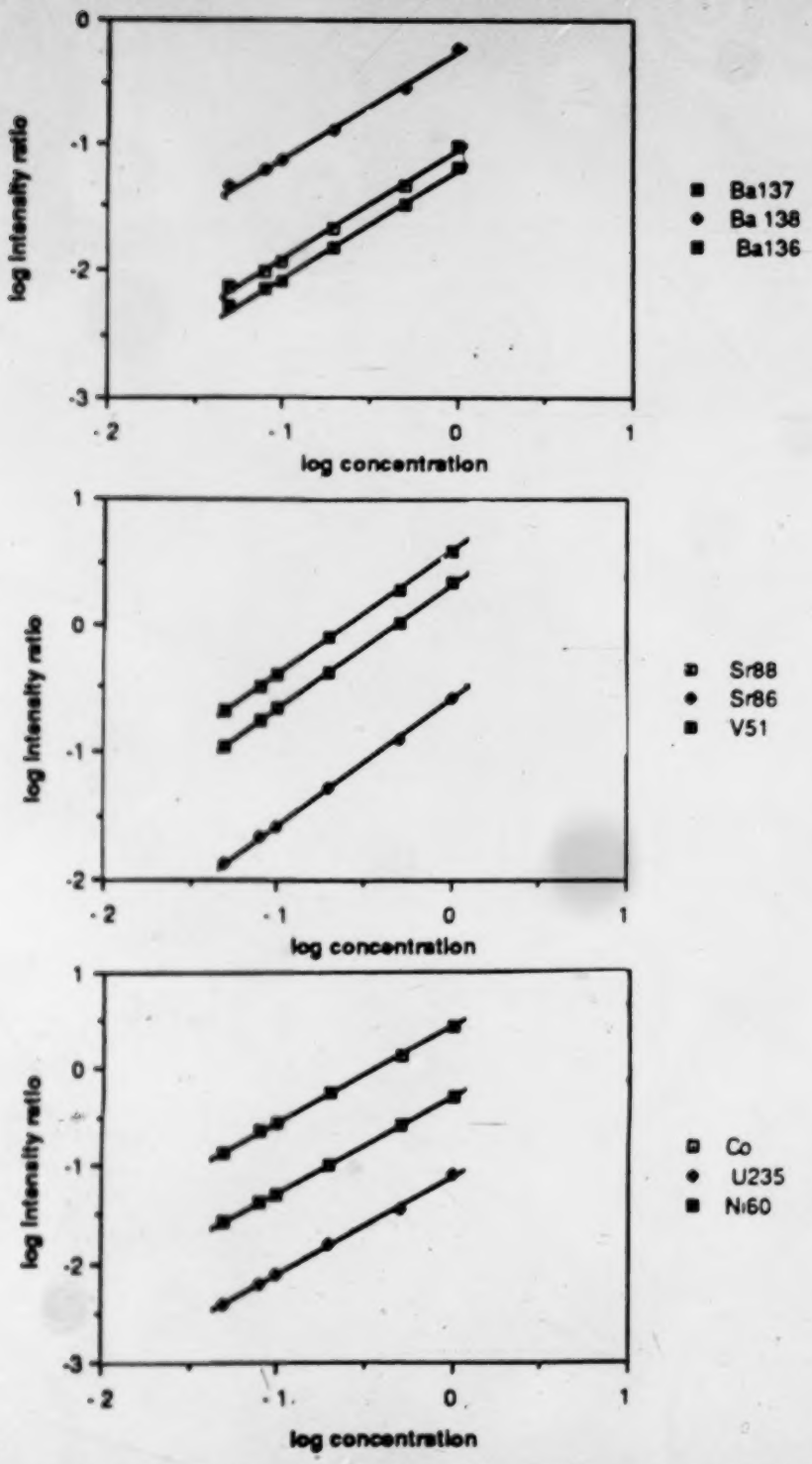

Figure 46. ICP-MS calibration curves for ^{136}Ba, ^{137}Ba, ^{138}Ba, ^{88}Sr, ^{86}Sr, ^{51}V, Co, ^{235}U

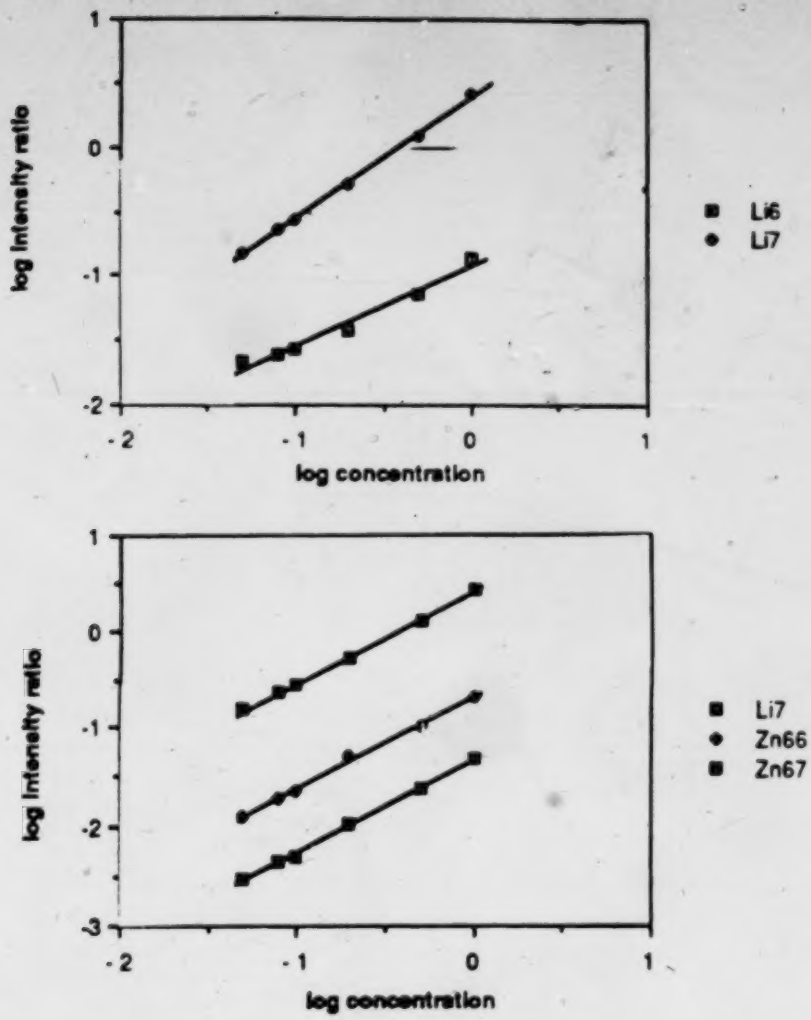

Figure 47. ICP-MS calibration curves for ^{6}Li, ^{7}Li, ^{66}Zn and ^{67}Zn

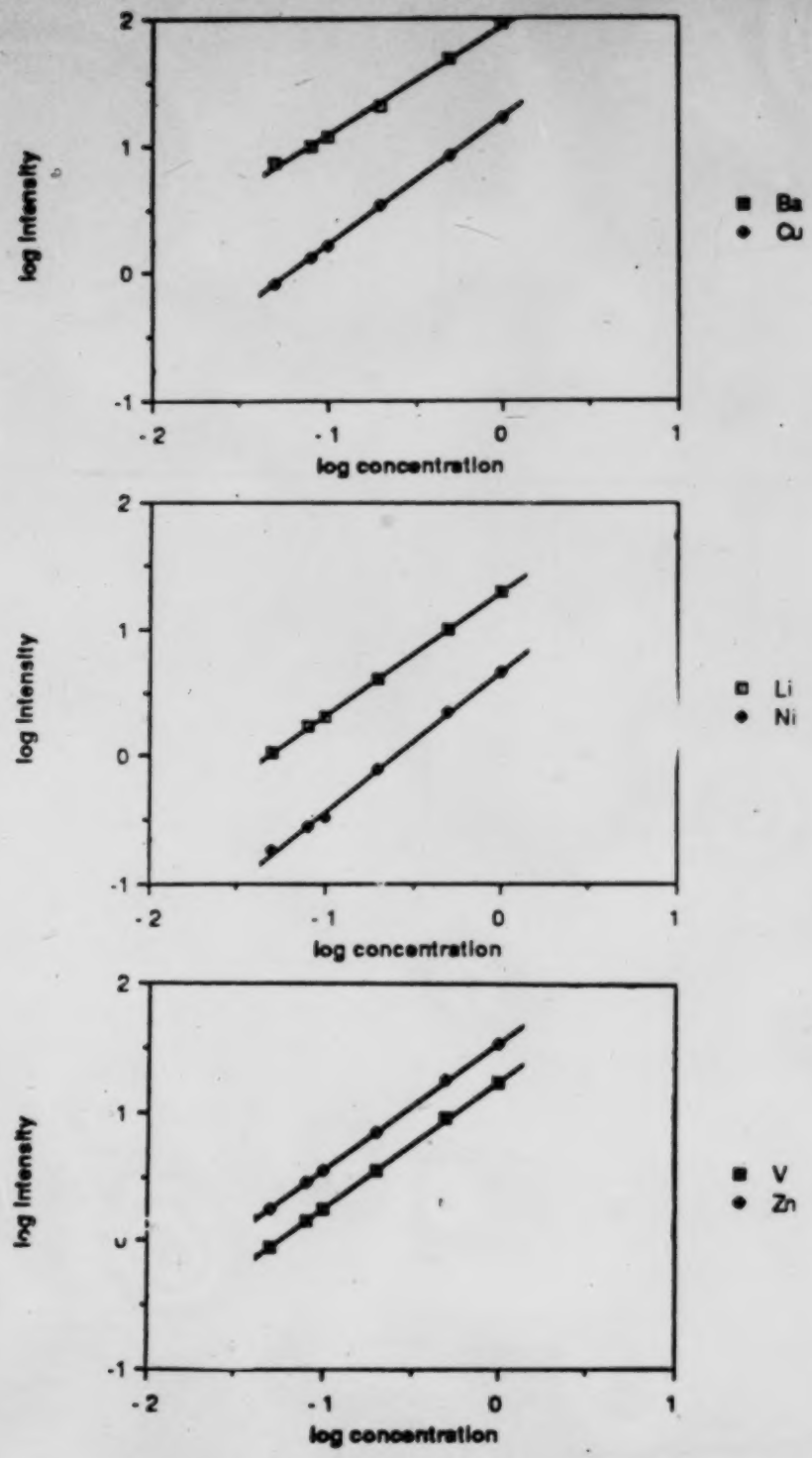

Figure 48. ICP-AES Calibration Curves for Ba, Cu, Li, Ni, V and Zn

Table XV. Slopes of ICP-MS and ICP-AES log-log calibration curves

	log i vs. log c*	log i vs. log c	log c vs. log i		log i vs. log c	log i vs. log c	log c vs. log i
ELEMENT	ICP-MS SLOPE	STD. ERR SLOPE	ICP-MS SLOPE	ELEMENT	ICP-AES SLOPE	STD. ERR SLOPE	ICP-AES SLOPE
Co	0.98	0.004	1.02	Ba	0.85	0.024	1.18
U235	0.98	0.016	1.02	Cu	0.998	0.004	1.00
Ni60	0.98	0.003	1.02	Li	0.973	0.006	1.03
Ni62	0.93	0.013	1.07	Ni	1.1	0.024	0.91
Cu63	0.96	0.004	1.04	V	0.99	0.003	1.01
Cu65	0.96	0.005	1.04	Zn	0.99	0.006	1.01
Li6	0.64	0.051	1.57				
Li7	0.95	0.017	1.05				
Zn66	0.93	0.025	1.07				
Zn67	0.93	0.020	1.08				
Sr88	0.98	0.007	1.02				
Sr86	0.99	0.010	1.01				
Ba137	0.86	0.030	1.16				
Ba138	0.86	0.027	1.17				
Ba136	0.85	0.023	1.17				
V51	0.98	0.003	1.03				

* c= concentration
i= ion count

possible contributors to the problem.

The analytical results obtained for both ICP-MS and ICP-AES are tabulated together in Tables XVI-XXI. Two or more isotopes were selected whenever possible for the ICP-MS results. The isotopes were selected so as to avoid major spectral overlap interference problems that would have resulted from nitrogen, oxygen and doubly charged species. Hence in some cases, the major isotope of the element was not used for analysis. Results obtained with the ICP-AES technique (Precision:0-20% RSD) were used to check the accuracy of the ICP-MS results (Precision:0.1-30% RSD).

In the absence of interference, the concentration obtained for all the isotopes of an element should be close to one another within experimental limits and should also be close to concentration values obtained using other techniques that are free from interference problems. Disagreement between such values is indicative of interference problems.

Comparing the concentrations obtained for the different isotopes, strontium and barium show very good agreement for all samples analyzed. This agreement is clearly shown in Figures 49 and 50 which show column plots for the concentration obtained from ^{138}Ba and ^{137}Ba and from ^{88}Sr and ^{86}Sr respectively in all the samples analyzed.

The other elements (Ni, Cu, Li and Zn) did not show good agreement between the two isotopes used for analysis. Figure 51 shows the plot for ^{66}Zn and ^{67}Zn Isotopes. The concentration reported from the ^{66}Zn was always higher than that of ^{67}Zn. The

Table XVI

ICP-MS and ICP-AES trace element analysis report for Sr and Ba In WW27-WW52

Sample number	ICP-MS Sr88 ppm	ICP-MS Sr86 ppm	ICP-AES Ba ppm	ICP-MS Ba137 ppm	ICP-MS Ba138 ppm	ICP-MS Ba136 ppm
WW27	0.74	0.74	0.016	0.017	0.015	0.017
WW28	0.51	0.52	0.029	0.030	0.028	0.028
WW29	0.47	0.46	0.077	0.076	0.077	0.078
WW30	0.10	0.11	0.018	0.019	0.018	0.020
WW31	0.17	0.17	0.012	0.013	0.013	0.013
WW32	0.07	0.07	0.018	0.020	0.018	0.017
WW33	0.12	0.12	0.016	0.015	0.016	0.016
WW34	0.11	0.11	0.0059	0.0067	0.0057	0.0067
WW35	0.43	0.44	0.0053	0.0068	0.0065	0.0075
WW36	0.16	0.16	0.10	0.11	0.10	0.099
WW37	0.34	0.34	0.24	0.25	0.251	0.25
WW38	0.36	0.36	0.011	0.014	0.013	0.013
WW39	0.90	0.91	0.017	0.019	0.019	0.019
WW40	0.87	0.87	0.44	0.40	0.40	0.40
WW41	0.76	0.75	0.035	0.037	0.036	0.035
WW42	0.50	0.51	0.0088	0.011	0.0095	0.010
WW43	0.52	0.52	0.030	0.031	0.030	0.031
WW44	0.56	0.58	0.016	0.019	0.017	0.017
WW45	0.16	0.17	0.11	0.11	0.10	0.098
WW46	0.59	0.59	0.042	0.045	0.045	0.042
WW47	0.25	0.25	0.17	0.15	0.15	0.15
WW48	0.38	0.39	0.053	0.056	0.054	0.055
WW49	0.10	0.10	0.021	0.021	0.021	0.022
WW50	0.71	0.72	0.045	0.045	0.044	0.046
WW51	0.23	0.23	0.034	0.038	0.037	0.038
WW52	1.5	1.5	0.015	0.016	0.015	0.015

Table XVII

ICP-MS and ICP-AES trace element analysis report for Sr and Ba

Sample number	ICP-MS Sr88 ppm	ICP-MS Sr86 ppm	ICP-AES Ba ppm	ICP-MS Ba137 ppm	ICP-MS Ba138 ppm	ICP-MS Ba136 ppm
WW53	0.97	0.98	0.056	0.062	0.058	0.056
WW54	0.11	0.11	0.053	0.053	0.055	0.056
WW55	0.14	0.14	0.070	0.082	0.079	0.080
WW56	1.30	1.31	0.020	0.022	0.021	0.019
WW57	0.24	0.24	0.099	0.10	0.10	0.10
WW58	0.19	0.19	0.076	0.081	0.081	0.084
WW59	0.69	0.68	0.76	0.83	0.81	0.84
WW60	1.1	1.1	0.019	0.020	0.019	0.018
WW61	0.48	0.48	0.44	0.47	0.46	0.48
WW62	0.73	0.74	0.019	0.019	0.020	0.020
WW63	0.60	0.60	0.032	0.030	0.029	0.029
WW64	0.008	0.008	<0.0038	0.0036	0.0037	0.0044
WW65	0.82	0.83	0.011	0.010	0.010	0.012
WW66	0.24	0.25	0.27	0.25	0.25	0.25
WW67	0.13	0.13	0.18	0.17	0.16	0.17
WW68	0.10	0.10	0.082	0.079	0.077	0.081
WW69	0.31	0.31	0.23	0.20	0.20	0.19
WW70	0.16	0.16	0.14	0.14	0.14	0.14
WW71	0.083	0.084	0.0094	0.013	0.012	0.014
WW72	0.19	0.19	0.16	0.13	0.14	0.13
WW73	0.60	0.60	0.026	0.024	0.024	0.025
WW74	0.61	0.62	0.026	0.025	0.025	0.027
WW75	0.29	0.29	0.15	0.12	0.12	0.12
WW76	0.052	0.052	0.029	0.026	0.025	0.025
WW77	1.1	1.1	0.81	0.72	0.73	0.73

Table XVIII

ICP-MS and ICP-AES trace element analysis report for Ni, Cu, V and Co in WW27-WW52

Sample number	ICP-MS Ni60 ppm	ICP-MS Ni62 ppm	ICP-MS Cu63 ppm	ICP-MS Cu65 ppm	ICP-MS V51 ppb	ICP-MS Co ppb
WW27	0.036	0.016	0.027	0.042	1.7	1.4
WW28	0.021	0.043	0.011	0.029	2.0	0.87
WW29	0.036	0.015	0.025	0.031	1.7	1.5
WW30	0.011	0.045	0.013	0.019	1.7	0.71
WW31	0.0042	0.10	0.024	0.040	1.6	0.25
WW32	0.0022	0.092	0.011	0.021	3.0	0.42
WW33	0.012	0.039	0.019	0.021	1.6	0.27
WW34	0.0038	0.045	0.047	0.052	1.7	0.39
WW35	0.0095	0.13	0.012	0.037	1.8	0.48
WW36	0.027	0.022	0.065	0.068	1.5	1.1
WW37	0.011	0.031	0.014	0.009	40	0.48
WW38	0.014	0.047	0.013	0.023	2.0	0.65
WW39	0.044	0.056	0.0057	0.034	1.9	1.8
WW40	0.020	0.061	0.011	0.008	30	0.82
WW41	0.026	0.049	0.0068	0.023	1.9	1.2
WW42	0.020	0.026	0.014	0.025	2.1	1.1
WW43	0.030	0.024	0.034	0.048	1.8	1.3
WW44	0.034	0.032	0.013	0.031	2.0	1.6
WW45	0.0065	0.031	0.014	0.010	21	0.45
WW46	0.040	0.018	0.033	0.046	2.0	1.6
WW47	0.0075	0.027	0.016	0.011	33	0.40
WW48	0.014	0.019	0.0061	0.012	2.6	0.81
WW49	0.0045	0.018	0.027	0.030	1.7	0.33
WW50	0.054	0.016	0.030	0.046	2.3	2.4
WW51	0.0092	0.017	0.0048	0.011	2.0	0.49
WW52	0.081	0.027	0.011	0.053	2.1	4.4

Table XIX

ICP-MS and ICP-AES trace element analysis report for NI, Cu, V and Co in WW53-WW77

Sample number	ICP-MS Ni60 ppm	ICP-MS Ni62 ppm	ICP-MS Cu63 ppm	ICP-MS Cu65 ppm	ICP-MS V51 ppb	ICP-MS Co ppb
WW53	0.037	0.0067	0.0056	0.012	1.8	1.5
WW54	0.0037	0.0095	0.0050	0.003	15	0.35
WW55	0.0042	0.0081	0.0061	0.004	18	0.27
WW56	0.10	0.029	0.019	0.088	3.9	4.1
WW57	0.0062	0.012	0.0080	0.010	13	0.33
WW58	0.0080	0.018	0.0056	0.009	9.7	0.39
WW59	0.023	0.0092	0.0042	0.003	31	1.0
WW60	0.058	0.026	0.0044	0.050	2.9	2.5
WW61	0.021	0.0052	0.019	0.018	19	1.1
WW62	0.042	0.0073	0.0081	0.023	2.3	1.8
WW63	0.031	0.021	0.026	0.060	2.2	1.5
WW64	0.0010	0.028	0.010	0.026	2.4	0.26
WW65	0.063	0.016	0.020	0.073	3.0	4.0
WW66	0.043	0.013	0.013	0.016	3.2	1.8
WW67	0.0037	0.016	0.018	0.018	2.0	0.20
WW68	0.0039	0.014	0.087	0.085	4.6	0.36
WW69	0.042	0.023	0.059	0.064	2.0	1.6
WW70	0.0084	0.022	0.74	0.73	3.7	0.80
WW71	0.0022	0.11	0.093	0.120	1.9	0.31
WW72	0.013	0.010	0.12	0.12	3.4	0.59
WW73	0.031	0.023	0.006	0.027	2.4	1.2
WW74	0.033	0.029	0.11	0.14	2.3	1.3
WW75	0.0068	0.022	0.042	0.045	2.5	0.40
WW76	0.0022	0.013	0.023	0.021	3.4	0.19
WW77	0.042	0.015	0.079	0.078	17	2.8

Table XX

ICP-MS and ICP-AES trace element analysis report for Li, Zn, and U in WW27-WW52

Sample number	ICP-AES Li ppm	ICP-MS Li6 ppm	ICP-MS Li7 ppm	ICP-AES Zn ppm	ICP-MS Zn66 ppm	ICP-MS Zn67 ppm	ICP-MS U238 ppb
WW53	0.14	0.15	0.14	0.027	0.039	0.028	1.4
WW54	0.042	0.10	0.054	0.079	0.091	0.058	1.4
WW55	0.049	0.11	0.061	0.20	0.21	0.14	1.2
WW56	0.12	0.16	0.12	0.20	0.23	0.16	27
WW57	0.049	0.089	0.056	<0.020	0.019	0.018	0.89
WW58	0.048	0.084	0.053	<0.020	0.020	0.016	1.5
WW59	0.045	0.093	0.053	0.11	0.11	0.077	1.5
WW60	0.098	0.14	0.097	0.026	0.043	0.041	1.5
WW61	0.027	0.072	0.033	<0.020	0.021	0.024	1.5
WW62	0.094	0.11	0.087	<0.020	0.021	0.019	1.1
WW63	0.073	0.12	0.065	<0.020	0.028	0.030	1.8
WW64	0.013	0.067	0.019	<0.020	0.026	0.024	2.0
WW65	0.11	0.16	0.087	0.19	0.21	0.15	15
WW66	0.027	0.047	0.031	0.27	0.26	0.17	1.0
WW67	0.023	0.053	0.028	<0.020	0.015	0.014	1.6
WW68	0.017	0.056	0.021	0.078	0.080	0.058	1.3
WW69	0.018	0.051	0.022	1.4	1.4	0.89	3.2
WW70	0.015	0.070	0.019	0.23	0.25	0.16	2.6
WW71	0.071	0.16	0.069	0.091	0.092	0.067	2.4
WW72	0.013	0.058	0.017	0.042	0.071	0.050	1.2
WW73	0.041	0.082	0.044	0.30	0.31	0.20	1.6
WW74	0.041	0.075	0.043	0.30	0.31	0.19	1.2
WW75	0.020	0.076	0.025	0.21	0.21	0.14	1.9
WW76	0.021	0.077	0.026	0.030	0.040	0.030	1.7
WW77	0.088	0.13	0.091	0.23	0.22	0.15	2.6

Table XXI

ICP-MS and ICP-AES trace element analysis report for Li, Zn, and U in WW53-WW77

Sample number	ICP-AES Li ppm	ICP-MS Li6 ppm	ICP-MS Li7 ppm	ICP-AES Zn ppm	ICP-MS Zn66 ppm	ICP-MS Zn67 ppm	ICP-MS U238 ppb
WW27	0.057	0.078	0.058	0.12	0.12	0.078	1.1
WW28	0.049	0.081	0.053	0.23	0.23	0.15	1.1
WW29	0.051	0.070	0.056	0.93	0.97	0.60	12
WW30	0.067	0.097	0.073	0.032	0.044	0.032	1.1
WW31	0.13	0.17	0.14	<0.020	0.028	0.025	1.2
WW32	0.057	0.096	0.066	0.11	0.12	0.077	1.6
WW33	0.086	0.11	0.095	0.075	0.081	0.055	0.93
WW34	0.080	0.11	0.090	0.039	0.048	0.032	1.3
WW35	0.14	0.19	0.15	0.20	0.21	0.14	1.5
WW36		0.030	0.014	0.12	0.13	0.083	1.7
WW37	0.070	0.15	0.093	0.79	0.81	0.51	1.6
WW38	0.067	0.10	0.082	0.79	0.84	0.52	1.4
WW39	0.081	0.10	0.095	0.070	0.091	0.065	1.1
WW40	0.14	0.24	0.15	<0.020	0.034	0.031	2.2
WW41	0.051	0.087	0.056	0.14	0.16	0.11	2.2
WW42	0.068	0.096	0.083	0.071	0.089	0.058	1.4
WW43	0.045	0.070	0.054	0.63	0.65	0.41	1.0
WW44	0.078	0.11	0.091	0.071	0.080	0.054	1.1
WW45	0.052	0.13	0.064	0.24	0.24	0.15	2.4
WW46	0.060	0.083	0.072	0.49	0.51	0.33	6.8
WW47	0.066	0.14	0.077	0.020	0.035	0.028	2.4
WW48	0.16	0.21	0.18	0.19	0.21	0.13	1.8
WW49	0.057	0.098	0.068	0.10	0.11	0.072	1.6
WW50	0.045	0.082	0.056	0.029	0.050	0.036	13
WW51	0.080	0.12	0.096	0.049	0.065	0.043	1.0
WW52	0.068	0.11	0.075	0.047	0.067	0.055	16

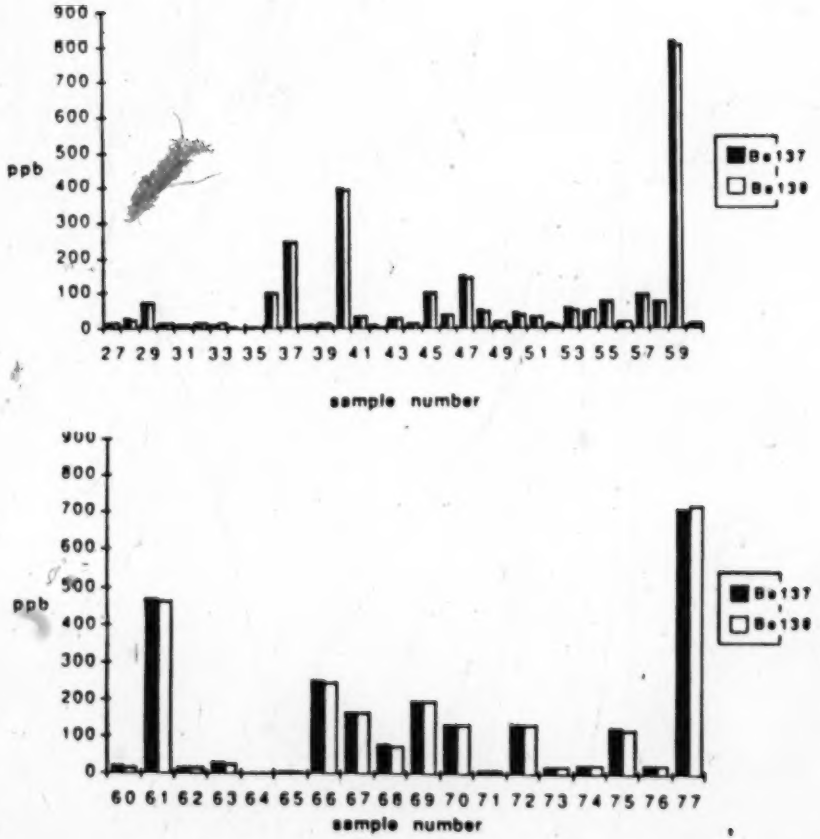

Figure 49. Column plots of ICP-MS concentration results of ^{137}Ba and ^{138}Ba

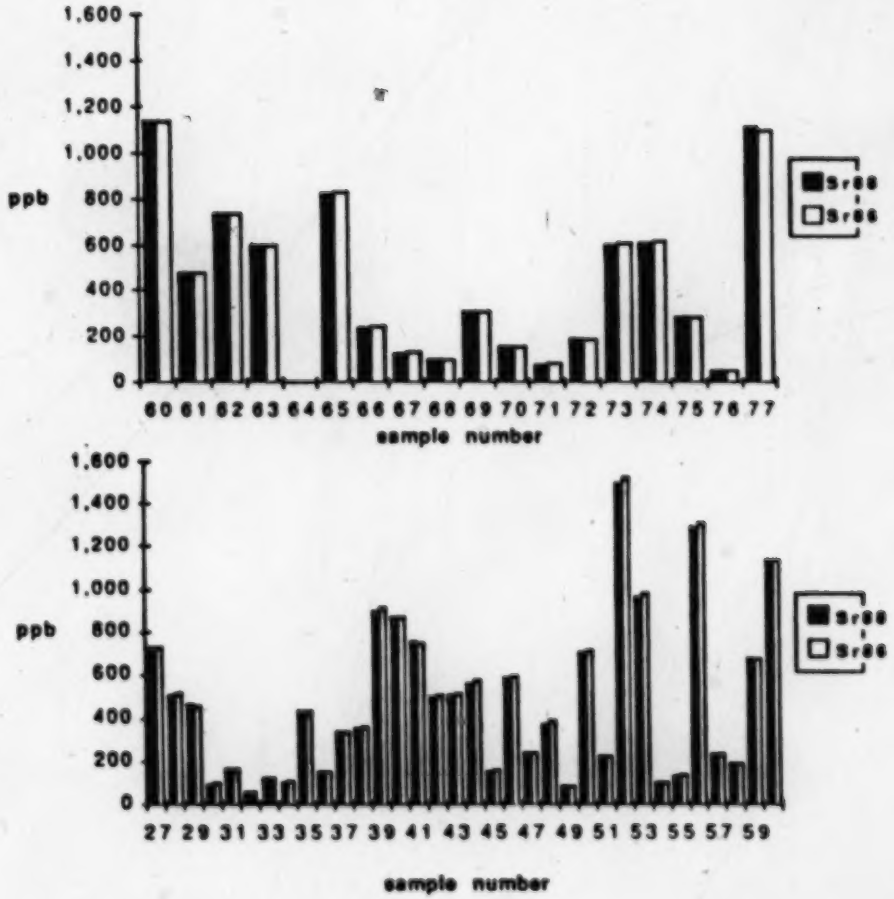

Figure 50. Column plots of ICP-MS concentration results of ^{86}Sr and ^{88}Sr

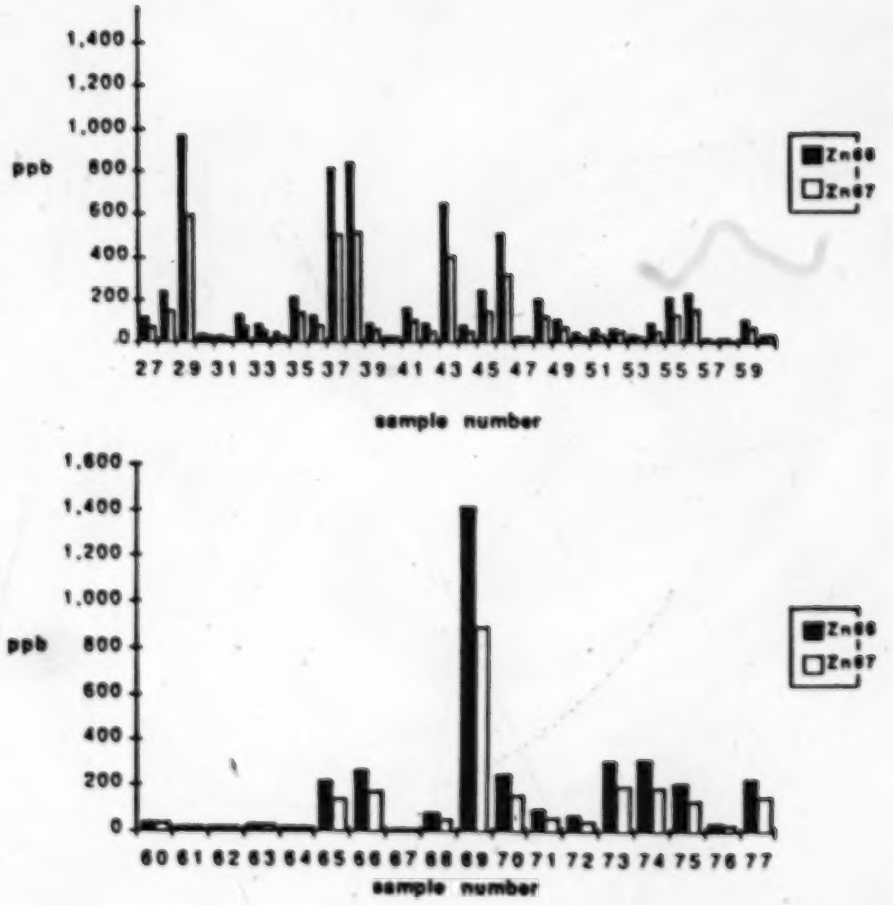

Figure 51. Column plots of ICP-MS concentration results of ^{66}Zn and ^{67}Zn

same trend can be observed for ^{6}Li and ^{7}Li, with concentrations reported from ^{6}Li being always higher than that of ^{7}Li. However, in this case such an observation is expected because of possible errors in the ^{6}Li calibration curve as indicated by its high slope (log c vs. log i) of 1.57. The disagreement between concentrations reported for the isotopes of nickel and copper can be accounted for by interferences arising from major elements in the matrix. Results illustrating these interferences are shown in the next section.

ICP-AES results were obtained for Ba, Li and Zn. The other elements (Vanadim, Cobalt, Nickel, Copper and Vanadium) were not detected by ICP-AES as they were present at concentration levels below the detection limit of the ARL 34000 ICP spectrometer. The strontium channel was not in operation during the analysis.

A plot of the results shown in Tables XVI-XXI for the ICP-MS and ICP-AES results for barium is shown in Figure 52. This figure format shows very clearly the agreement between the two results. Similar plots for Li ands Zn are shown in Figures 53 and 54. Figure 53 shows that the ^{7}Li ICP-MS results agree better with the ICP-AES results then with the ^{6}Li ICP-MS results, showing that the ^{7}Li results are more accurate. Similarly the plots for the ICP-AES results of Zn (Figure 54) show agreement with those of the ^{66}Zn ICP-MS results, indicating that the ICP-MS results of ^{66}Zn are more accurate than those of ^{67}Zn. The low Isotope abundance of ^{67}Zn (4.1%) compared with that of ^{66}Zn 27.8% and possible interferences from $^{35}C\ ^{16}O^{16}O$ may be responsible for the inaccuracy of the ^{67}Zn results.

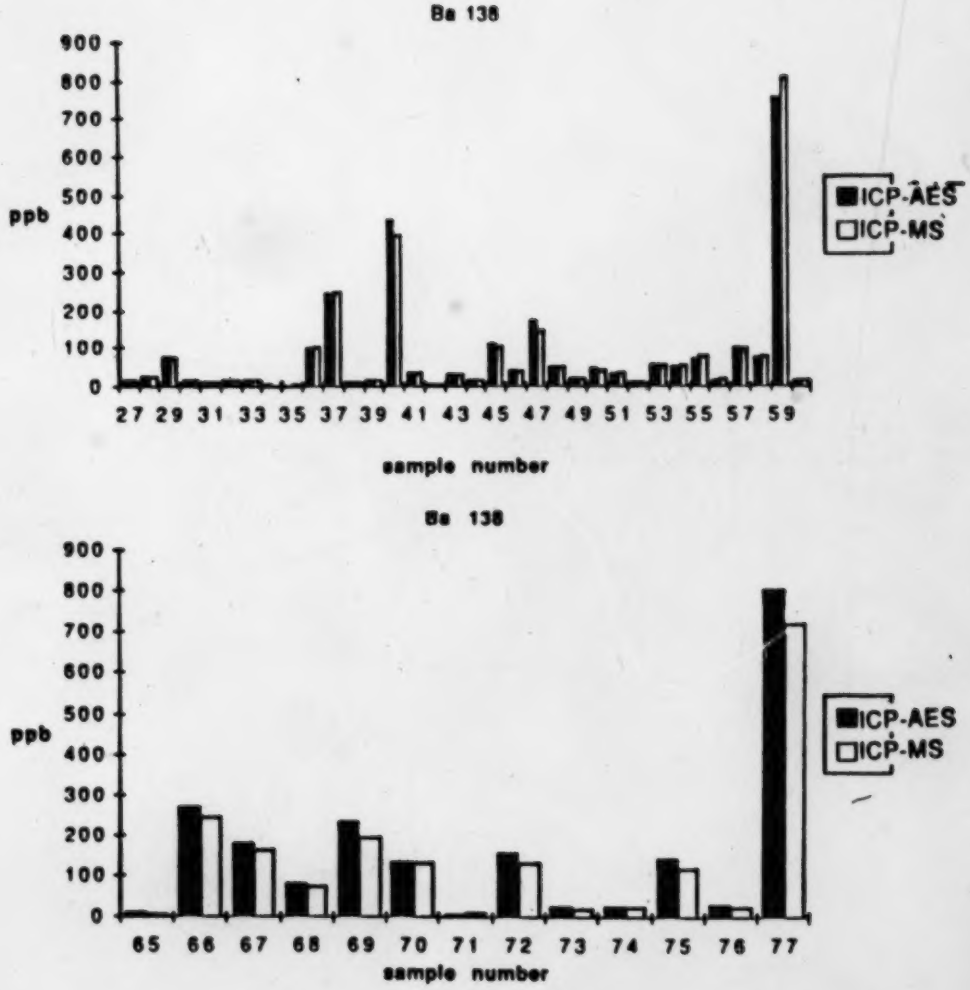

Figure 52. Column plots of ICP-MS and ICP-AES concentration results of Ba

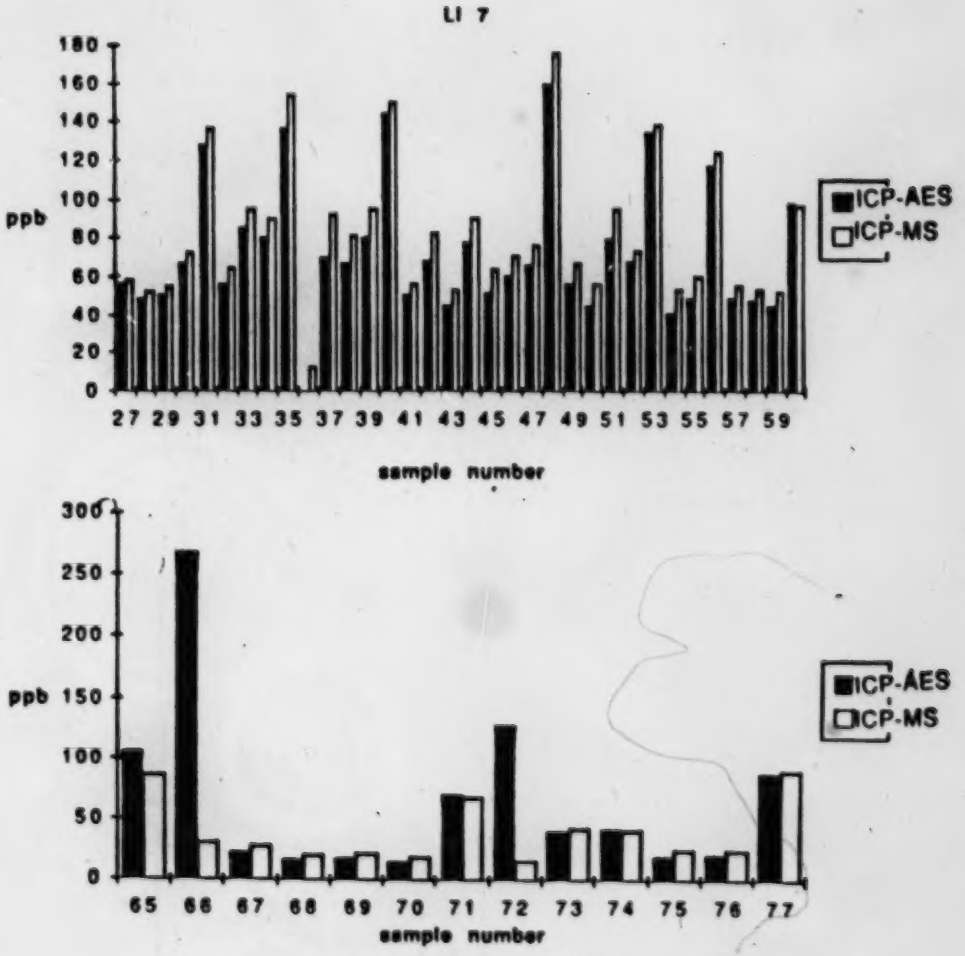

Figure 53. Column plots of ICP-MS and ICP-AES concentration results of LI

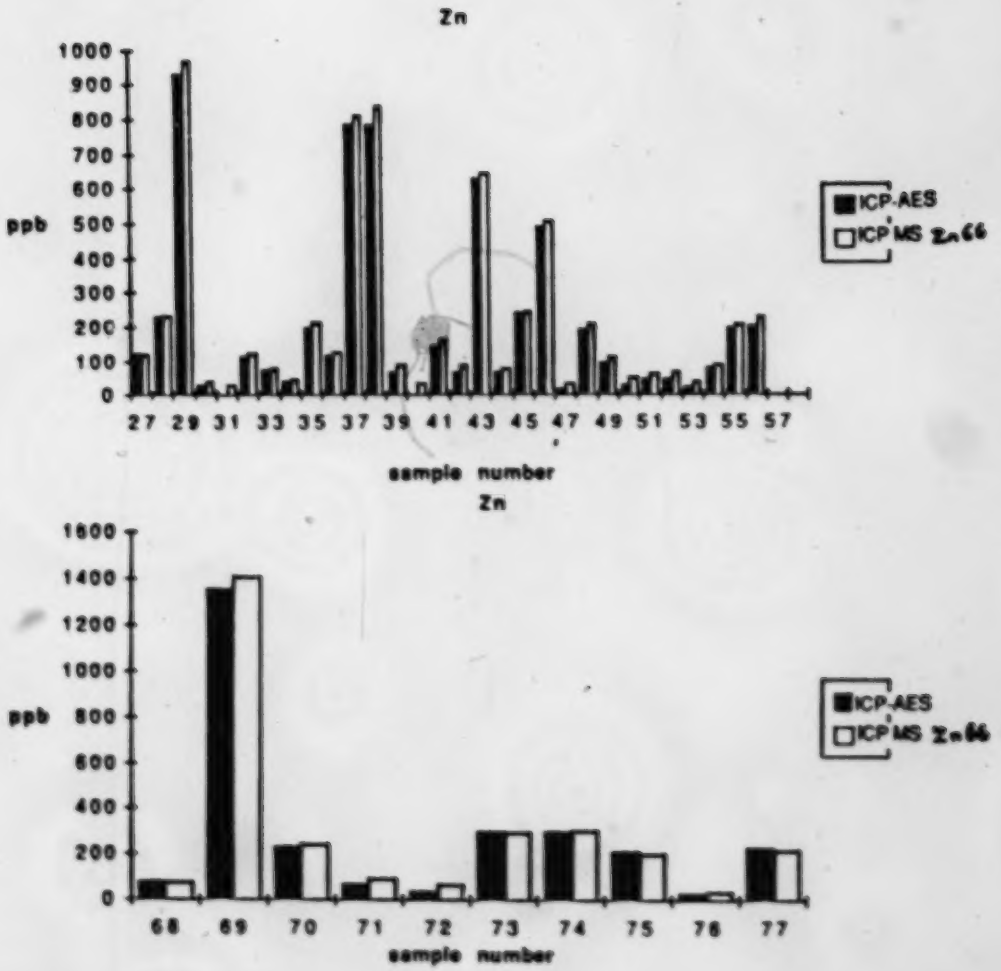

Figure 54. Column plots of ICP-MS and ICP-AES concentration results of Zn

Tables XXII-XXV show a comparison of the precision obtained with ICP-MS and ICP-AES for Li and Zn. In most cases it was observed that precision was better with the ICP-AES technique or that there was no significant difference between the two techniques. The F-test of standard deviations was used and conclusions based on 90% and 95% confidence limits are tabulated.

Detection limits for ICP-MS and ICP-AES are shown in Table XXVI. Detection limit is defined here as the elemental concentration that would give a net intensity equal to twice the standard deviation of the background signal. Background standard deviation was determined using 5 repeats for the ICP-MS analysis and 11 integrations for the ICP-AES analysis. All results obtained were lower for ICP-MS indicating that the technique is more sensitive than ICP-AES.

D. Spectral Interference Assessment in ICP-MS

As mentioned in the previous section, discrepancies in the ICP-MS analytical results for the nickel and copper isotopes are due to isobaric spectral overlap interferences. In order to develop analytical methodologies which would make use of the low detection limit capability of ICP-MS, these interferences arising from the common major elements in the type of sample of interest must be assessed. Such studies would help in establishing criteria for quality assurance of analytical results and hence help in improving the quality of data reported.

Table XXII

Precision comparison of ICP-MS and ICP-AES results for Li in WW27-WW52

Sample#	ICP-AES Li std dev ppm	ICP MS Li std dev ppm	F Statistic	90% confidence	95% confidence
27	0.0008	0.0018	5.3360	same	same
28	0.0008	0.0012	2.2375	same	same
29	0.0003	0.0009	8.9566	same	same
30	0.0009	0.0015	2.9434	same	same
31	0.0012	0.0043	14.0510	ICP-AES better	same
32	0.0008	0.0010	1.5236	same	same
33	0.0010	0.0019	3.4254	same	same
34	0.0012	0.0026	4.7734	same	same
35	0.0011	0.0049	20.1399	ICP-AES better	ICP-AES better
36		0.0004			
37	0.0011	0.0021	3.3398	same	same
38	0.0003	0.0012	18.4798	ICP-AES better	same
39	0.0013	0.0041	9.9648	ICP-AES better	same
40	0.0007	0.0159	479.3454	ICP-AES better	ICP-AES better
41	0.0020	0.0014	0.5133	same	same
42	0.0005	0.0023	24.1472	ICP-AES better	ICP-AES better
43	0.0005	0.0018	13.0964	ICP-AES better	same
44	0.0005	0.0032	46.9210	ICP-AES better	ICP-AES better
45	0.0003	0.0026	96.5702	ICP-AES better	ICP-AES better
46	0.0019	0.0016	0.6972	same	same
47	0.0005	0.0039	53.3033	ICP-AES better	ICP-AES better
48	0.0003	0.0049	235.8528	ICP-AES better	ICP-AES better
49	0.0006	0.0015	7.2228	same	same
50	0.0003	0.0015	30.1332	ICP-AES better	ICP-AES better
51	0.0010	0.0018	2.8405	same	same
52	0.0005	0.0029	27.4008	ICP-AES better	ICP-AES better

Table XXIII

Precision comparison of ICP-MS and ICP-AES results for Li in WW53-WW77

Sample#	ICP-AES Li std dev ppm	ICP MS Li std dev ppm	F Statistic	90% confidence	95% confidence
53	0.0011	0.0027	6.2468	same	same
54	0.0015	0.0009	0.3466	same	same
55	0.0003	0.0019	44.4513	ICP-AES better	ICP-AES better
56	0.0011	0.0050	22.2995	ICP-AES better	ICP-AES better
57	0.0003	0.0010	12.3806	ICP-AES better	same
58	0.0003	0.0008	7.4830	same	same
59	0.0003	0.0019	49.3401	ICP-AES better	ICP-AES better
60	0.0003	0.0051	300.7215	ICP-AES better	ICP-AES better
61	0.0005	0.0014	8.1342	same	same
62	0.0003	0.0011	15.4094	ICP-AES better	same
63		0.0052			
64		0.0012			
65		0.0075			
66	0.0166	0.0006	0.0013	same	same
67	0.0009	0.0008	0.9185	same	same
68	0.0003	0.0007	4.1529	same	same
69	0.0010	0.0003	0.0957	same	same
70	0.0009	0.0005	0.3379	same	same
71	0.0008	0.0041	23.5261	ICP-AES better	ICP-AES better
72	0.0051	0.0008	0.0234	same	same
73	0.0006	0.0007	1.5226	same	same
74	0.0010	0.0008	0.6876	same	same
75	0.0015	0.0008	0.2881	same	same
76	0.0012	0.0007	0.3306	same	same
77	0.0008	0.0042	27.4625	ICP-AES better	ICP-AES better

Table XXIV

Precision comparison of ICP-MS and ICP-AES results for Zn in WW27-WW52

Sample#	ICP-AES Zn std dev ppm	ICP MS Zn std dev ppm	F Statistic	90% confidence	95% confidence
27	0.0037	0.0042	1.2979	same	same
28	0.0025	0.0098	14.9045	ICP-AES better	same
29	0.0093	0.0165	3.1426	same	same
30	0.0003	0.0029	98.2693	ICP-AES better	ICP-AES better
31		0.0015			
32	0.0038	0.0034	0.8301	same	same
33	0.0026	0.0052	3.9672	same	same
34	0.0008	0.0014	2.8592	same	same
35	0.0012	0.0050	17.4393	ICP-AES better	same
36	0.0052	0.0047	0.8131	same	same
37	0.0079	0.0065	0.6771	same	same
38	0.0055	0.0055	1.0110	same	same
39	0.0033	0.0053	2.6136	same	same
40		0.0025			
41	0.0037	0.0019	0.2756	same	same
42	0.0012	0.0039	10.3398	ICP-AES better	same
43	0.0063	0.0110	3.0190	same	same
44	0.0011	0.0027	6.5550	same	same
45	0.0022	0.0114	28.2321	ICP-AES better	ICP-AES better
46	0.0035	0.0060	2.9759	same	same
47	0.0009	0.0031	12.2886	ICP-AES better	same
48	0.0038	0.0057	2.2167	same	same
49	0.0012	0.0028	5.9913	same	same
50	0.0019	0.0012	0.3629	same	same
51	0.0009	0.0021	5.0231	same	same
52	0.0008	0.0028	12.1365	ICP-AES better	same

Table XXV

Precision comparison of ICP-MS and ICP-AES results for Zn in WW53-WW77

Sample#	ICP-AES Zn std dev ppm	ICP MS Zn std dev ppm	F Statistic	90% confidence	95% confidence
53	0.0017	0.0025	2.2805	same	same
54	0.0005	0.0056	138.2795	ICP-AES better	ICP-AES better
55	0.0022	0.0103	22.9467	ICP-AES better	ICP-AES better
56	0.0026	0.0113	18.8164	ICP-AES better	same
57		0.0013			
58		0.0010			
59	0.0013	0.0036	7.1040	same	same
60	0.0008	0.0055	50.1596	ICP-AES better	ICP-AES better
61		0.0014			
62		0.0015			
63		0.0035			
64		0.0030			
65	0.0010	0.0086	81.8413	ICP-AES better	ICP-AES better
66	0.0064	0.0057	0.7730	same	same
67		0.0018			
68	0.0010	0.0048	22.9529	ICP-AES better	ICP-AES better
69	0.0054	0.0371	47.0533	ICP-AES better	ICP-AES better
70	0.0014	0.0055	16.1615	ICP-AES better	same
71	0.0017	0.0118	50.3730	ICP-AES better	ICP-AES better
72	0.0015	0.0034	5.2440	same	same
73	0.0048	0.0083	2.9208	same	same
74	0.0039	0.0113	8.2364	same	same
75	0.0013	0.0027	4.4717	same	same
76	0.0013	0.0023	3.2120	same	same
77	0.0027	0.0047	2.8998	same	same

Table XXVI

ICP-MS and ICP-AES detection limits

ELEMENT	ICP-MS DL (ppb)	ICP-AES DL (ppb)
Co	0.031	N/A
Ba	0.11	0.38
U	0.49	N/A
Ni	0.21	13
Cu	0.20	2.2
Li	0.18	1.7
Sr	0.081	N/A
V	0.10	2.5
Zn	0.30	3.5

Figure 55 shows a column plot of the concentration values obtained for ^{60}Ni Isotope versus sample number and a similar plot for Ca obtained using ICP-AES. These plots show a very strong pattern correlation between ^{60}Ni and Ca indicating that a calcium species interferes with ^{60}Ni. A look at the possible Ca interferences in Table VII shows that $^{43}Ca^{16}OH$ and $^{44}Ca^{16}O$ are most likely responsible for this interference. The table also shows that ^{61}Ni, ^{62}Ni and ^{64}Ni will also suffer from Ca interference due to $^{44}Ca^{16}OH$, $^{46}Ca^{16}O$ and $^{48}Ca^{16}O$ respectively.

Figure 56 shows column plots of ^{62}Ni and Na while Figure 57 shows column plots of ^{62}Ni and Ca. The ^{62}Ni plots appear to follow the same pattern as the Na plot for samples WW27-35. Beyond sample WW35 there is no clear pattern. Since both calcium and sodium can interfere with ^{62}Ni, calcium producing $^{46}Ca^{16}O$ and sodium producing $Na_2{}^{16}O$ as shown in Table VII, this complex pattern is not unexpected. Most of the samples below WW35 have very little Ca, thus the predominant interference will originate from Na. Above WW35 there is a significant amount of both Ca and Na in most of the samples thus the interference on ^{62}Ni will depend on both Ca and Na, hence a complex process was observed.

Both $Na^{40}Ar$ and $^{46}Ca^{16}OH$ should interfere with ^{63}Cu. $Na^{40}Ar$ should be the more significant interferent because of the fact that argon was used as the plasma gas. The column plot for ^{63}Cu (Figure 58), however, does not show very similar variations in the ^{63}Cu and Na plots. A previous study done in our lab showed a strong correlation

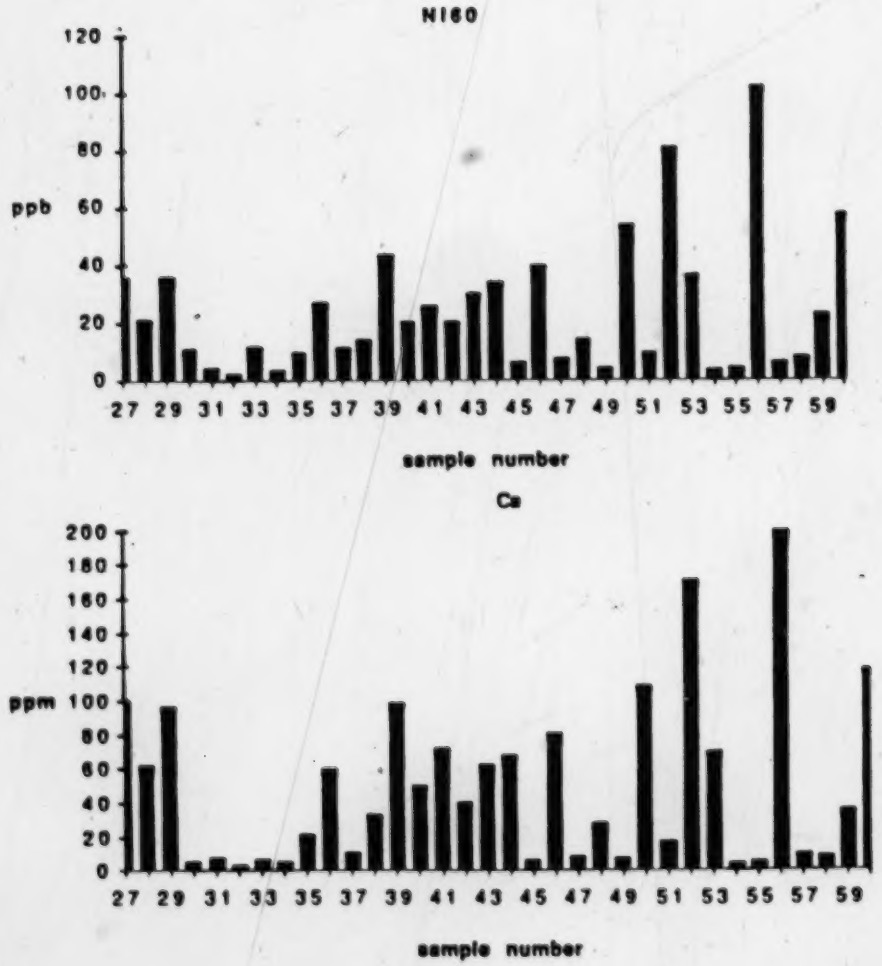

Figure 55. Column plots of ^{60}Ni and Ca

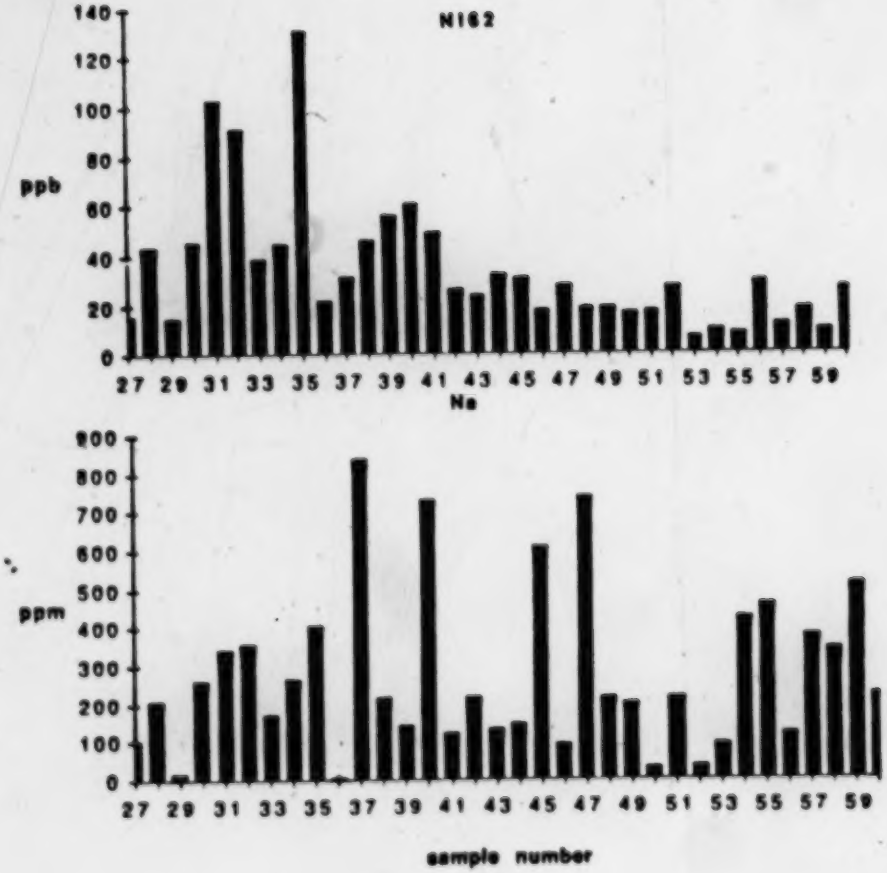

Figure 56. Column plots of ^{62}Ni and Na

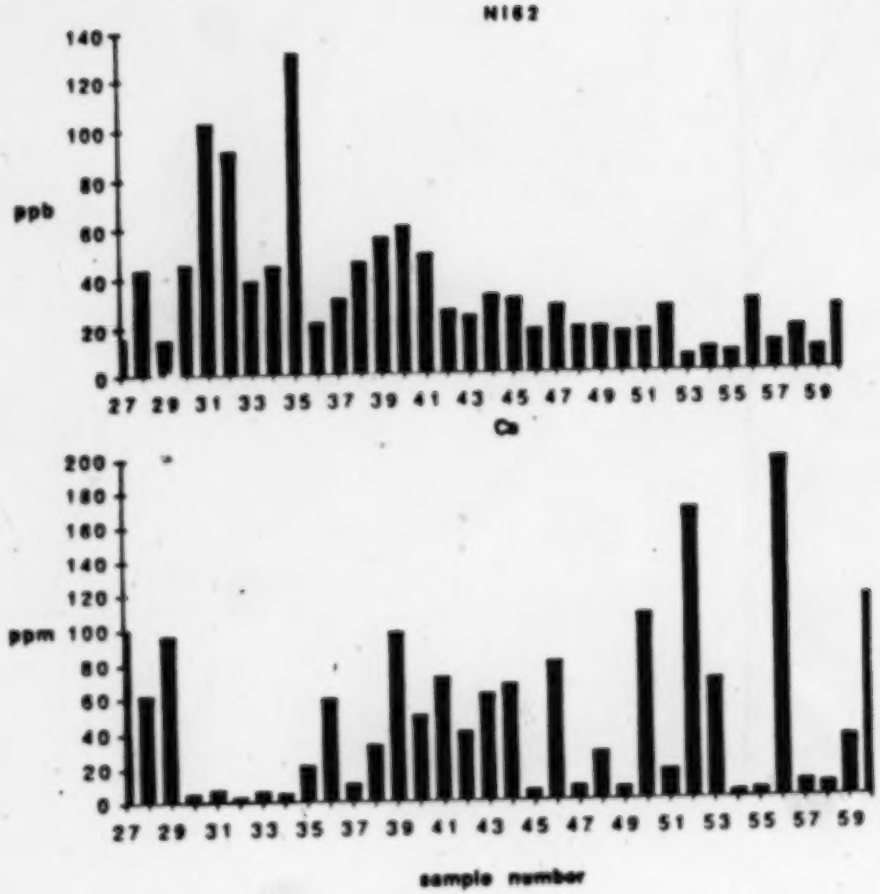

Figure 57. Column plots of ^{62}Ni and Ca

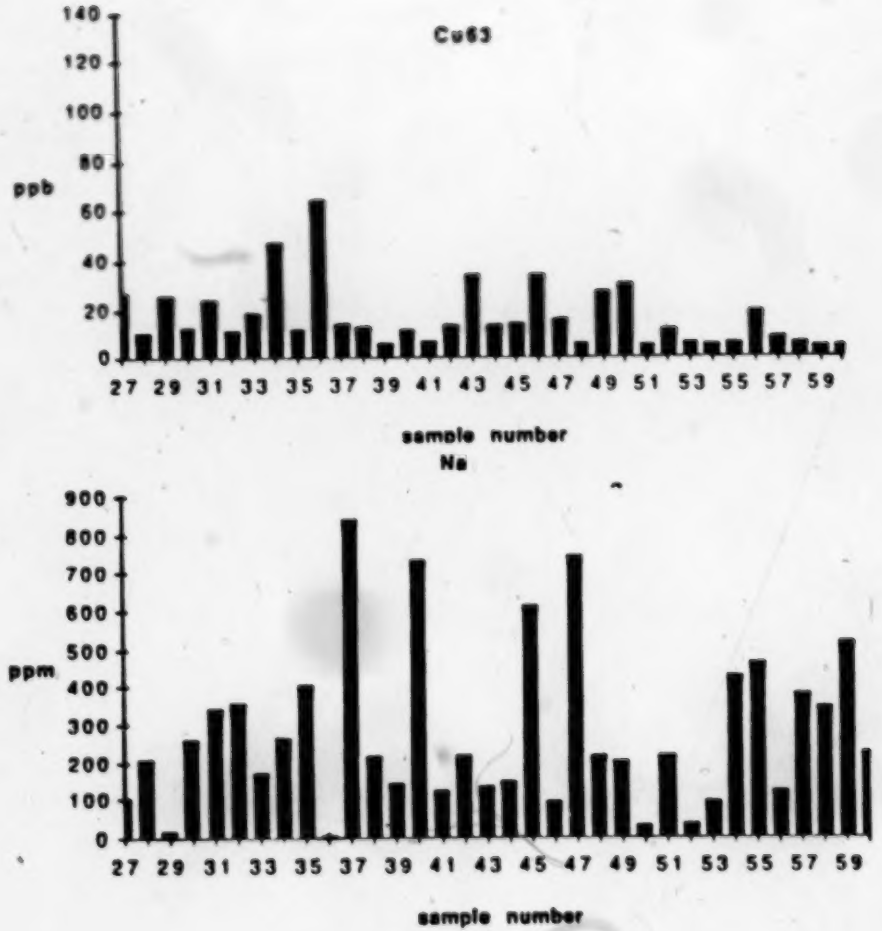

Figure 58. Column plots of ^{63}Cu and Na

between ^{63}Cu and Na but the samples used for that study had much higher Na matrix concentrations than those used for this study.

^{65}Cu Line plots are shown in Figure 59. Table VI shows that sulfur interferes with ^{65}Cu because it gives $^{33}S^{16}O^{16}O$ and $^{33}S^{32}S$. The line plots show that the concentration measured from the ^{65}Cu isotope follows a similar variation among the samples as the sulfur concentration.

The column plots in Figure 60 show the difference between the concentrations obtained with the ^{65}Cu and ^{63}Cu plotted against sample number (top plot) and the sulfur concentration plotted against sample number (bottom plot). Here it can be observed that the concentration obtained with ^{65}Cu is always greater than that obtained with ^{63}Cu if sulfur is present in the sample and always less if the sulfur concentration is negligible. This indicates that the concentration report from the ^{65}Cu isotopes is very likely to be erroneous due to sulfur interference. Since the difference is very small if the sulfur concentration is very small it also indicates that the ^{63}Cu results are likely to be accurate. This would explain the observation that the ^{63}Cu results do not correlate with the Na results as observed in Figure 58. Thus Na is not present at a high enough level in the samples to interfere with the ^{63}Cu results.

Table XXVII shows that the major isotope of vanadium (^{51}V) has interference from $^{35}Cl^{16}O$. Since the vanadium results are very low and since Cl is a major anion in the samples, the results are likely to be inaccurate.

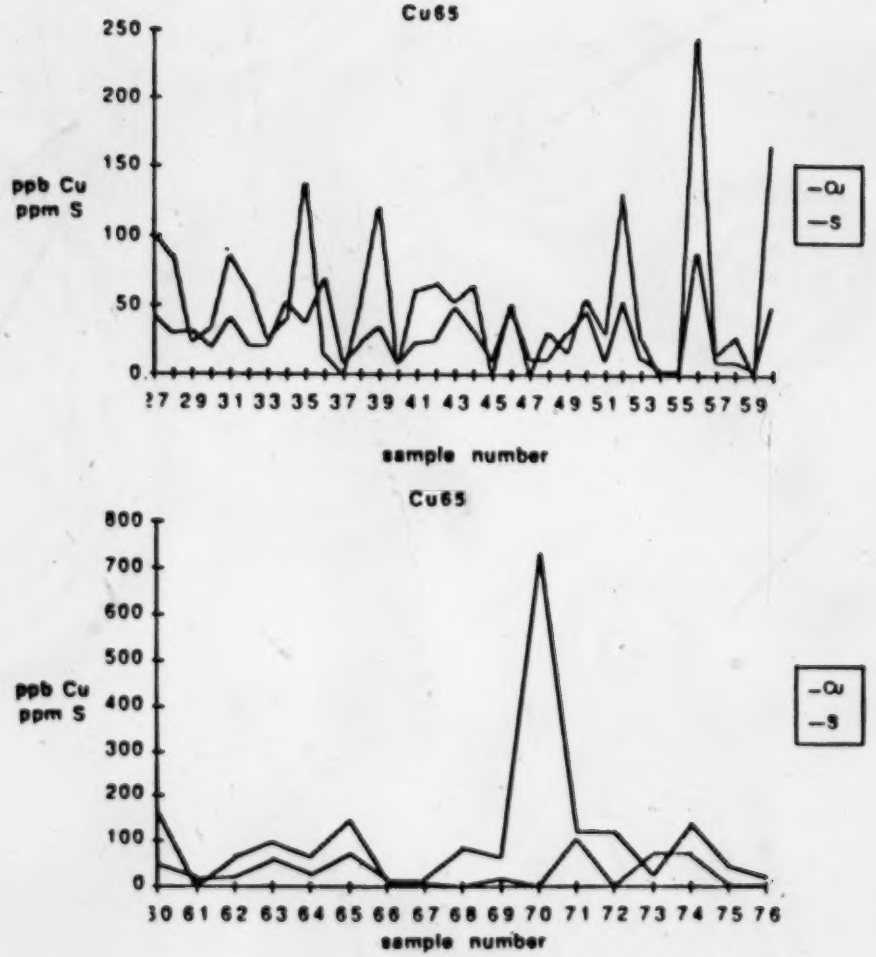

Figure 59. Line plots of ^{65}Cu and S

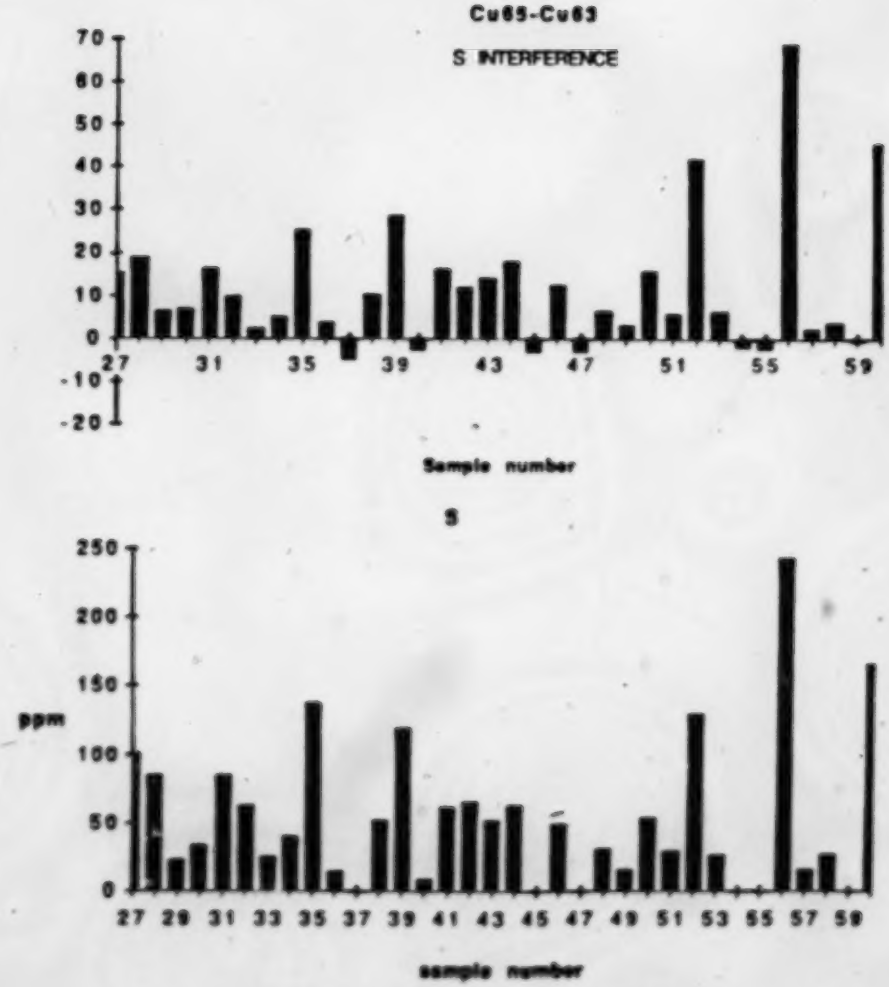

Figure 60. Column plots of ^{65}Cu-^{63}Cu and S

Table XXVII. Isobaric interfering species associated with Cl

Element	Mass	%Abund.	Assoc. species	Mass	Affected elements (% abund.)
Cl	35	75.77	CH	36	Ar(0.34), S(0.02)
Cl	37	24.23	CH	38	Ar(0.06)
Cl	35	75.77	$Cl^{14}N$	49	Ti(5.46)
Cl	37	24.23	$Cl^{14}N$	51	V(99.76)
Cl	35	75.77	$Cl^{16}O$	51	V(99.76)
Cl	37	24.23	$Cl^{16}O$	53	Cr(9.51)
Cl	35	75.77	$Cl^{16}OH$	52	Cr(83.76)
Cl	37	24.23	$Cl^{16}OH$	54	Fe(5.82), Cr(2.38)
Cl	35	75.77	$Cl^{16}O^{16}O$	67	Zn(4.11)
Cl	37	24.23	$Cl^{16}O^{16}O$	69	Ga(60.16)
Cl	35	75.77	$Cl^{35}Cl$	70	Ge(20.51), Zn(0.62)
Cl	37	24.23	$Cl^{35}Cl$	72	Ge(27.4)
Cl	35	75.77	$Cl^{40}Ar$	75	As(100)
Cl	37	24.23	$Cl^{40}Ar$	77	Se(7.58)

CHAPTER VI

Conclusions

ICP-MS is a very promising technique for rapid multielement trace analysis. Its excellent sensitivity and low detection limits which have been shown in data presented here, surpass those of ICP-AES and many other spectroscopic techniques. The ability to do isotope ratio analysis and qualitative/semiquantitative analysis in a very short time is also a big plus. However, from the results presented it is clear that both isobaric spectral overlap interferences and matrix induced signal suppression interferences can be very serious and can lead to erroneous analytical results. The analyte signals in ICP-MS also depend on ICP parameters, particularly nebulizer flowrate and power both of which must be kept constant during trace analysis. Parameter plots of these two variables show characteristic patterns which are similar for most elements and therefore aid in the selection of compromise instrument settings without much loss in sensitivity.

Table XXVIII shows the results of ICP-MS semi-quantitative and quantitative trace element analysis for some of the groundwater samples. It can be seen that the semi-quantitative analysis results are close to the corresponding quantitative analysis results. Most of the semi-quantitative results are within a factor of 3 of the corresponding quantitative results.

Although the precision values obtained in ICP-MS are not as good as those of ICP-AES, RSD values obtained are comparable with those obtained in some other analytical techniques. Precision

Table XXVIII

ICP-MS semiquantitative and quantitative trace analysis results comparison

	SEMI-QUANT	QUANT	SEMI-QUANT	QUANT	SEMI-QUANT	QUANT	SEMI-QUANT	QUANT
sample #	Ba ppm	Ba 138 ppm	Sr ppm	Sr ppm	Zn ppm	Zn66 ppm	Li ppm	Li7
WW39	0.027	0.019	2.0	0.90	0.16	0.091	0.47	0.095
WW40	0.61	0.40	2.5	0.87	0.071	0.034	1.0	0.15
WW41	0.060	0.036	1.9	0.76	0.27	0.16	0.29	0.056
WW43	0.048	0.030	1.2	0.52	1.2	0.65	0.24	0.054
WW44	0.026	0.017	1.3	0.56	0.025	0.080	0.39	0.091
WW45	0.18	0.10	0.51	0.16	0.44	0.24	0.37	0.064
WW46	0.064	0.045	1.3	0.59	0.94	0.51	0.29	0.072
WW47	0.24	0.15	0.67	0.25	0.065	0.035	0.39	0.077
WW48	0.069	0.054	0.79	0.38	0.34	0.21	0.52	0.18
WW49	0.032	0.021	0.22	0.10	0.22	0.11	0.24	0.068
WW50	0.076	0.044	2.0	0.71	0.099	0.050	0.23	0.056
WW52	0.032	0.015	5.0	1.5	0.14	0.067	0.36	0.075
WW53	0.071	0.058	2.1	0.97	0.081	0.039	0.43	0.14
WW54	0.082	0.055	0.30	0.11	0.17	0.091	0.23	0.054
WW55	0.11	0.079	0.33	0.14	0.35	0.21	0.22	0.061
WW56	0.035	0.021	3.6	1.30	0.41	0.23	0.41	0.12
WW57	0.13	0.10	0.51	0.24	0.025	0.019	0.19	0.056
WW58	0.099	0.081	0.45	0.19	0.035	0.020	0.18	0.053
WW59	0.80	0.81	1.5	0.69	0.20	0.11	0.19	0.053
WW60	0.031	0.019	2.8	1.1	0.053	0.043	0.37	0.097
WW61	0.24	0.46	0.51	0.48	0.012	0.021	0.06	0.033
WW62	0.030	0.020	1.7	0.73	0.059	0.021	0.30	0.087
WW63	0.040	0.029	1.4	0.60	0.015	0.028	0.21	0.065
WW65	0.017	0.010	2.1	0.82	0.34	0.21	0.30	0.087
WW66	0.21	0.25	0.45	0.24	0.39	0.26	0.080	0.031
max(semi/quant)		2.1		3.4		2.8		6.7

values are affected by random errors during measurement, errors due to sample preparation and sample introduction and changes in the sampler orifice diameter due to salt particle deposits.

At present most samples have to be in aqueous solution before analysis by ICP-MS, however, samples can also be introduced via electrothermal vaporization and directly using electrode cups made from a variety of materials.

ICP-MS is a fairly new technique with great promise. However, there still remains a lot to be done for it to occupy a major place in industry and routine analysis laboratories. Most of the different types of isobaric interferences have been presented in the literature but very little has been done in the development of analytical methodologies. For this to be accomplished, interferences caused by major elements in different samples have to be studied, the concentration of the interfering element at which the interference becomes important must be determined and possible interference correction procedures studied. The development of sample introduction techniques is also very important. Taking these steps should help in paving the way towards extending the analytical applications of ICP-MS.

Bibliography

1. W. Stum and J.J. Morgan, "Aquatic Chemistry", Wiley (Interscience); New York (1970).
2. J.W. Moore and E.A. More, "Environmental Chemistry", Academic Press, New York (1976).
3. C.N. Sawyer and R.L. McCarty, "Chemistry For Environmental Engineering", McGraw-Hill, New York (1978).
4. R.E. Thiers, Methods Biochem. Anal., 5, 237 (1975).
5. P. MacCarthy and R.W. Klusman, Anal. Chem. 59(12), 308R-337R (1987).
6. K.H. Mancy editor, "Instrumental Analysis for Water Pollution," Ann Arbor Science Publishers, Michigan (1971).
7. L.L. Ciaccio editor, "Water and Water Pollution Handbook", Volume 1, Dekker, New York (1971).
8. L.L. Ciaccio, Ibid., Volume 2, (1971).
9. L.L. Ciaccio, Ibid., Volume 3, (1972).
10. L.L. Ciaccio, Ibid., Volume 4, (1973).
11. R.A. Minear and L.H. Keith, "Water Analysis" Academic Press, N.Y. (1982).
12. E.B. Sandell "Colorimetric Determination of Traces of Metals", Third Edition, Interscience, New York (1965).
13. X. Yan, L. Liu, X. Zhu, Z. Zhang, B. Tang and X. Zhang, Fenxi Ceshi Tongbao, 4, 28-30 (1985).
14. H.S. Rathore, S.K. Sharma, K. Kuman, Ann. Chim. (Rome), 74, 873-80 (1984).

15. R. Mavrodineau, editor, Analytical Flame Spectroscopy", Macmillan 1970.

16. J.A. Dean and T.C. Rains, editors "Flame Emission and Atomic Absorption Spectrometry", Volume 1, Dekker, 1969.

17. J.A. Dean and T.C. Rains, editors. "Flame Emission and Atomic Absorption Spectrometry", Volume 2, Dekker, 1971.

18. ASTM, "Manual on Industrial Water and Industrial Waste Water" /2d ed, The Society, Philadelphia (1985).

19. C.G. Hsu and D.C. Locke, Anal. Chim. Acta, 153, 313-18, (1983).

20. Z.I. Sukhareva, A.P. Zolotareva, A.I. Ryzak, Zovod. Lab. 49, 36 (1983).

21. J.M. Lo, J.C. Yu, R.I. Hutchison, C.M. Wai, Anal Chem., 54, 2536-9 (1982).

22. K.R. Sperling, B. Baar, Z. Freseneius, Anal Chem., 314, 21-4 (1983).

23. A. O'Ulivo, R. Fulol, R., Pupoff, Talanta, 32, 103-109 (1985).

24. H. Tao, A. Mujazaki, K. Bansho Kogai, 20, 137-144 (1985).

25. H. Han, W. Wang, Hnanjing Huaxne, 4, 52-57 (1985).

26. A.W. Morris, Analytica Chim Acta, 1968, 42, 397.

27. P. Chechet, G. Eschalier, Anal Chim Acta, 156, 295-9 (1984).

28. A.T. Ellis, D.E. Leyden, W. Wegscheider, B.B. Jabwaski, W.B. Bodnar, Anal Chim Acta, 142, 73-87 (1982).

29. A.T. Ellis, D.E. Leyden, W. Wegscheider, B.B. Jabwaski,

W.B. Bodnar, Anal Chim Acta, 142, 89-100 (1982).

30. S. Imai, M. Muroi, A. Hamaguehe and M. Koyama, Anal. Chem., 55, 1215-19 (1983).

31. R.R. Greenberg and H.M. Kingston, Anal. Chem. 55, 1160-5 (1983).

32. C. Brihaye and G. Duyckaerts, Anal. Chim. Acta, 148, 51-7 (1983).

33. R. Audruzzi, A. Trazza and G. Marrosu, Anal. Lett., 15, 1565-84 (1982).

34. A. Hu, R.E. Dessy and A. Granedi, Anal. Chem., 55, 320-8 (1983).

35. I. Drabaek, P.P. Madsen and J. Soerensen, Int. J. Environ. Anal. Chim Acta, 144, 183-8 (1982).

36. G.O. Foss, H.J. Svec and R.J. Conzemius, Anal. Chim. Acta, 147, 151-62 (1983).

37. I.R. Shelpakova, A.I. Saprykiu, T.A. Chanysheva and I. Yudelevich, G. ZH. Anal. Khim., 38, 581-5 (1983)

38. W.M. Blakemore, P.H. Casey and W.R. Collins, Anal. Chem., 56, 1376-9 (1984).

39. A.S. Buchanan and P. Hannaker, Anal. Chem., 56, 1379-82 (1984).

40. I.T. Urasa, Anal Chem., 56, 904-8 (1984).

41. V.A. Fassel and R.N. Kinsley, Anal. Chem. 46 (13), 1110A-1120A (1974).

42. V.A. Fassel and R.N. Kinsley, Anal. Chem. 46 (13) 1155A-1164A (1974).

43. N. Furuta, Spectrochim. Acta. 41B, 1115 (1986).

44. N. Furuta, Spectrochim. Acta. 40B, 1013-1022, (1985).

45. P.W.J.M. Boumans, Editor, "Inductively Coupled Plasma Emission Spectroscopy", Part 2. Applications and Fundamentals. Wiley Interscience, New York (1987).

46. A. Montaser and D.W. Golightly, Editors, "Inductively Coupled Plasmas in Analytical Atomic Spectrometry", VCH Publishers, New York (1987).

47. P.W.J.M. Boumans, "Theory of Spectrochemical Excitation", Higler Watts, London/Plenum Press, New York (1966).

48. R.S. Houk, V.A. Fassel, G.D. Flesch, H.J. Svec, A.L. Gray and C.E. Taylor, Anal. Chem. 52, 2283-2289 (1980).

49. R.S. Houk, H.J. Svec and V.A. Fassel, Appl. Spectrosc., 35, 380-384 (1981).

50. R.S. Houk, A. Montaser and V.A. Fassel, Appl. Spectrosc 37, 425-428 (1983).

51. D.F. Douglas, E.S.K. Quan and R.G. Smith, Spectrochim. Acta., 38B, 39-48 (1983).

52. A.R. Date and A.L. Gray, Analyst 106, 1255-1267 (1981).

53. A.R. Date and A.L. Gray, Analyst 108, 159-165 (1983).

54. A.R. Date and A.L. Gray, Spectrochim. Acta. 38B, 29-37 (1983).

55. A.R. Date and A.L. Gray, Analyst 108, 1033-1050 (1983).

56. R.S. Houk and D.F. Douglas, Prog. Anal. At. Spectrosc. 8, 1-18 (1985).

57. A.L. Gray, Spectrochim. Acta. 41B 1525-1537 (1985).

58. S.H. Tan and G. Horlick, Appl. Spectrosc. 40, 445-460 (1986).

59. M.A. Vaughan and G. Horlick Appl. Spectrosc. 40, 434-445 (1986).

60. S.H. Tan, G. Horlick, J. Anal. At. Spectrom. 2, 745-763 (1987).

61. G. Horlick, S.H. Tan, M.A. Vanghan and C.A. Rose, Spectro Chim. Acta, 40B, 1555, (1985).

62. G. Zhu, and R.F. Browner, Appl. Spectrosc. 41, 56 (1987).

63. D.C. Gregoire, Spectrochim. Acta. 42B, 895 (1987).

64. H. Kawaguchi, T. Tanaka, T. Nakawura, M. Monshita, and A. Mizuiki, Anal. Sci. 3, 305 (1987).

65. D. Beauchemin, J.W. McLaren and S.S. Berman, Spectrochim. Acta, 42B, 467 (1987).

66. S.R. Koirtyohann, J.S. Jones and D.A. and Yates, Anal. Chem. 52, 1965-1966 (1980).

67. G. Horlick and M. Vaughan, J. Anal. At. Spectrom. In Press.